2016-04-13

Numerical Modeling of Intervertebral Disc Degeneration and Repair

Qiaoqiao Zhu
University of Miami, qqz_whu@hotmail.com

UNIVERSITY OF MIAMI

NUMERICAL MODELING OF INTERVERTEBRAL DISC DEGENERATION AND REPAIR

By

Qiaoqiao Zhu

A DISSERTATION

Submitted to the Faculty
of the University of Miami
in partial fulfillment of the requirements for
the degree of Doctor of Philosophy

Coral Gables, Florida

May 2016

UNIVERSITY OF MIAMI

A dissertation submitted in partial fulfillment of
the requirements for the degree of
Doctor of Philosophy

NUMERICAL MODELING OF INTERVERTEBRAL DISC DEGENERATION AND REPAIR

Qiaoqiao Zhu

Approved:

Weiyong Gu, Ph.D. Professor of Mechanical and Aerospace Engineering and Biomedical Engineering	Chun-Yuh Huang, Ph.D. Associate Professor of Biomedical Engineering
Alicia R. Jackson, Ph.D. Assistant Professor of Biomedical Engineering	Fotios Andreopoulos, Ph.D. Associate Professor of Biomedical Engineering
Mark D. Brown, M.D., Ph.D. Professor of Orthopaedics	Guillermo Prado, Ph.D. Dean of the Graduate School

ZHU, QIAOQIAO (Ph.D., Biomedical Engineering)
Numerical Modeling of Intervertebral Disc Degeneration and Repair (May 2016)

Abstract of a dissertation at the University of Miami.

Dissertation supervised by Professor Weiyong Gu
No. of pages in text. (154)

Intervertebral disc (IVD) is the largest avascular structure in the human body and its main function is to support mechanical loading and to provide the flexibility for the spine system. Degenerative disc disease (DDD) is related to low back pain which affects more than 600 million people worldwide. One of the challenges in modeling DDD is that the biological, mechanical, chemical, and electrical events in IVD are coupled at different levels. It is important to develop a numerical model to understand the biophysics and pathophysiology in IVD (a biological system).

A multiscale and multi-physics model was developed based on a cell-activity-coupled mechano-electrochemical continuum mixture theory. In this model, the phenomena at the solute (or solvent) level (e.g., diffusion and/or reaction of ions, nutrients, growth factors, and interstitial fluid), cellular level (e.g., cell metabolism and viability), and tissue level (e.g., disc volume and shape) are accounted for. The model also includes the interactions among biological (cell activity), chemical [osmolarity, pH, extracellular matrix (ECM) synthesis and degradation], electrical (charges on ECM and solutes), and mechanical (loading and tissue swelling) events in the IVD. Numerical results were obtained by solving a dozen of partial differential equations using a finite element method. This model has been successfully used to simulate the degenerative progression of the IVD (up to 55 years) due to poor nutrition supply. The predicted distributions of water content in the IVD

were consistent with those from direct measurements published in the literature. This result was also consistent with those observed in MRI images of IVDs in human patients.

The model was also used to study kinetics of charged antibiotics (for treating disc infections) and effects of dynamic loading on cell viability (for preventing degeneration) in the IVD. The model has also been used to investigate the long-term efficacy (up to 10 years) of cell therapies for disc repair (i.e., in silico clinical trials). This model can be used not only to provide insights into the mechanisms of disc degeneration, but also to develop new diagnostic tools and to optimize new therapeutic strategies for degenerated discs.

ACKNOWLEDGEMENTS

I would like to thank my advisor, Dr. Weiyong Gu, for his guidance and direction in my Ph.D. study. I appreciate greatly your patience, insightful advice, continuous support and understanding in my research. I am also grateful for your guidance and advice in life, which has helped me grow into a more refined person.

I would also like to thank my committee members, Dr. Chun-Yuh Huang, Dr. Mark D. Brown, Dr. Alicia R. Jackson, and Dr. Fotios Andreopoulos. Thank you for sharing your expertise and offering valuable advice to this work.

Special thanks to all the members of the Tissue Biomechanics Lab and of the Mechanobiology Lab: Tai-yi Yuan, Francesco Travascio, Michele Baldoni, Chong Wang, Lauren Vernon, Daniella Gonzales, Yu Fu (Jason) Wang, Xue (Sherry) Yin, Amaris Genemaras, Lingtu Meng, for their support and encouragement. I especially want to thank Xin Gao for offering me great advice and help both on research and in life. I feel so fortunate to have you walk with me during this journey.

Most of all, I wish to express my deep love and appreciation to my family, my parents, and my younger brother, for your unconditional love and support and always standing aside me through the ups and downs of my life.

Table of Contents

List of Figures

List of Tables

Chapter 1 Specific Aims and Structure of This Dissertation

1.1 Specific Aim

The intervertebral disc (IVD) degeneration is strongly associated with low back pain [1-3], a leading cause of disability with an estimation of more than 600 million people suffered worldwide [4]. Understanding the cause and progression of IVD degeneration is crucial for developing effective treatment strategies for degenerated discs, yet changes of disc behaviors during the degeneration initiation and progression are challenging to be quantified, due to the nonlinear interactions among the biological, chemical, electrical and mechanical signals within the disc. Thus, the general objective of this project is to develop a realistic computational model for simulating the IVD degeneration, to systematically elucidate the complicated relationships between the cell biology and the mechanical, chemical, and electrical signals in the extracellular environment, and to develop new strategies for preventing or treating disc degeneration. In order to achieve these goals, the following specific aims will be addressed:

Specific Aim 1: To develop a comprehensive numerical model to study the biological, chemical, electrical, and mechanical events in the disc during IVD degenerative progression and repair. The multiphasic mixture theory [5, 6] will be extended to couple the interactions between biological activities and mechanics. A mathematical model for the relationship between human disc cell viability and extracellular glucose concentration will be developed and incorporated into the multiphasic mixture theory framework. A constitutive model for the proteoglycan (PG) synthesis/degradation will be developed and implemented into multiphasic mixture theory framework.

Specific Aim 2: To simulate the changes in tissue composition, extracellular environment, and morphology with the progression of disc degeneration. Changes in cell density, PG content, water content, disc deformation, extracellular mechanical signal, and nutritional level with the progression of disc degeneration will be quantitatively analyzed.

Specific Aim 3: To simulate the changes in tissue composition, extracellular environment, and morphology during the process of disc repair. The repair processes in the degenerated discs treated with cell implantation, or other biological therapies (GAG synthesis rate increase, GAG degradation rate decrease) will be quantitatively investigated. The long term efficacy of these treatment strategies will be investigated. Several critical issues related to cell therapy such as the number of cells needed, the time for repair required, the nutrition level demanded by the implanted cells, the long term treatment outcomes (such as 5, 10 or more years) will be addressed.

1.2 Structure of This Dissertation

In Chapter 2, an introduction of the background of the IVD and its structure, composition, function, degeneration, repair, and current status of numerical modeling is presented.

In Chapter 3, the development of a cell-activity coupled multiphasic mixture theory which couples the biology (cell viability, metabolic activities, synthetic activities) and mechanics [including the solid deformation, fluid flow, and solutes transport (diffusion, convection, and binding] to characterize the biomechanics and mechanobiology of IVDs is developed. The gap between the interaction between the cell biology and its extracellular environment is filled.

In chapter 4, a numerical study on the effects of nutrition supply and dynamic loading on cell viability is presented.

In Chapter 5, numerical studies on the initiation and progression of disc degeneration (up to 55 years) related to poor nutrition supply are presented. Changes in cell density, PG content, water content, disc deformation, and extracellular mechanical signal and nutritional level with the progression of disc degeneration are investigated.

In Chapter 6, a numerical study on the effect of nutritional pathway on disc degeneration patterns (spatial distributions of cell density, PG content, water content, etc.) is presented. The distributions of cell density, PG content, and water content in the disc with different nutritional supplies and pathways are studied numerically.

In Chapter 7, numerical studies on the long-term efficacy (up to 10 years) of biological therapies (e.g., cell implantation, biosynthetic activities stimulation, biodegradation activities inhibition) for disc repair (i.e., in silico clinical trials) are presented. Changes in cell density, PG content, water content, disc deformation, extracellular mechanical signal, and nutritional level with the process of disc repair are investigated.

In Chapter 8, numerical studies on kinetics of charged antibiotics (for treating disc infections) are presented. The penetration of differently charged antibiotics (positively, negatively, and uncharged) into human lumbar discs are quantitatively analyzed and compared to understand the effect of electrical charge on the kinetics of antibiotic penetration into the IVD.

In Chapter 9, numerical studies on water content distributions in degenerated discs are presented. We hypothesized that the patterns of water content distribution in the discs are related to the intensity patterns observed in T2-weighted MRI images. To test this hypothesis, the variations of water content distribution in the disc during degenerative progression and repair processes are investigated.

In Chapter 10, the major findings of the study are discussed and summarized.

Chapter 2 Background and Significance

This chapter introduces the background information on human intervertebral discs (IVD) physiology and pathophysiology, and reviews the current status of the numerical models related to IVD simulations with discussions on the limitations of previous models.

2.1 Intervertebral Disc Structure and Anatomy

The intervertebral discs (IVDs) are the main joints of the spinal column, lying between the vertebral bodies (Fig. 2.1). The major role of these discs are transmitting mechanical loads generated by body weight and muscle activities, providing flexibility to the spine, and allowing for the spinal bending, flexion and torsion [7].

The IVDs are not uniform in structure, but generally consist of three different parts: a nucleus pulposus (NP) in the center, surrounded circumferentially by the annulus fibrosus (AF) and superiorly and inferiorly by a thin layer of cartilaginous endplate (CEP), see Figure 2.2. Only the NP and inner AF are superiorly and inferiorly covered by the CEP, as shown in Figure 2.2B. The NP is a gel-like material in healthy discs which contains mostly water. The AF is a more solid-like composite material which consists of 15-25 layers of concentric lamellae composed of collagen fibers. The fibers orient parallel within each lamella, and run an alternating pattern between the layers at an angle approximately 60^{o} to the vertical axis (Fig. 2.3). This pattern of alternating layers of collagen fibers provides high tensile strength to the AF. The AF region of the disc functions primarily to constrain the gelatinous NP and to withstand the tensile forces applied to it by the compressed NP. The CEP consists of a thin layer of hyaline cartilage. The CEP functions to limit the exchange of solutes between NP and its surrounding vasculatures above the

CEP, to constrain the NP from leaking out through the top and bottom of the disc, and to evenly distribute the mechanical loading across the disc and the adjacent vertebral bone.

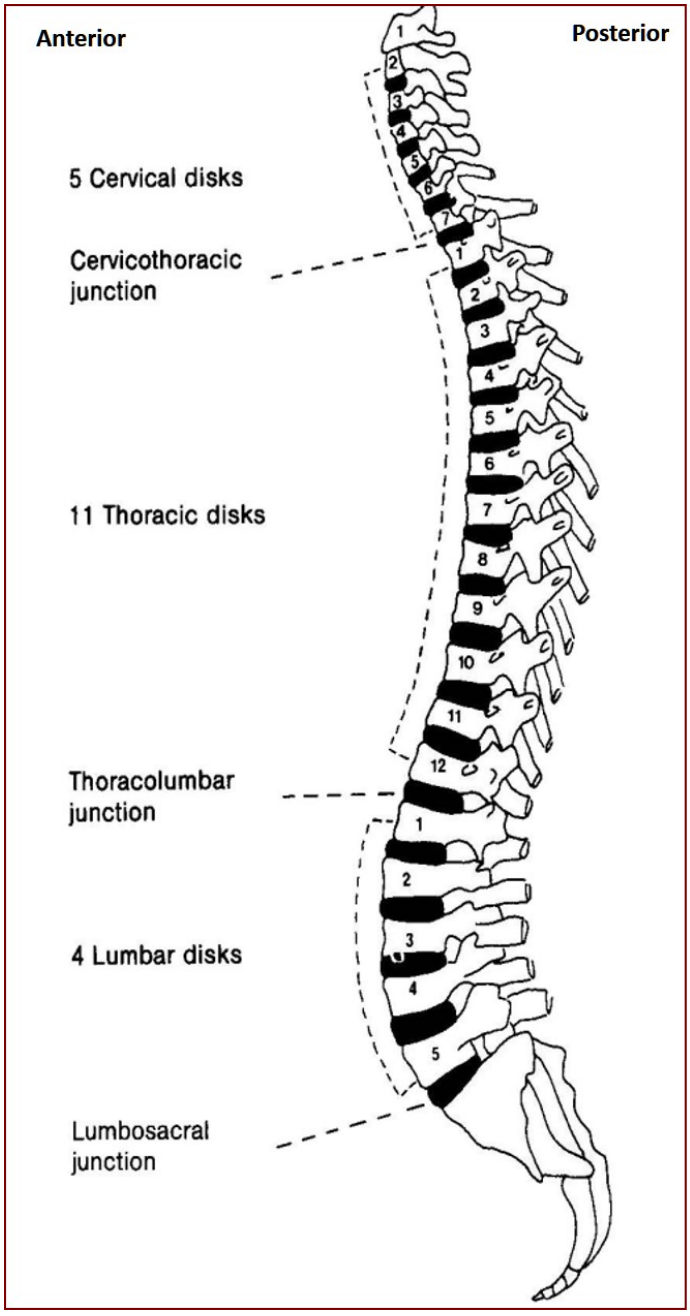

Figure 2. 1: A schematic of the human spine column (adapted from Kramer 1981).

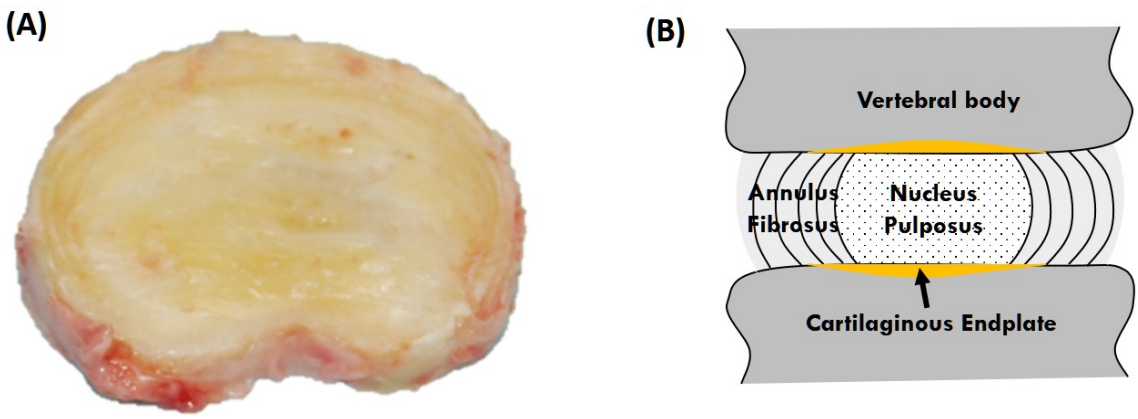

Figure 2. 2: (A) A human lumbar disc (L2-3, 41 years old, non-degenerated, adopted from [7]). (B) A schematic of the disc components.

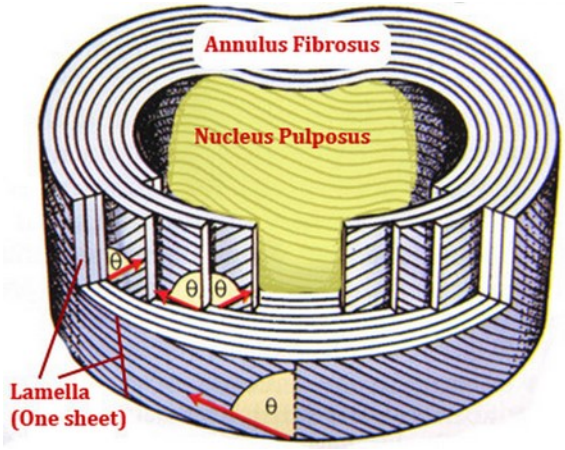

Figure 2. 3: A schematic of the AF lamellar structure (source: http://www.chirogeek.com/).

2.2 IVD Tissue Composition

The IVD consists of a sparse population of cells and an abundant extracellular matrix formed by a framework of macromolecules filled with water. The macromolecules and their interactions with water determines the disc structural integrity and mechanical functions. The cells synthesize the macromolecules and maintain and repair the extracellular matrix (ECM). These disc cells also synthesize the digestive proteinases [e.g., matric metalloproteinases (MMP), aggrecanases] [8-10] which function to degrade the proteins that make up the framework of the matrix. The balance between synthesis, breakdown, and accumulation of matrix components determines the integrity of the matrix, and correspondingly the mechanical properties of the disc [7]. The matrix integrity is also important for maintaining the avascularity and aneural nature of the healthy disc [7].

Matrix components

The major components of a disc are water, proteoglycans (PG), and collagen [11-13]. PGs are large composite molecules in the disc [13]. The majority type of PG in the disc is aggrecan [14]. The PGs are responsible for maintain tissue hydration through the osmotic pressure generated by its negatively charged side chains [15]. PGs, together with water and collagen, give the disc stiffness and resilience to compression [3].

The collagen network is formed mostly of type I and type II collagen fibrils [16, 17]. It makes up approximately 70% and 20% of the dry weight of the AF and the NP, respectively [16]. The collagens provide tensile strength to the disc [3].

The different components have distinct biochemical composition and structure. The NP and inner AF regions contain higher quantities of water and PG than those in the outer AF

region [13, 17]. The outer AF however has larger amount of collagen content (primarily type I collagen), compared to that in the NP and inner AF regions. The collagen type in the NP and inner AF are predominantly type II. The ratio of collage type I and collagen type II decreases from the outer AF to the inner AF. The CEP contains mostly type II collagens.

Cells

The cells in the NP and innermost zone of AF are spheroidal and chondrocyte-like, while the cells in the outer AF are elongated and fibroblast-like, and cells in the endplate are rounded chondrocytes [3, 18]. The cell density is low in the disc, with an average of 5800 cells/mm^3 over the disc [18]. The cell density varies by region. NP has the lowest cell density: 4000 cells/mm^3, AF has a relatively larger cell density of 9000 cells/mm^3, and the CEP has the largest cell density: approximately 15000 cells/mm^3 [18].

Disc cells require nutrients to survive and function. Their main supply of energy is provided by glycolysis [19]. An adequate level of glucose is essential for maintaining the viability of disc cells, and if the glucose concentration drops below a certain level within the disc, such as 0.5 mmol/L, the cells would start to die [20]. The concentrations of glucose, oxygen, and lactate acid in the disc depend both on the rate of nutrient transport and cellular metabolic rates.

Due to avascular, the nutrients have to be transported into the disc and the metabolic wastes be transported out the disc through the matrix. Thus, the transport properties of these nutrients are significantly influenced by the matrix composition and organization.

2.3 Intervertebral Disc Degeneration

There is no unanimously accepted definition of degeneration yet. It is generally found that with degenerative progression, the discs undergo striking alterations in volume, shape, structure, and composition that decrease motion and alter the mechanical functions of the discs. The NP becomes less gel-like, more stiff and fibrous, the interface between NP and AF becomes blurred. In some degenerated discs, there are tears/fissures in the AF, and nerves and blood vessels are observed in the degenerated discs [21]. Researchers have reported that more than 50% of the cells in the adult discs are necrotic [22]. Boos et al. found that decrease in endplate blood vessels at the early age (e.g., 3-10 years old) is detrimental to the maintenance of the disc matrix integrity [23].

The most characteristic biochemical change in the degenerated disc is the loss of PG, especially in the NP and inner AF regions [12]. This loss of PG causes a fall in the osmotic pressure [24] and resultantly a loss of water content in the disc [12], this may cause stress redistributions within the disc and consequently inappropriate stress concentrations in the AF [25-27]. The changes of the collagen content are not obvious in degenerated discs. However, the type and the distribution of the collagen alter with the disc degeneration [7]. It is thought that these changes are initially originated from disturbances in biology of cells in the disc [26, 28].

The causes of disc degeneration are still not fully understood. It is generally thought that poor nutrition, abnormal mechanical loading, and genetic factors are the most important factors leading to the disc degeneration [7].

Nutrition Supply. The disc is avascular and the cells rely on blood vessels at disc margins to supply nutrients and remove metabolic waste through two pathways: the CEP-NP pathway and the AF periphery pathway [29-31]. Survival of NP cells depends primarily on the nutrients supplied through the CEP-NP pathway, and the AF cells mostly rely on nutrients supplied through the AF periphery pathway [29, 32-34].

Disc cells require nutrients such as glucose to maintain alive and active. The cells do not survive long in low glucose concentration and low pH value environment [20, 35]. However they can survival long under low oxygen condition [35] because the cell metabolism is found mainly to be anaerobic [36]. The cell activities are very sensitive to the nutrients and pH at extracellular environment [37-39]. Nutrition supply can be restricted by a fall in endplate permeability [40-43] or a decrease in blood supply [44, 45].

Mechanical Loading. It is shown that mechanical loading affects the cell viability [46], cell metabolism [47], disc morphology and composition [48]. One study suggested that the overloading caused disc degeneration through the mitochondrial apoptotic pathway in disc cells [49].

Dynamic loading effects on the cell viability and activities have been studied and the results of these studies suggest that the cell responses depend on the loading magnitude, frequency, and duration [50]. Chronically loaded compression on discs has been found to decrease disc thickness, increase axial and angular stiffness, and decrease PG contents [48]. Static compression was reported to initiate disorganization of the AF, increase in apoptosis, and down regulation of collagen II and aggrecan gene expression, in a magnitude-dependent manner [51]. A more detailed review can be seen in Setton and Chen (2006) [52].

Genetic factors. It has been reported that familial predisposition may exist for disc degeneration [53, 54]. Twin studies have shown that genetic predisposition plays a significant role in disc degeneration [55-57]. Other studies have found that mutations of two collagen type genes are associated with lumbar disc degeneration and sciatica in a Finnish population [58, 59], and that a polymorphism in the aggrecan gene is associated with early disc degeneration in a Japanese population [60]. Other studies with transgenic mice also demonstrated that mutations in gene of matrix components such as aggrecans and collagens can cause disc degeneration [61-63]. Mutations in genes of macromolecules other than the matrix components such as a polymorphism in the promotor region of the MMP-3 is also found to be associated with rapid degeneration in elderly Japanese population [64].

2.4 Treatment

Traditional treatment methods for disc degeneration involve conservative treatments (e.g., physiotherapy, core strengthening and other exercise modalities) and surgical interventions (such as spinal fusion or prosthetic disc replacement) [65]. Although these treatments alleviate some symptoms, they cannot stop the degenerative progression, nor restore the structure or function of the disc [65]. The long-term efficacy of these treatments is not promising either, as many treated patients experience recurrent pain, reduced spinal mobility, and/or adjacent segment degeneration [65]. New therapies aiming to halt and/or regenerate the disc degeneration are of crucial significance in treating disc degeneration-related spinal disorders. Regenerative therapies such as the biological therapy have been intensively studied in recent years. The idea of the biological therapy is to restore disc

structure and function through implanting functional cells, stimulating the matrix synthesis, and/or inhibiting the matrix degradation activities in the disc [66, 67].

Cell implantation has been applied to a few clinical trials (a detailed review can be found in Benneker et al [67] and Sakai and Andersson [66]). These clinical trials showed positive treatment outcomes; including increases in tissue water content and disc height in the patients under therapy[68-72], except one study in which no improvement in pain relief after one-year follow-up was reported [73]. These studies showed a great potential of the cell therapy in retarding and/or reversing disc degeneration. Nonetheless, many critical issues in relation to the therapies are unaddressed, such as the number of cells needed, the time required for repair, the nutrients demanded by the implanted cells, and the long-term (such as 5, 10, or more years) efficacy of biological therapies. These issues are challenging and costly to address experimentally. Numerical simulations are an alternative means to investigate the process of disc degeneration or regeneration quantitatively and can provide insights into the complicated biological, chemical, electrical, and mechanical events in discs under pathophysiological conditions, which might be difficult to measure directly or simultaneously.

2.5 Numerical Models of IVD

Currently, the published numerical studies on IVD usually focus on the mechanical behaviors of the disc (a detailed review can be found in Schmidt et al (2013) [74]). These models may be generally categorized into 3 types in consideration of the disc materials: single phase models [75-77], biphasic models [78-83], and multiphasic mechano-electrochemical models [84-86]. In single phase models, the NP was usually treated as an

ideal fluid and the AF as a solid. The AF was treated either as a linear orthotropic elastic material [75, 87] or isotropic elastic material [88], or nonlinear orthotropic elastic material [89], or a composite material [90, 91]. These models can be used to estimate the overall mechanical behavior of the disc, however, these models cannot characterize the interstitial fluid flow in the AF and swelling pressure. In biphasic models, the disc was considered as a mixture of fluid and solid. These models are able to characterize the interstitial fluid flow and the flow caused time dependent viscoelastic behavior of the discs. However, the mechano-electrochemical effects, such as the swelling effects, cannot be depicted with these models. A shortcut is to add the swelling pressure term to the total mixture stress based on the Lanir's assumption that the electro-chemical equilibrium in the tissue is achieved instantaneously [92]. This approach is called biphasic-swelling model, and it has been used as an approximation to include the mechano-chemical effects [93]. The diffusivity of ions in this type of model is assumed to be infinitely large, which is not physiologically relevant. The multiphasic mixture models described the disc as a mixture of solid, fluid, and solutes (e.g., ions, nutrients) [84]. All the mechano-electrochemical phenomena in the disc tissue can be described.

These models provide a foundation for understanding mechanical and electrochemical behaviors of charged hydrated tissues, however, these theories have mainly focused on the mechanics and transport of the tissue, how these mechanical and electrochemical behaviors influence the biological activities within the tissue cannot be depicted with these models, yet it is extremely important to explore these issues because interactions between cell biology and its extracellular mechano-electrochemical environment play significant roles in tissue growth and remodeling.

2.6 Significance

Low back pain is a prevalent health problem which affects more than 600 million people worldwide [4, 94, 95]. Approximately 70% of the population suffers from low back pain at some point of their lifetime [96]. It is the leading cause of work-related disability [97] and causes an enormous economic burden on individuals, families, and society as a whole [98-100]. For example, it was estimated that the total cost of low back pain ranges from $100 to $200 billion per year in the United States alone (two thirds of which is attributed to indirect cost, including lost wages, or reduced/ lost productivity) [101].

Although the exact cause of low back pain is still not definitive, intervertebral disc degeneration is found to be strongly associated with it [1-3]. Despite numerous studies have investigated intervertebral disc degenerations, to date there still lacks a thorough understanding on the mechanisms of initiation and progression of the disc degeneration. It is generally thought that the imbalance in matrix synthesis and degradation may initiate the degeneration process and proceed this process. The balance of the biosynthetic and degradative activities however is determined by the cell viability and activity in the disc. The cells, as having been reported by numerous studies, are affected by many extracellular factors such as local nutrition concentration, mechanical signals, growth factors, etc. How the variations of external nutrition supply and/or mechanical loading affect the nutrition concentration, cell responses, mechanical signal distributions, tissue composition and structure changes within the disc are largely unknown. How the changes in tissue composition and structure in turn affect the nutrition and mechanical signals and their effects on the cell responses, are largely unknown either. Answers to these questions would

significantly increase our understanding of the mechanisms of disc degeneration and shed light on the effective treatment of disc degeneration.

Chapter 3 A Cell Activity Coupled Multiphasic Mixture Theory

3.1 Introductory Remarks

Mixture theory has been successfully applied to the study of cartilaginous tissues for over three decades. Biphasic mixture theory was developed by Mow and co-workers [102] for the hydrated soft tissues. In this theory, the tissue is modeled as a mixture of solid phase and fluid phase. This theory can be used to characterize the motion and deformation and fluid flow in hydrated soft tissues. Lai and co-workers expanded the biphasic theory into a triphasic mixture theory, in which the charged hydrated soft tissues (such as articular cartilage and IVDs) were modeled as a mixture of solid phase, fluid phase and ion phase [6]. This theory can be used to describe not only the deformation and fluid flow but also swelling effects of the charged hydrated tissues as well. Gu and co-workers further extended the triphasic theory to describe the swelling phenomenon and passive transport of multi-electrolytes into the charged hydrated soft tissues and through cell membranes.

These theories could provide a foundation for understanding mechanical and electrochemical behaviors of charged hydrated tissues, however, these theories have mainly focused on the mechanics and transport of the mixture, how these mechanical and electrochemical behaviors influence tissue biological behavior was not considered with these theories, yet it is extremely important to explore these issues because interactions between cell biology and its extracellular mechano-electrochemical environment play significant roles in tissue growth and remodeling.

To these ends, the cell metabolism (consumption of nutrients such as glucose, oxygen, and production of metabolic waste such as lactate) were incorporated into the multiphasic

mixture theory by Huang and Gu [103]. Later, Jackson and co-workers incorporated the cell viability (which is nutrient concentration dependent) into this extended multiphasic mixture theory [104]. This theoretical model of nutrient concentration dependent cell viability was first proposed by Shirazi-Adl and co-workers [105]. In this model, it is assumed that the cell density is a linear function of glucose concentration [105]. A significant problem of this model is that the resurrection of dead cells would occur when the glucose level recovers after falling below certain threshold value for cell survival (e.g., 0.5 mM for bovine disc cells [20]). Another limitation of this model is that it cannot be used to analyze cell viability in a time-dependent process under dynamic situations.

The objective of this chapter is to develop such a theory-a cell biology incorporated multiphasic mixture theory-for cartilaginous tissues.

3.2 The Cell Activity-Coupled Multiphasic Mixture Theory

The tissue is considered as a mixture of intrinsically incompressible elastic solid phase (with cells and PG fixed to it), interstitial fluid phase, and solute phase with multiple species (including charged ions like Na^+, Cl^-, and neutral molecules such as glucose, oxygen, lactate, etc.). The driving forces for the transport of interstitial fluid and solutes are the gradients of (electro)chemical potentials.

Momentum Balance Equation for the Mixture

$$\nabla \cdot \boldsymbol{\sigma} = 0\,, \tag{3.1}$$

Continuity Equation for the Mixture

$$\nabla \cdot \left(\boldsymbol{v}^{s} + J^{w} \right) = 0\,, \tag{3.2}$$

Mass Balance Equations for Solutes

$$\frac{\partial \left(\phi^{w} c^{\alpha} \right)}{\partial t} + \nabla \cdot \left(J^{\alpha} + \phi^{w} c^{\alpha} v^{s} \right) = Q^{\alpha}\,, \tag{3.3}$$

where $\boldsymbol{\sigma}$ is the total stress of the mixture, $\boldsymbol{v}^{s}$ is the velocity of the solid phase, J^{w} is the volume flux of water relative to the solid phase, ϕ^{w} is the water volume fraction (also known as tissue porosity or water content), c^{α} is the molar concentration (per unit fluid volume) of solute α, J^{α} is the molar flux of solute α relative to the solid phase, and Q^{α} is the cellular metabolic rate of solute α per unit tissue volume. The velocity of the solid phase $\boldsymbol{v}^{s}$, total stress $\boldsymbol{\sigma}$, volume flux of water (J^{w}), and molar flux of solute α (J^{α}) can be expressed as:

$$\mathbf{v}^{s} = \frac{\partial \mathbf{u}}{\partial t}\,, \tag{3.4}$$

$$\boldsymbol{\sigma} = -p\mathbf{I} + \lambda tr\left(\mathbf{E}\right)\mathbf{I} + 2\mu\mathbf{E}\,, \tag{3.5}$$

$$J^{w} = -k\left(\rho_{T}^{w} \nabla \mu^{w} + \sum_{\alpha} H^{\alpha} c^{\alpha} M^{\alpha} \nabla \tilde{\mu}^{\alpha} \right), \tag{3.6}$$

$$J^{\alpha} = H^{\alpha} c^{\alpha} J^{w} - \frac{D^{\alpha} \rho^{\alpha}}{RT} \nabla \tilde{\mu}^{\alpha}, \tag{3.7}$$

where $\boldsymbol{u}$ is the solid displacement, p is the fluid pressure, $\mathbf{I}$ is the identity tensor, λ and μ are the Lamé constants of the solid matrix, $\mathbf{E}$ is the infinitesimal strain tensor for the solid matrix, k is the hydraulic permeability, ρ^{α} is the apparent mass density of solute α, ρ_T^w is the true mass density of water, H^{α} is the convection coefficient (hindrance factor) of solute α, M^{α} is the molar weight of solute α, D^{α} is the diffusivity of solute α, R is the universal gas constant and T is the absolute temperature.

Cell Metabolism

The cellular metabolic rates of oxygen, glucose, and lactate (per unit tissue volume) and pH are given as follows [103, 106, 107] :

$$Q^{O_2} = -\frac{V'_{\max}(pH - 4.95)c^{o_2}}{K'_m(pH - 4.59) + c^{o_2}} \rho^{cell}, \tag{3.8}$$

$$Q^{lactate} = \exp(-2.47 + 0.93pH + 0.16c^{o_2} - 0.0058c^{o_2{}^2}) \rho^{cell} \frac{c_g}{c_g + k_m^l}, \tag{3.9}$$

$$Q^{glucose} = -0.5 Q^{lactate}, \tag{3.10}$$

$$pH = -0.1 c^{lactate} + 7.5, \tag{3.11}$$

where $V'_{\max}$ is the maximum consumption rate of oxygen, K'_m is the Michaelis-Menten constant for oxygen, k_m^l is the Michaelis-Menten constant for lactate, and ρ^{cell} is the cell

density. More details of the theoretical formulation can be found in our previous studies [5, 103, 108-111].

The metabolic rates of sodium ion (Na^+) and chloride ion (Cl^-) are related to the rate of fixed charge density change (Q^F), see Eq. (3.20) below.

Cell Density

A new theoretical formulation for rate of cell density change has been developed. These equations are typically developed based on the principles of physiology and experimental observations on microbial cell growth [112] :

$$\frac{\partial\left(\phi^w \rho^{cell}\right)}{\partial t} + \nabla \cdot \left(\phi^w \rho^{cell} v^s\right) = \zeta \times \rho^{cell}, \tag{3.12}$$

where ρ^{cell} is cell density, and ζ is essentially the rate of normalized cell density change. We propose that the rate ζ of cell density change in the IVD tissue in general depends on the glucose concentration as follows:

$$\zeta = \alpha_1 \cdot \left(\frac{c_g - c_{g_0}}{c_g + k_1} - \frac{\left|c_g - c_{g_0}\right|}{c_g + k_2}\right), \tag{3.13}$$

where c_g is glucose concentration (in mM), c_{g_0} is the threshold glucose concentration necessary for IVD cell survival; below which cells begin to die. The positive parameters α_1, k_1 and k_2 are determined by the biology of IVD cells.

Previous experimental studies have shown that IVD cell death is initiated when glucose levels fall below 0.5 mM, and at 0.2 mM, all cells die in three days [113-115]. Based on

these studies and the assumption that cell density does not change for glucose concentration values above $0.5\,\text{mM}$, we have that $c_{g_0} = 0.5\,\text{mM}$, $k_1 = k_2 = 0.2\,\text{mM}$ and $\alpha = 1\,\text{day}^{-1}$. So Eq. (3.13) becomes

$$\zeta = \alpha \cdot \left(\frac{c_g - 0.5}{c_g + 0.2} - \frac{\left|c_g - 0.5\right|}{c_g + 0.2}\right). \tag{3.14}$$

Proteoglycan (PG) Content

In the model, the PG content is estimated by the chondroitin sulfated GAG content. The conservation of mass for GAG is:

$$\frac{\partial\left(c^{GAG}\right)}{\partial t} + \nabla \cdot \left(c^{GAG}\mathbf{v}^{s}\right) = Q^{GAG}, \tag{3.15}$$

where c^{GAG} is the molar concentration (per tissue volume) of GAG, $\mathbf{v}^{s}$ is the velocity of solid matrix, and Q^{GAG} is the synthetic/degradation rate of GAG (per tissue volume).

The rate of GAG synthesis/degradation is assumed to be related to the cell density and GAG content by:

$$Q^{GAG} = \lambda_1 \rho^{cell} - \lambda_2 c^{GAG}, \tag{3.16}$$

where λ_1 is the GAG synthesis rate per cell and λ_2 is the GAG degradation rate. The value of λ_2 is related to the half-life of GAG turnover reported in literature [116]. Q^{GAG} is assumed to be zero in discs under a normal/healthy condition before the process of disc degeneration starts. Thus,

$$\lambda_1 = \lambda_2 c_0^{GAG} / \rho_0^{cell} \quad , \tag{3.17}$$

where c_0^{GAG} and ρ_0^{cell} are the GAG content and cell density at healthy state prior to the degeneration process. The experimental results for the rates of GAG synthesis in nucleus pulposus (NP), inner annulus fibrosus (AF), and outer AF are (2.6±3.5) $\times 10^{-5}$, (2.9±4.2) $\times 10^{-5}$, and (1.1±0.9) $\times 10^{-5}$ mmol/g dry weight/hr, respectively [117].

Electroneutrality:

$$c^+ = c^- + c^F \, , \tag{3.18}$$

where c^+ and c^- are the concentrations of sodium ion and chloride ion, respectively; and c^F is the fixed charge density which is related to GAG concentration by assuming 2 moles of charge per mole of GAG in the tissue [118]:

$$c^F = 2c^{GAG} \, . \tag{3.19}$$

From Eq. (3.18), it follows that

$$Q^+ = Q^- + Q^F \quad , \tag{3.20}$$

where Q^+ is the chemical reaction rate for sodium, Q^- is the rate for chloride, and Q^F is the rate for the fixed charge density with $Q^F = 2Q^{GAG}$ because of Eq. (3.19).

Thus, the biological, chemical, electrical, and mechanical events are coupled in the disc.

Chapter 4 Effect of Nutrition and Dynamic Compression on Cell Viability

4.1 Introductory Remarks

Intervertebral disc (IVD) cells play a vital role in maintaining IVD health and function, as they synthesize both anabolic molecules for maintaining the extracellular matrix and catabolic molecules responsible for matrix breakdown [119]. Reduction of cell density in IVDs may diminish the total number of macromolecules produced for maintaining or repairing the matrix structure, lead to tissue disorganization and, consequently, result in IVD degeneration and dysfunction [26, 115].

IVD cells need nutrients to survive. It has been shown that viability of IVD cells is mainly dependent on glucose concentration [20, 35, 120]. Due to the avascular nature of the tissue, nutrients (e.g., glucose and oxygen) and metabolic wastes (e.g., lactic acid) need to be transported in and out the tissue by diffusion (mainly for small molecules) and convection (mainly for large molecules) from CEP and AF peripheral vasculatures outside disc boundaries. Most of the NP cells rely on nutrients supplied through the CEP route while the cells in the AF region are mainly nurtured through the AF peripheral pathway [7, 18, 20, 29, 121, 122]. Adequate nutrient supply has long been regarded as a crucial factor for maintaining normal activities and viability of IVD cells [20, 29, 35, 114, 122, 123]. Decrease of nutrition supply at IVD boundary such as seen in patients with cigarette smoking, malnutrition, or disorders like blood aneurysms, leads to cell death and the development of IVD degeneration [124-126].

Mechanical loading has been shown to affect cellular matrix synthesis of disc cells [127-133], cell viability [46, 134], and transport of nutrients within the IVD tissue [109, 135-141].

However, few quantitative analysis of effects of nutrition supply and mechanical loading on the cell viability has been reported in literature. Thus, the objectives of this study was to analyze and predict how cell viability would be affected by the alteration in the extracellular microenvironment that results from disturbances in nutrition deprivation, degeneration, and dynamic loading in the realistic, human IVDs in a time-dependent manner using a finite element model developed based on the cell-activity coupled multiphasic mixture theory stated in Chapter 3.

4.2 Methods

The geometry of the IVD was generated based on an L2-3 human lumbar disc (41 year old, male, non-degenerated), see Figure 4.1A. The IVD was modeled with three distinct regions: nucleus pulposus (NP), annulus fibrosus (AF), and cartilaginous endplate (CEP).

Some assumptions were made on the disc geometry. The IVD was assumed to be symmetric about the transverse (mid-axial) and mid-sagittal planes, but not the mid-coronal plane. Thus, an upper quarter of the IVD was modeled (Fig. 4.1B) due to such assumed symmetries. The IVD was meshed with 13,981 quadratic Lagrange tetrahedral elements (Fig. 4.1D) using COMSOL software (COMSOL 4.2a, COMSOL, Inc., MA). The weak form of FEM formulation was based on the work by Sun et al. [142].

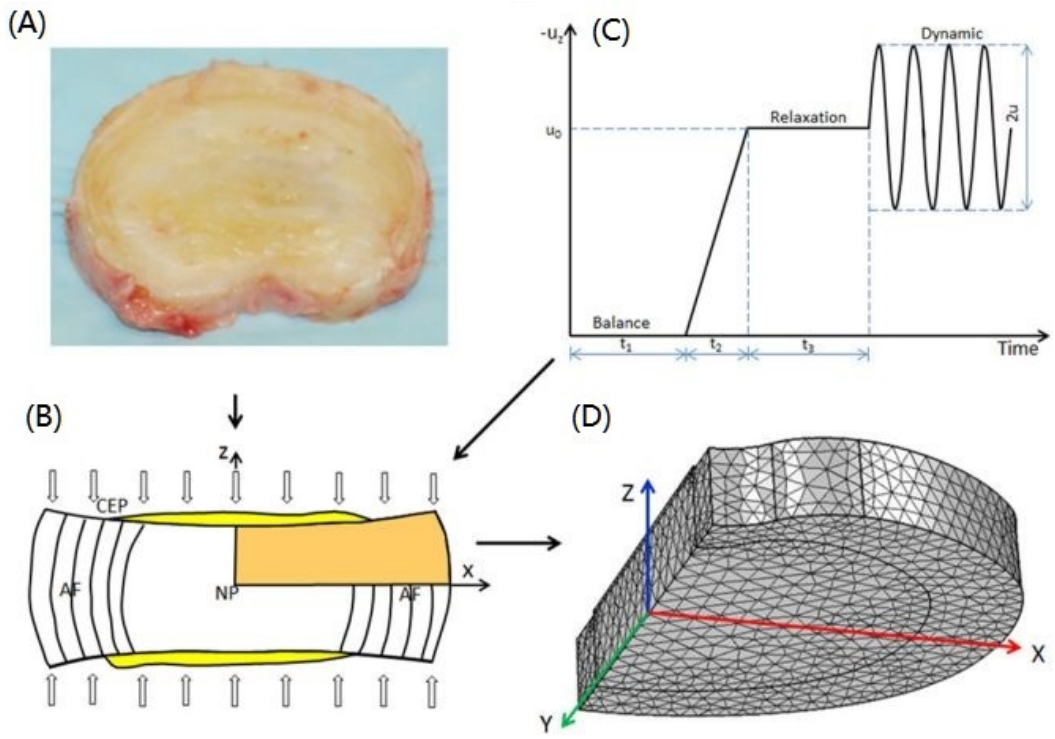

Figure 4. 1: (A) A picture of the human lumbar disc (L2-3, non-degenerated); (B) A schematic of the upper quarter used in this study; (C) the time history of the displacement (u_0) boundary; and (D) mesh of the upper quarter used in the finite element model.

Both non-degenerated and degenerated IVDs were analyzed. The material properties used in the model came from experiments [18, 109-111, 121, 143-146], details were listed in Table 4.1. Boundary and initial conditions were listed in Table 4.2.

For the healthy human disc, the glucose concentration used was 4 mM, and 5 mM, and the oxygen concentration 5.1 KPa and 5.8 KPa at the NP-CEP boundary and the AF periphery, respectively [147]. This nutrition level was defined as the normal nutrition level at disc boundaries. The deprivation of nutrition supply at IVD boundary was simulated by

reduction in nutrition level at the NP-CEP and AF periphery boundaries. The effects of 100%, 75%, 60%, 50%, and 30% of normal nutrition level at both boundaries on cell viability were simulated. In these simulations, both non-degenerated and degenerated IVDs were first equilibrated with normal nutrition boundary and initial conditions as listed in Table 4.2, for 10 days, then followed by a reduction of nutrition level at the boundaries for another 10 days.

Effects of mechanical compressions on cell viability were modeled as the following: the IVD was initially equilibrated with aforementioned initial and boundary conditions for a period of time t_1 (t_1=10 days), followed by a ramp compression [10% axial compression within a period of t_2 (t_2 =1 hour)]. After stress relaxation for a period of t_3 (t_3=5 days) at this new configuration, for dynamic compression cases, axial sinusoidal compression was applied to the tissue for another 5 days, see Figure 4.1C. For static compression cases, displacement was maintained at u_0 for another 5 days after t_3.

In addition, the effect of glucose threshold value (c_{g0}) on cell viability was also investigated with non-degenerated IVDs. Three different threshold values (i.e., c_{g0}=0.7 mM, 0.5 mM, 0.3 mM) were used in the simulations. In these simulations, the disc was equilibrated with 50% of normal nutrition level at both boundaries for 10 days at each threshold value.

Table 4. 1: Material properties of the IVD used in the finite element analysis

IVD Properties	Regions	Non-degenerated	Degenerated
Reference water content $\emptyset_0^w$ [a]	AF	0.75	0.68
	NP	0.86	0.78
	CEP	0.60	0.3
Thickness (mm)	AF	10	9
	NP	10	9
	CEP	0.6	0.6
ρ_0^{cell} (cells/mm^3) [b]	AF	9000	
	NP	4000	
	CEP	15000	
c^F (mol/m^3) [c]	AF	150	125
	NP	250	175
	CEP	90	90
Parameters for diffusivity [d] $\frac{D^\alpha}{D_0^\alpha} = exp[-A\left(\frac{r_\alpha}{\sqrt{k}}\right)^B]$	AF	A=1.29 B=0.372	
	NP	A=1.25 B=0.681	
	CEP	A=1.29 B=0.372	
Parameters for permeability [e] $k = a(\frac{\phi^w}{1-\phi^w})^n$	AF	a=0.00044 nm^2 n=7.193	
	NP	a=0.00339 nm^2 n=3.240	
	CEP[f]	a=0.0248 nm^2 n=2.154	
Elasticity constants [g]	AF	$\lambda = 300\ kPa$ $\mu = 100\ kPa$	$\lambda = 700\ kPa$ $\mu = 150\ kPa$
	NP	$\lambda = 15.6\ kPa$ $\mu = 0.18\ kPa$	$\lambda = 25.8\ kPa$ $\mu = 0.61\ kPa$
	CEP	$\lambda = 100\ kPa$ $\mu = 200\ kPa$	$\lambda = 100\ kPa$ $\mu = 200\ kPa$

[a] Calculated from results in [148, 149].
[b] From [18].
[c] Calculated from results in [104, 149].
[d] From [110].
[e] From [150].
[f] From [104].
[g] From [104, 144, 151, 152].

Table 4. 2: Boundary and initial conditions used in the finite element analysis

<table>
<tr><td colspan="2" rowspan="2">Boundary Conditions</td><td colspan="3">Initial Conditions</td></tr>
<tr><td>NP</td><td>AF</td><td>CEP</td></tr>
<tr><td>AF peripheral</td><td>$c^{glucose} = 5\ mM$
$c^{O_2} = 5.8\ kPa$
$c^{lactate} = 0.9\ mM$
$c^{Na^+} = c^{Cl^-} = 0.15\ M$
$\sigma_{xx} = \sigma_{xz} = \sigma_{xy} = 0$</td><td colspan="3" rowspan="4">$u = 0$
$v = 0$
$w = 0$
$c^{glucose} = 4mM$
$c^{O_2} = 5.1\ kPa$
$c^{lactate} = 0\ mM$
$c^{Na^+} = c^{Cl^-} = 0.15\ M$</td></tr>
<tr><td>CEP top</td><td>$c^{glucose} = 4mM$
$c^{O_2} = 5.1\ kPa$
$c^{lactate} = 0.8\ mM$
$c^{Na^+} = c^{Cl^-} = 0.15\ M$
$u_z = 0$ for no compression
$u_z \neq 0$ for compression
$\sigma_{zx} = \sigma_{zy} = 0$</td></tr>
<tr><td>Mid-plane (z=0)</td><td>$j_z^{water} = j_z^{glucose} = j_z^{O_2} = j_z^{lactate} = j_z^{Na^+} = j_z^{Cl^-} = 0, u_z = 0, \sigma_{zx} = \sigma_{zy} = 0$</td></tr>
<tr><td>Plane (x=0)</td><td>$j_z^{water} = j_z^{glucose} = j_z^{O_2} = j_z^{lactate} = j_z^{Na^+} = j_z^{Cl^-} = 0, u_x = 0, \sigma_{xy} = \sigma_{xz} = 0$</td></tr>
</table>

4.3 Results

Effects of Nutrition Level at IVD Boundary on Cell Viability

Cell density decreased substantially with reduction of nutrition level at disc boundaries in non-degenerated discs (Fig. 4.2). Cell death was initiated primarily near the NP-AF interface on the mid-plane (Fig. 4.2B). The NP region was more affected, compared with the AF region (Fig. 4.2C).

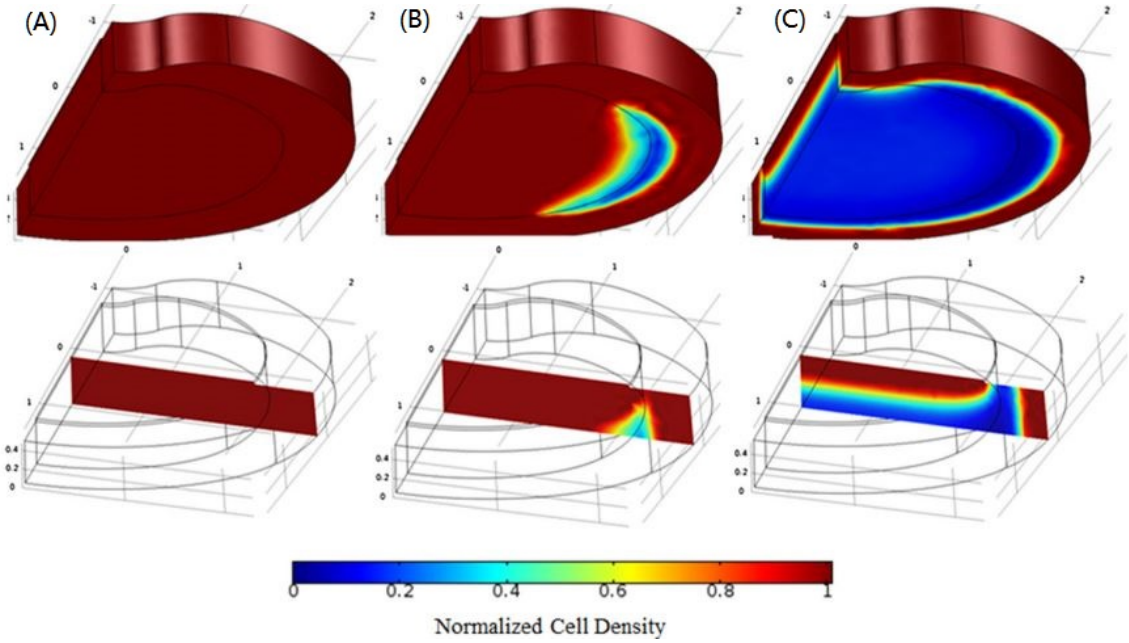

Figure 4. 2: Effects of nutrition level reduction at IVD boundaries on cell density change in a non-degenerated after the nutrition level decreased for 10 days. (A) Normal nutrition level (i.e., 100%); (B) 50% of normal level; (C) 30% of normal level.

This effect of nutrition level reduction on cell density was more pronounced in degenerated IVDs. After the end of 10-day of nutrition reduction (50%), the minimum glucose concentration in the degenerated IVD was slightly lower than that in non-degenerated IVDs (Fig. 4.3A), but the difference in minimum cell density between the degenerated and non-degenerated IVDs was significant (Fig. 4.3B). The minimum cell density decreased monotonically with time even though the minimum glucose concentration recovered in IVDs (Fig. 4.3).

Effects of Dynamic Compression on Cell Viability

Dynamic compression with different combinations of magnitude u (u=10% ± 2.5%, ± 5%) and frequency f (f=1, 10, 20 cycle/day) were simulated. It was found that dynamic compressions did not affect the cell viability in non-degenerated IVDs, compared with that in the static cases, because the glucose levels in the non-degenerated IVDs did not fall below the threshold value (i.e., 0.5 mM) for cell survival. The cell density in the degenerated disc with dynamic compression was higher compared with that with static compression (Fig. 4.4). For example, the minimum value of normalized cell density was 0.37 in disc with static compression (Fig. 4.4A), compared to the value of 0.62 in the same disc with dynamic compression (10% ± 2.5%, 20 cycle/day), see Figure 4.4D. The degree of improvement in cell viability in degenerated depended both on loading frequency and amplitude.

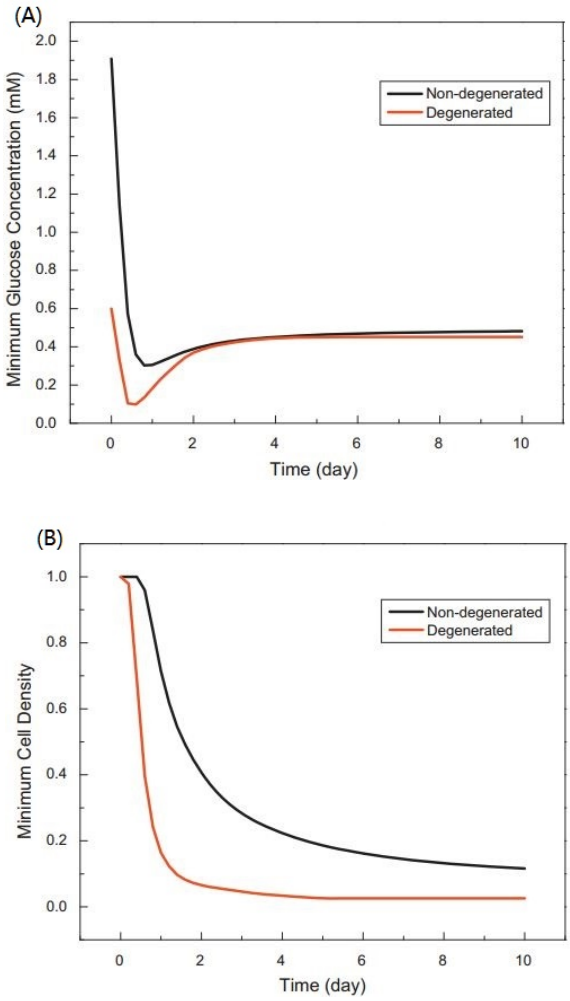

Figure 4. 3: Effect of degeneration on cell density and glucose concentration in the IVD with 50% of normal nutrition level at the end of a 10-day period. (A) Minimum glucose concentration and (B) minimum cell density.

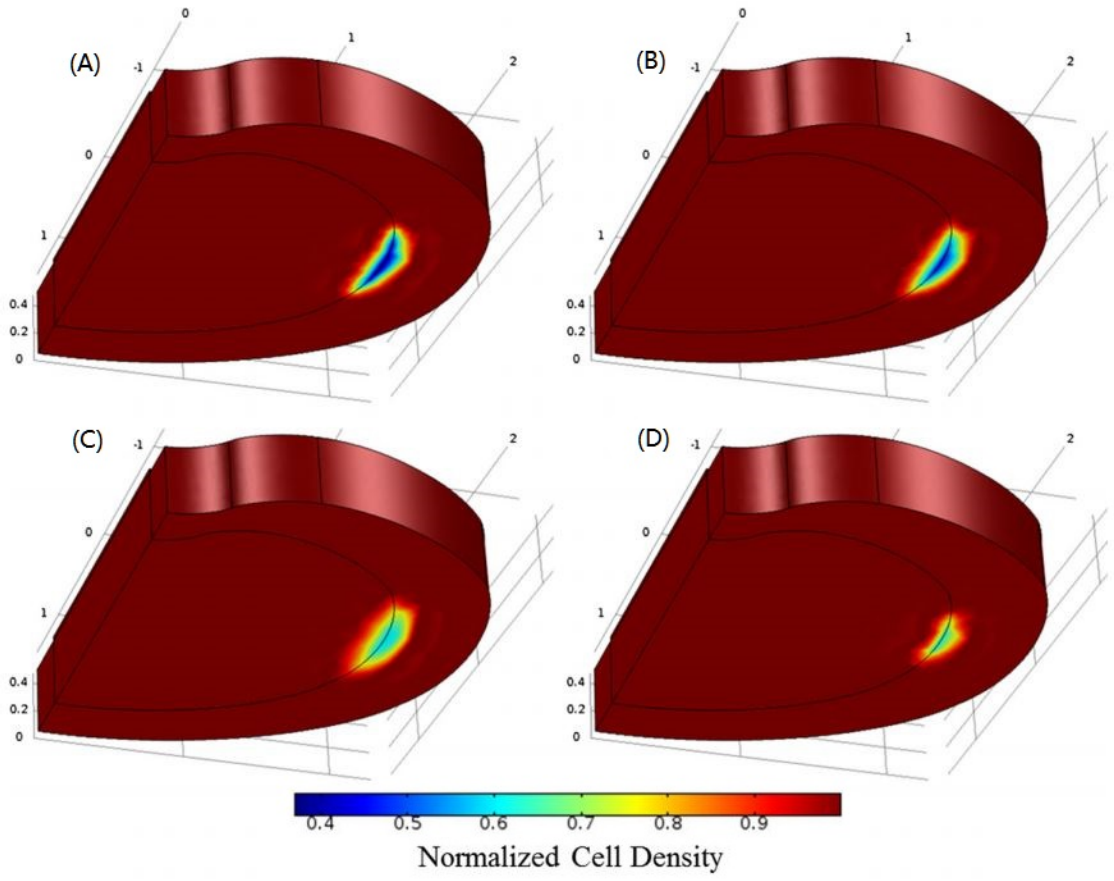

Figure 4. 4: Effects of dynamic compression on cell density distribution in degenerated IVDs: (A) 10% static compression; (B) dynamic compression (10% ± 2.5%, 1 cycle/day); (C) dynamic compression (10% ± 5%, 1 cycle/day); and (D) dynamic compression (10% ± 2.5%, 20 cycles/day).

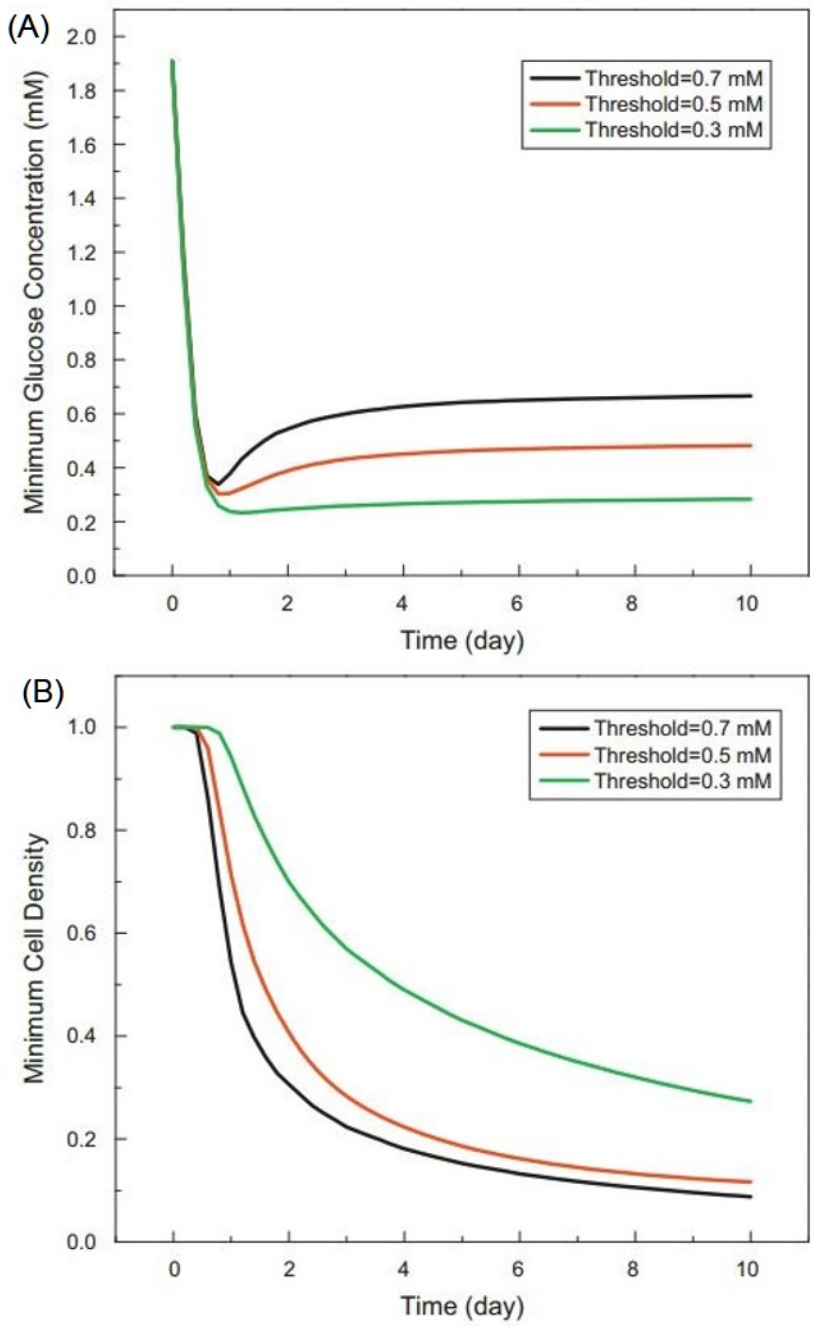

Figure 4. 5: The change of (A) minimum glucose concentration and (B) minimum cell density (both are normalized) in the non-degenerated IVDs with 50% of normal nutrition level at IVD boundary, with variations of threshold values.

4.4 Discussion

In this study, the effects of reduction of nutrition levels at disc boundaries, disc degeneration, and dynamic compression on cell viability in IVDs in a time-dependent manner were investigated. To this end, a novel constitutive model for cell viability was developed based on the experimental data [20, 35, 120], and incorporated into the mechano-electrochemical mixture theory to regulate the cell density.

This new constitutive model can more realistically predict cell viability in the IVD, without the peculiar phenomenon of resurrection of dead cells when glucose level recovers (Figs. 4.3 and 4.5). For the case where a degenerated IVD is statically compressed by 10% [104], our current model predicts that at steady state, the minimum glucose concentration in disc is 0.495 mM and the minimum cell density is 0, compared to the predicted values of 0.292 mM for minimum glucose concentration and 0.309 for normalized minimum cell density in the same disc using the previous model for cell viability [104, 105]. In addition, our calculation shows that the affected volume (defined as the domain where more than 5% of cells die) is only 2.67% of the total volume (NP, AF, and CEP) of IVD predicted by our model, compared to the value of 34.19% predicted by the previous cell viability model (in which resurrection od dead cells would occur). This is because in the previous model for cell viability, the cell density was assumed to be linearly related to the glucose concentration (in the range of 0.2 mM to 0.5 mM) [105]. However, in reality, when the glucose concentration is lower than the threshold value (i.e., 0.5 mM), the cell density would continue to decline until the glucose concentration recovers to the threshold value, or cell density would reach to zero. Our current model can correctly predict this phenomenon (Figs. 4.3 and 4.5). These comparisons also indicate that predicted results

are sensitive to the choice of the constitutive models for cell viability, thus it is important to have a more realistic constitutive model for cell viability in order to investigate the mechanobiology of IVD numerically.

These results indicate that perturbations in nutrition supply at boundaries because of factors like aging, blood aneurysms, and/or smoking [124-126] could all adversely influence the activities and viability of disc cells, and resultantly, disc function. Our results demonstrate that as the nutrition level at boundaries falls below ~60% of normal value, cell death begins to initiate near the NP-AF interface on the mid-plane and spread toward the inner NP region. When the nutrition level on the disc edge drops below~ 30% of normal level, most of the cells at the mid-plane of the NP region will die in non-degenerated discs (Fig. 4.2). For degenerated case, the drop in nutrition level at the disc boundary caused larger magnitudes of cell death (compared to that in the non-degenerated case). This may be because reduced diffusivity and permeability due to that lower fluid content decreases the nutrients transport through the CEP to NP cells, which consequently reduces the nutrients distribution around the cells.

The finding that dynamic compression improves cell viability is mainly due to the fact that dynamic compressions increase the diffusivities of nutrients, and improve the concentration of cell nutrition, which aid in maintain cell metabolism and viability. This will consequently promote synthesis and maintenance of the matrix, which will in turn prevent or retard the degeneration of the IVD. Our findings are in agreement with reports from the literature [127-129, 132, 153]. Since dynamic compression is a more typical mechanical loading regime for the human discs (as compared with static compressions),

our results under dynamic compressions are indicative of real time compression effects on nutrition transport and cell viability in the human discs.

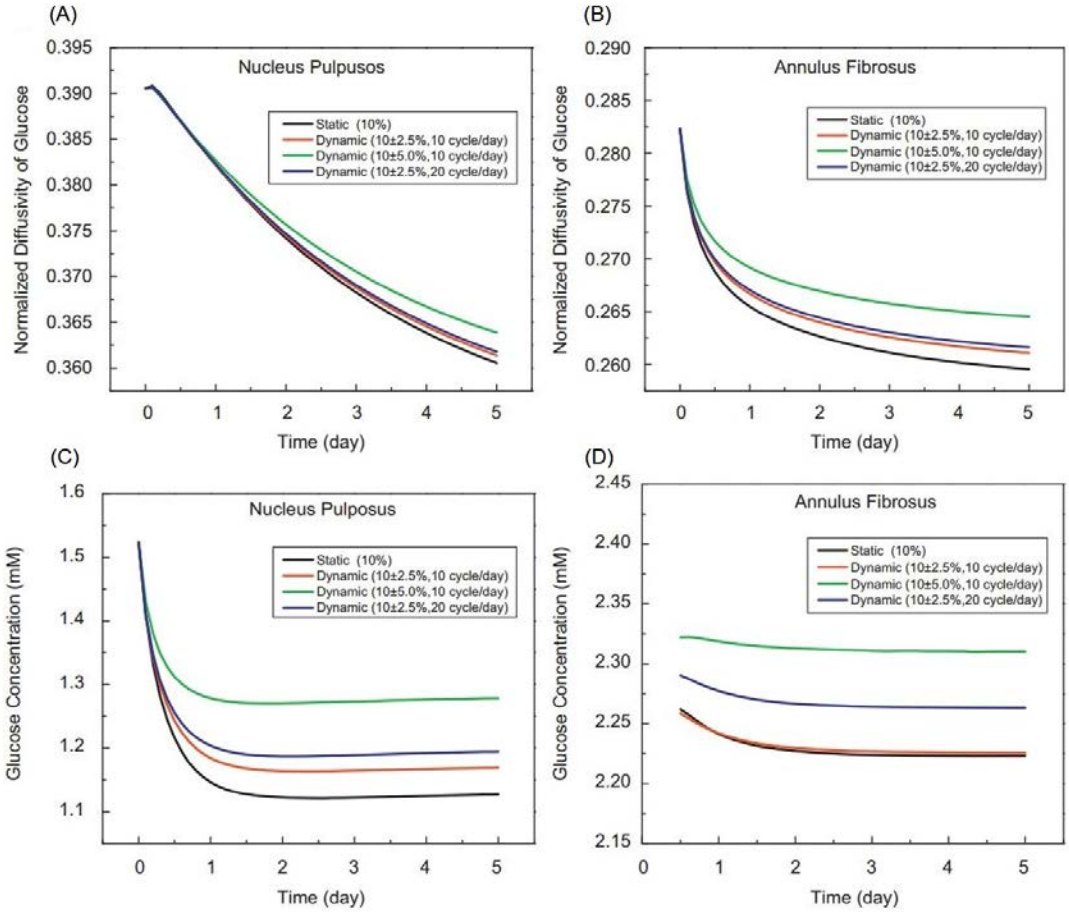

Figure 4. 6: Effect of dynamic compression on: glucose diffusivity change in (A) NP and (B) AF; and on glucose concentration change in (C) NP and (D) AF, in the degenerated IVDs.

Our findings on the location (i.e., near NP-AF interface) of cell death initiation differs from the previous study by Shirazi-Adl et al. (2010) [105], which found that the initiation of cell death was located in the center of the NP region. This may be due to different material

properties and different cell density models used. However, our finding is in agreement with experimental results reported by Walsh and Lotz [50], which found that cells at the NP-AF interface (i.e., outer NP cells, inner and middle AF cells) were more affected than the other parts under dynamic loading.

One limitation of this study was that only glucose has been considered in our cell viability model. Even though it has been reported that inclusion of pH did not significantly influence cell viability (compared with the consideration of glucose alone in the cell viability model [105]), future works are necessary to explicitly incorporate pH factor into our cell viability model to more accurately investigate and predict the cell viabilities and functions in the IVD. Another limitation was that the anisotropic properties of the AF were not taken into consideration in this study. This will be included in our future studies.

In summary, this work numerically analyzed the effects of reduction of nutrition levels at disc boundaries, disc degeneration, and dynamic compression on cell viability in a realistic, three-dimensional disc in a time-dependent manner. A new constitutive model for cell viability has been developed based on experimental data. This model is capable of predicting cell density distributions as well as both the region and time at which cells start to die within the disc under different biological and physical conditions. The present numerical simulation is a valuable supplement to experimental studies of cell viability and transport of nutrients in avascular, hydrated, cartilaginous tissues under nutrition deprivation, disc degeneration, and mechanical loading conditions.

Chapter 5 Simulation of Disc Degeneration Progression

5.1 Introductory Remarks

During disc degeneration, the disc undergoes a cascade of changes in biological, chemical, electrical, and mechanical events, leading to the loss of cellularity and compromised cellular activities, reduction of proteoglycan (PG) and water contents, decrease in disc volume, and resultantly failure in tissue structure and functions [13, 28, 149, 154, 155].

The disc cells play a vital role in maintaining the IVD structure and function [65]. The cells live in a complicated mechano-electrochemical environment, and their activities and viability are regulated by mechanical signals (e.g., deformation, stress, fluid flow), electrical signals (e.g., streaming potential, current), and biochemical signals (e.g., osmotic pressure, glucose levels, pH, growth factors, etc.) within the environment [26, 156]. The cells synthesize both the anabolic components for matrix maintenance and the catabolic molecules responsible for matrix breakdown [119]. In the healthy condition, the balance between anabolic and catabolic activities is maintained by the cells. Disruption of this balance would result in loss of matrix component and damage of tissue structure and consequently failure in function.

The mechanical behaviors of the disc have been extensively studied with experiments (see reviews [157-160]). These studies have significantly advanced the understanding of the biomechanics of human discs. Based on these data, a number of numerical models have been developed for the study of the mechanical behaviors of the discs (see a recent review [74]).

Cell viability was first included into the transport model for disc by Shirazi-Adl et al.[105], the influences of nutrient environment on cell viability was investigated numerically with this model, however, this model did not include the coupled mechano-electrochemical effects on the transport of the nutrients within the disc. Recently, we developed a new constitutive model for disc viability and incorporated it into the tri-phasic model [161]. Using this model, we studied the effects of mechanical compression and disc degeneration on the cell viability within the coupled mechano-electrochemical environment.

However, there seems no numerical model that is able to describe the continuous temporal and spatial changes of the tissue composition and mechanical behavior during disc degenerative progression. The knowledge of quantitative changes in these signals in the disc with degenerative progression is crucial for understanding the mechanobiology in the disc as well as for developing a new diagnostic method for detecting disc degeneration. Therefore, the objective of this chapter is to numerically analyze and simulate the biological, chemical, electrical, and mechanical events within the intervertebral disc (IVD) during tissue degeneration for the understanding the pathophysiology of IVD.

5.2 Finite Element Methods

Geometry and Mesh

The disc was considered as an inhomogeneous material with two distinct regions, namely, NP and AF (Fig. 5.1). In this study, the disc was attached to the vertebra to restrain the relative motion of the solid phase on the disc-vertebra interface, see Fig. 5.1B. Since the vertebra is about 10 times stiffer than the disc, the effect of the vertebra height on disc deformation was believed to be negligible. Thus, only a small part (5mm height) of the

vertebra was included in the model to reduce the computational cost. The vertebra was modeled as a single-phase solid with linear elastic mechanical properties.

Due to symmetry, only the upper right quarter of the disc was modeled. The mesh consisted of 7888 quadratic Lagrange hexahedral elements. The finite element model of the disc was developed with COMSOL software (COMSOL 4.3b, COMSOL, Inc., MA) based on the method developed by Sun et al. [142]. The configuration of the disc at mature, healthy condition before degeneration was chosen as the reference configuration, and the total stress tensor in this study was defined as the difference in stress between current configuration and reference configuration. The boundary conditions were similar to the study in Chapter 4, except for the load boundary condition in the axial direction. The axial load was assumed to be constant during disc degeneration.

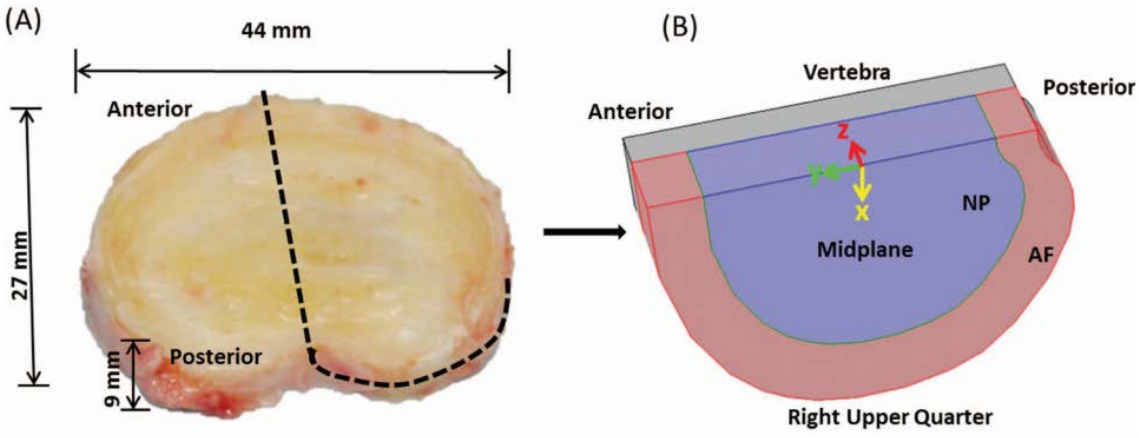

Figure 5. 1: (A) Geometry and size of the disc from a human lumbar spine (L2-3, non-degenerated, vertebra is not shown). (B) Schematic of the right upper quarter of the disc and the vertebra used in the finite element model.

Material Properties

The distribution of mechanical properties in the disc was inhomogeneous, and values were assigned on the basis of experimental results [162-164]. That is, the 2 Lame constants of elasticity (i.e., λ and μ) for each region were: λ=0.391 MPa in the NP, it linearly increased from 0.391 to 1.009 MPa from innermost to outer most AF; μ=0.009 MPa in the NP, and it linearly increased from 0.009 to 0.291 MPa from innermost to outer most AF. The mechanical property of the vertebra was set to λ=86.5 MPa, and μ=57.5 MPa, according to the experimental results [165].

The cell density in the healthy disc before degeneration was set to be 4000 cells/mm^3 in the NP and 9000 cells/mm^3 in the AF [18]. The fixed charge density and water content distributions in the healthy disc before degeneration were taken from measurement from a 27 year-old, healthy lumbar disc [15]: the fixed charge density was 0.343 M in the NP, and it linearly decreased from 0.343 to 0.163 M from the innermost to the outermost AF; the water content (volume fraction) was 0.85 in the NP, and it linearly decreased from 0.85 to 0.7 from the innermost to the outermost AF.

The GAG degradation rate (λ_2) is related to the half-life (τ) of GAG turnover, by $\lambda_2 = \ln 2 / \tau$, where the value of τ is equal to 11 years for IVD tissues [116]. Q^{GAG} was assumed to be zero in mature, healthy disc (before the process of disc degeneration starts). Thus, the value of GAG synthesis rate per cell λ_1 could be estimated by the following relationship: $\lambda_1 = \lambda_2 c_0^{GAG} / \rho_0^{cell}$, where c_0^{GAG} and ρ_0^{cell} were the GAG content and cell

density at the healthy state within the mature, healthy disc before degeneration. The half-life of the PG turnover was set to be 11 years [116].

The loss of PG content within the disc during the progression of disc degeneration may change the amount of solid mass. However, to what extent the solid mass may change is not clear and the related data is limited in the literature. Since the disc degeneration is a very slow process for most cases, in this study we assumed that the rate of change in solid mass was zero.

Boundary Conditions

The top surface (z=0.95 cm) of the vertebra was set to move freely in the axial direction while constrained in the horizontal directions (i.e., the displacements were zero in the horizontal directions). The difference in the axial stress (between current and that at healthy state) was set to be zero on this surface. There was no relative motion for solid phase at the disc-vertebra interface (z=0.45 cm). The lateral surfaces of AF and vertebra were set to be traction free. The mid-sagittal plane (x=0) and the mix-axial plane (z=0) were assumed to be symmetric plane. An impermeable boundary condition was used at the interface between AF and the vertebra, while free draining boundary condition was used at the interface between NP and the vertebra as well as at the AF periphery.

The concentrations of nutrients and metabolic wastes in the blood were reported to be: 5.6 mM for glucose concentration, 6.4 kPa for oxygen tension, and 1mM for lactate concentration [147, 166, 167]. The effect of cartilage endplate (CEP) on nutrition supply was considered by adjusting the boundary conditions at the interface between NP and CEP [25]. Values for glucose concentration, oxygen tension, and lactate concentration at the

CEP-NP boundary were 3.2 mM, 3.6 kPa, and 2.15 mM on the NP surface adjacent to the endplate; respectively; and at the AF periphery boundary were 5 mM, 5.8 kPa, and 0.9 mM, respectively [25, 147, 168]. These values were used as the reference values in this study.

The effect of the thin layer CEP on water flow in the disc in the current case was not believed to be significant because the degenerative process is very slow (no fluid pressurization effect). For other cases (such as a disc under dynamic loading), it is important to include the CEP in the model [161].

Simulation of Disc Degeneration

The disc degeneration was simulated by the reduction of the nutrition supply at the disc boundaries. In order to calculate the initial conditions for glucose, oxygen, lactate, ions, and other signals in the healthy disc before degeneration, the disc was initially equilibrated under the reference values at boundary (i.e., glucose, oxygen, and lactate concentrations were 3.2 mM, 3.6 kPa, and 2.15 mM on the NP surface adjacent to the endplate, and were 5 mM, 5.8 kPa, 0.9 mM on the AF periphery). The equilibrium distributions of glucose, oxygen, lactate, and other signals in the healthy disc with the reference values were calculated and used as the initial condition for the following simulations.

For the degeneration induction, the glucose and oxygen concentrations at disc boundaries were decreased linearly to a certain level in 3 days. Cases with different rates of nutrition reduction were also investigated (see Discussion). The beginning of the glucose and oxygen concentrations decrease was marked as the start point of the degeneration process (t=0).

The case in which glucose concentration was 1 mM at NP-vertebra interface and 1.5 mM at AF periphery, and oxygen tension was 1.28 kPa at the NP-vertebra interface and 1.74 kPa at AF periphery are presented.

5.3 Results

Cell Density and Glucose Concentration Change with Disc Degeneration

The cell density and glucose concentration distribution with disc degeneration are shown in Fig. 5.2. At this nutrition level at boundary, cell death started from the NP-AF interface in the lateral direction (Fig. 5.2A), where the lowest glucose concentration located (Fig. 5.2B). The cell death then extended toward the NP center, where glucose concentration was lower than the threshold value for cell survival (i.e., 0.5 mM [20]), see Fig. 5.2B. The cell density reached a steady state (defined as its relative change been less than 0.005%/day) in about 30 days (Fig. 5.2A and Fig. 5.3). The glucose concentration was seen initially decreased, then followed by a recovery in the initially decreased regions (Fig. 5.2B). The glucose reached new equilibrium in 40 days (the relative change of glucose concentration is less than 0.005%/day).

The PG content (estimated by GAG content) distribution with disc degeneration is shown in Fig. 5.2C. A decrease in PG content began to take place around 100 days after the glucose level was decreased, starting from the mid-plane near the NP-AF interface in the lateral direction and expanding toward the NP center. The loss of PG content was observed in the NP region under lowered nutrition supply condition. The averaged PG content change (percentage of current value to the value at healthy state) averaged over the whole disc is shown in Fig. 5.3. It was found that the PG content decreased exponentially in time,

and reached a steady state (defined as its relative change being <0.005%/year) after 55 years of degeneration.

Degenerative Changes in Water Content

The variation of water content distribution with the progression of disc degeneration is presented in Fig. 5.2D. The water content decreased in the NP and inner to middle AF regions, while it did not change significantly in the outer AF regions (Fig. 5.7). Variation of spatial distributions of water content followed a similar pattern to the changes of PG distribution. However, in the temporal scale, it lagged behind the PG content change (Fig. 5.2D and Fig. 5.3). The decrease of water content started after 300 days of degeneration. The relative water content change (percentage of current value to the value at healthy state) averaged over the whole disc is shown in Fig. 5.3. There was an 8.91% decrease in water content after 55 years. The disc volume decreased with the progression of the disc degeneration (Fig. 5.3). After 55 years of degeneration, there was a 9.08% reduction in the disc volume. Simulated distributions of GAG and water contents in the disc after 27 years (around 54 years of age) are consistent with the experimental results of human discs (averaged 54 years) reported by Iatridis et al. [155], see Fig. 5.4.

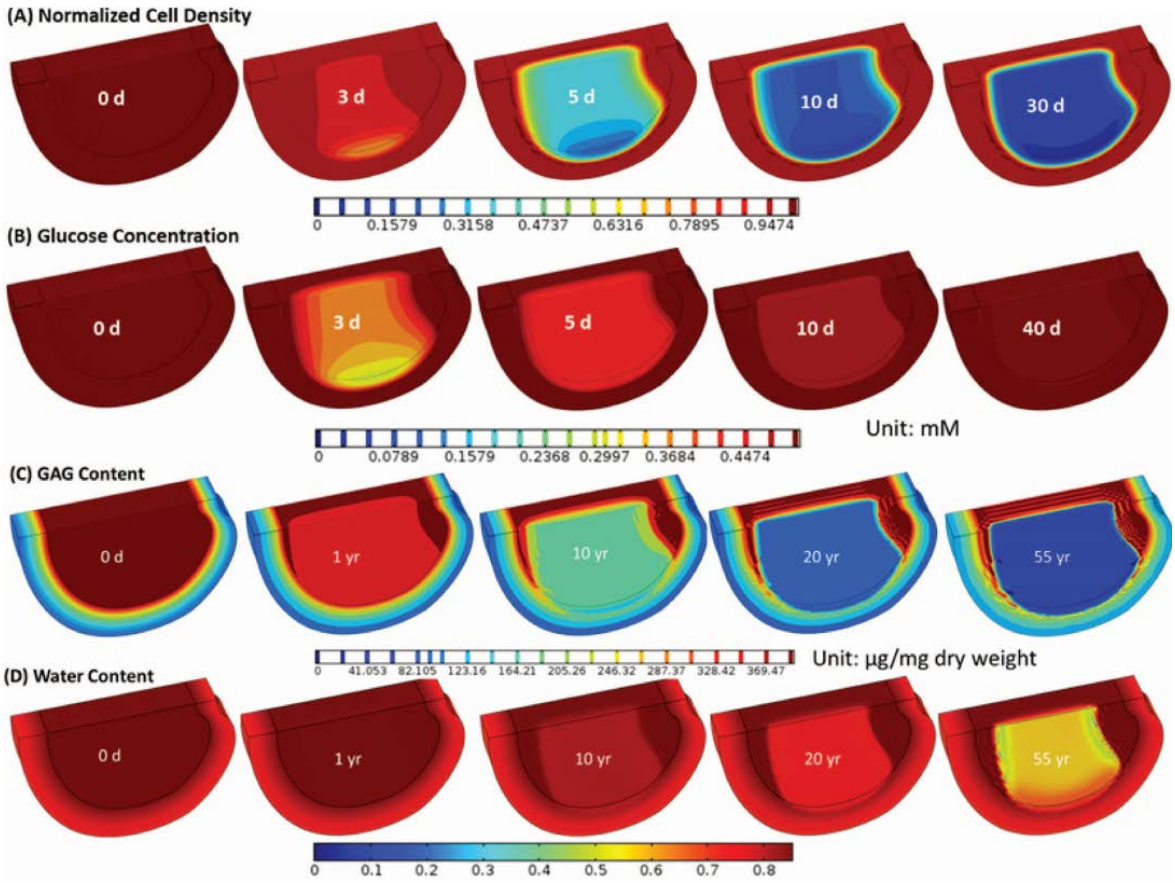

Figure 5. 2: (A) Normalized Cell density, (B) Glucose concentration (unit: mM), (C) GAG content (unit: µg/mg dry weight), and (D) water content (volume fraction) change with disc degeneration progression.

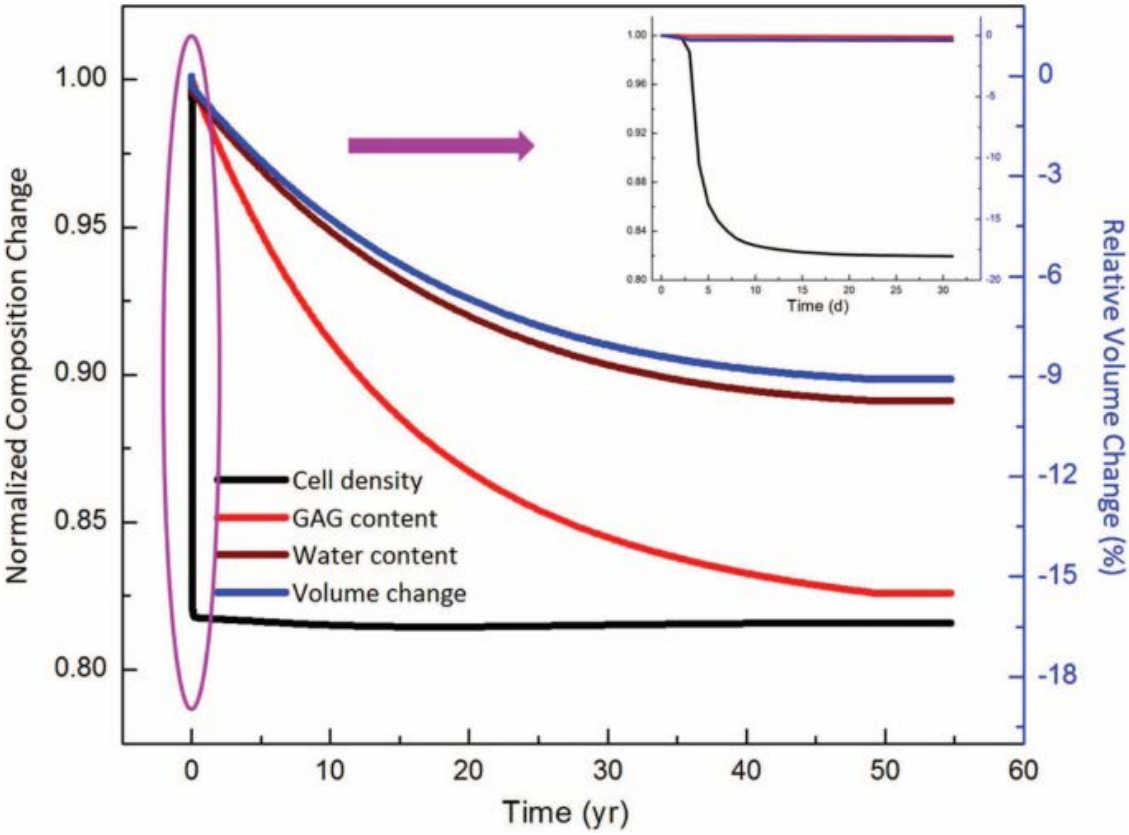

Figure 5. 3: The temporal change of normalized cell density, GAG concentration and water content averaged on the whole disc region. GAG: glycosaminoglycan.

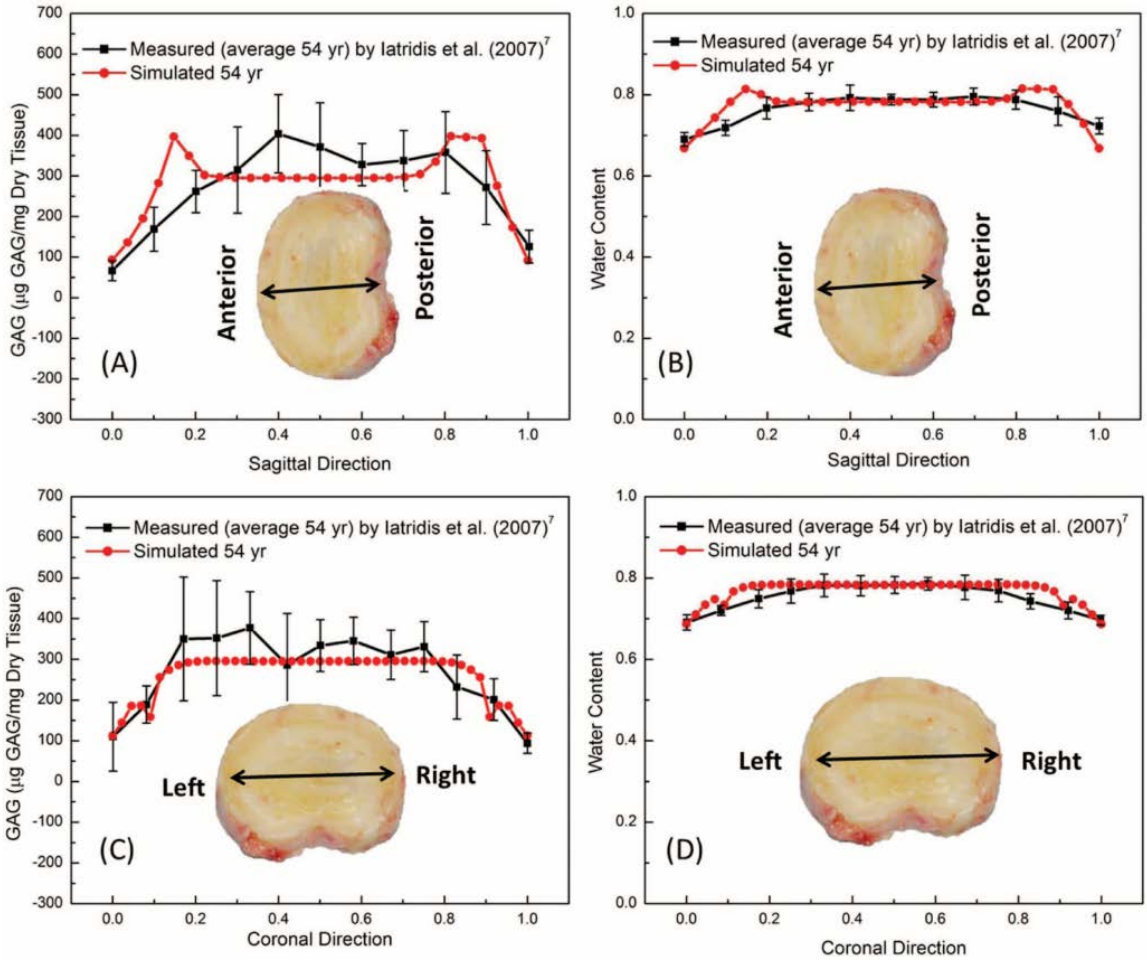

Figure 5. 4: Comparisons between our predicted results and the experimental results from the study by Iatridis et al.[155] of the 54-year-old human lumbar disc: (A) GAG content and (B) water content in the sagittal direction; and (C) GAG content and (D) water content in the coronal direction. GAG: glycosaminoglycan

Fixed Charge Density

In the healthy state, the fixed charge density distribution in the disc is shown in Fig. 5.5A ('before degeneration'). With the progression of disc degeneration, the fixed charge density decreased significantly in the NP and in the inner and middle AF regions (Fig. 5.5),

with the inner and middle AF regions near the mid-axial plane (z=0) experienced the most severe loss of fixed charged density (Fig. 5.5).

Fluid Pressure

Changes in fluid pressure and its distributions with disc degenerative progression were similar to those for fixed charge density change (Fig. 5.6). The NP and the inner to middle AF regions experienced a significant decrease in the fluid pressure, with the largest decrease shown in the inner to middle AF regions (Fig. 5.6).

Von Mises Stress

As stated previously in the Methods, all the stresses reported in this study were the difference between values at current state and that at healthy state. It was shown that the Von Mises stress increased with the degenerative progression (Fig. 5.8). The increases in the outer AF region were seen larger than that in the rest of the regions (Fig. 5.8).

Deformation

The disc volume decreased by 7.2%, 11.7%, and 15.4% after 10, 20, and 40 years of degeneration, respectively (Fig. 5.9). The disc height decreased with the degenerative progression, with 6.0%, 9.9%, and 13.0% after 10, 20, and 40 years of degeneration, respectively. The disc was also shown to shrink radially inward toward the center (Fig. 5.9).

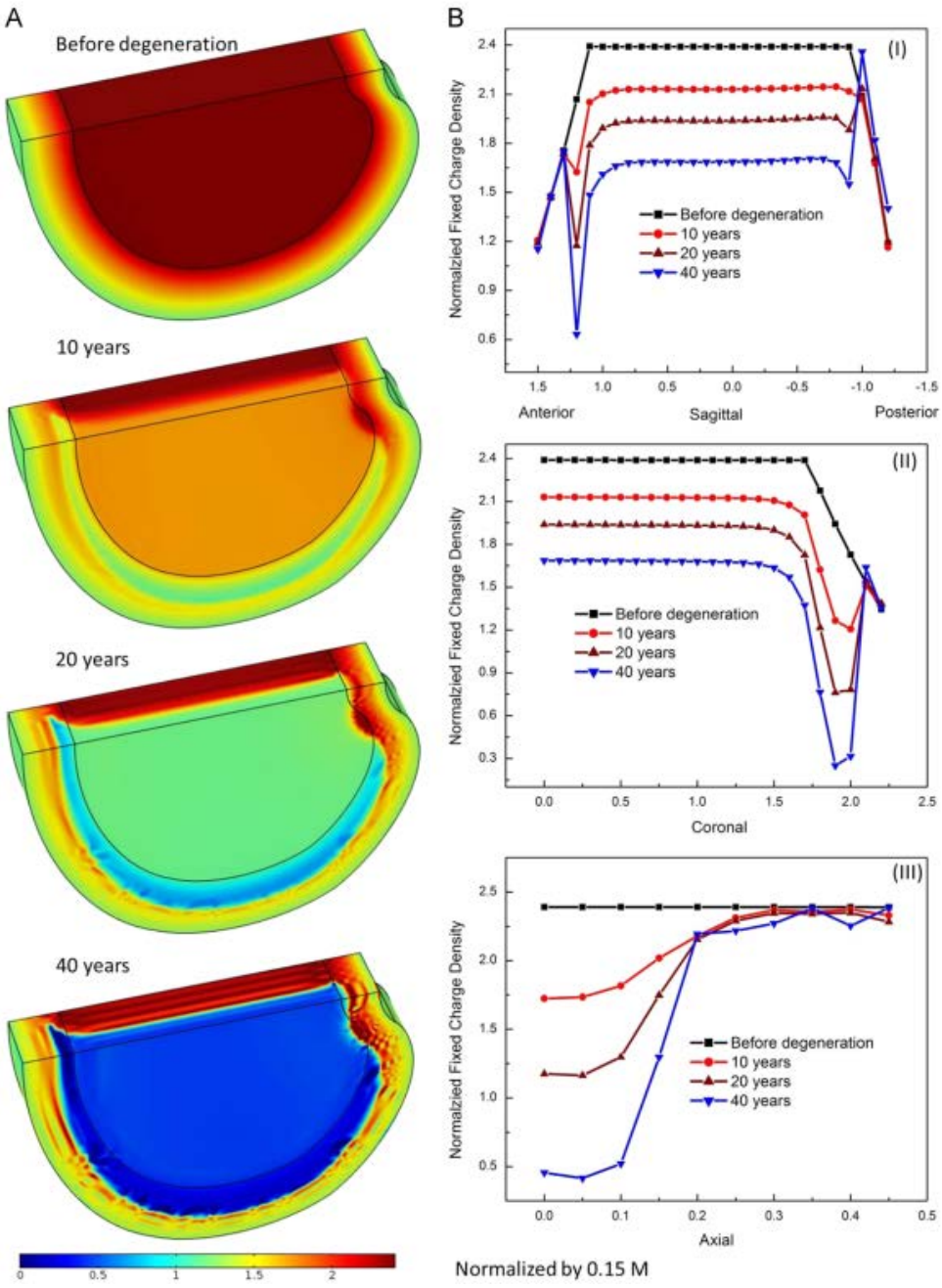

Figure 5. 5: (A) 3D distributions of fixed charge density (normalized by 0.15 M) within the disc before degeneration, after 10, 20 and 40 years of degeneration. (B) Variations of fixed charge density (normalized by 0.15 M) with the progression of disc degeneration: (I) in the sagittal direction (averaged over the disc thickness) at x=0; (II) in the coronal direction (averaged over the disc thickness) at y=0; and (III) in the axial direction (averaged over the horizontal plane in the NP).

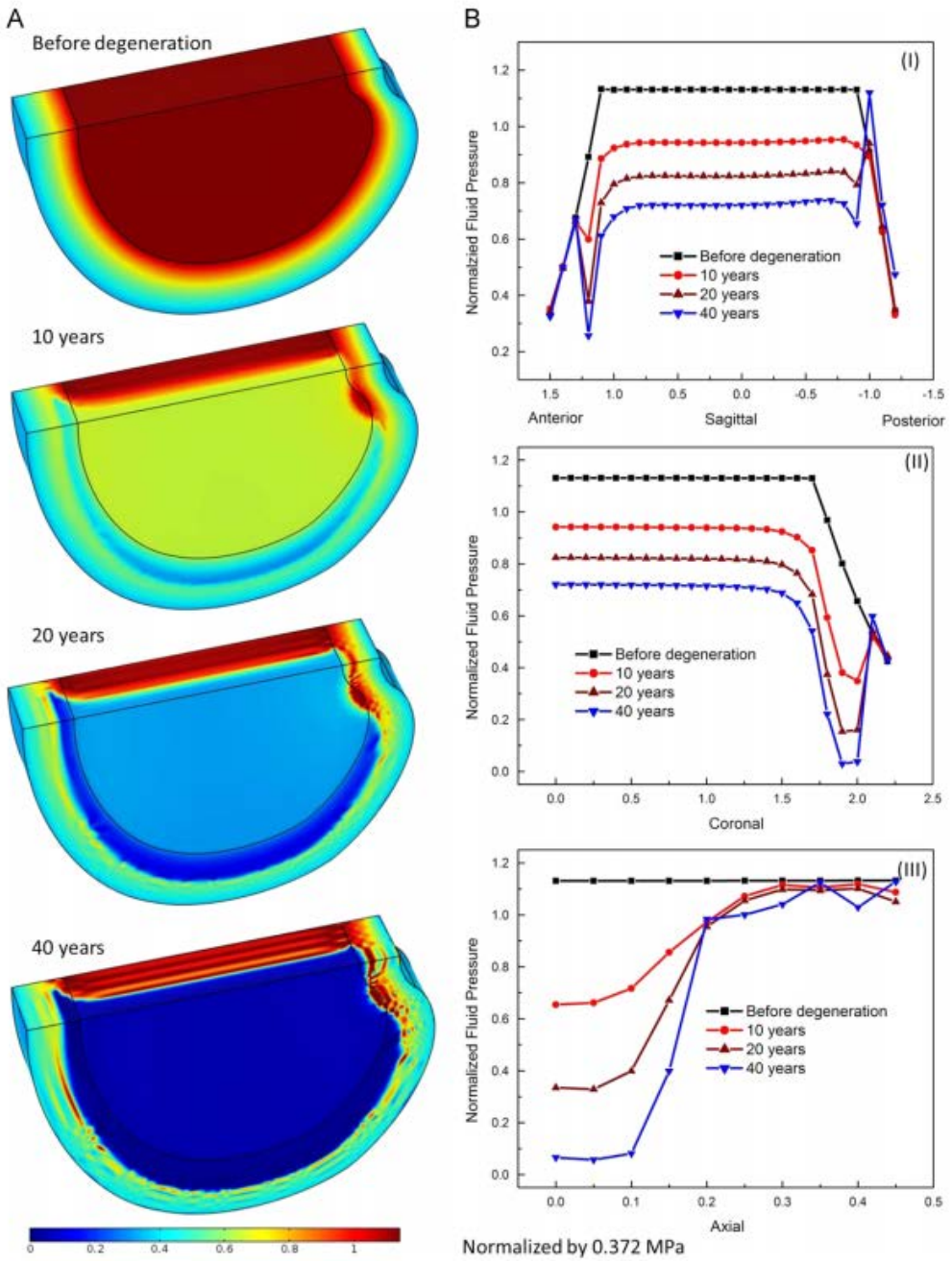

Figure 5. 6: (A) 3D distribution of fluid pressure (normalized by 0.372 MPa) before degeneration, after degeneration for 10, 20, and 40 years within the disc. (B) The variations of fluid pressure (normalized by 0.372 MPa) with the progression of disc degeneration: (I) in the sagittal direction (averaged over the disc thickness) at x=0; (II) in the coronal direction (averaged over disc thickness) at y=0; and (III) in the axial direction (averaged over the x-y plane in the NP).

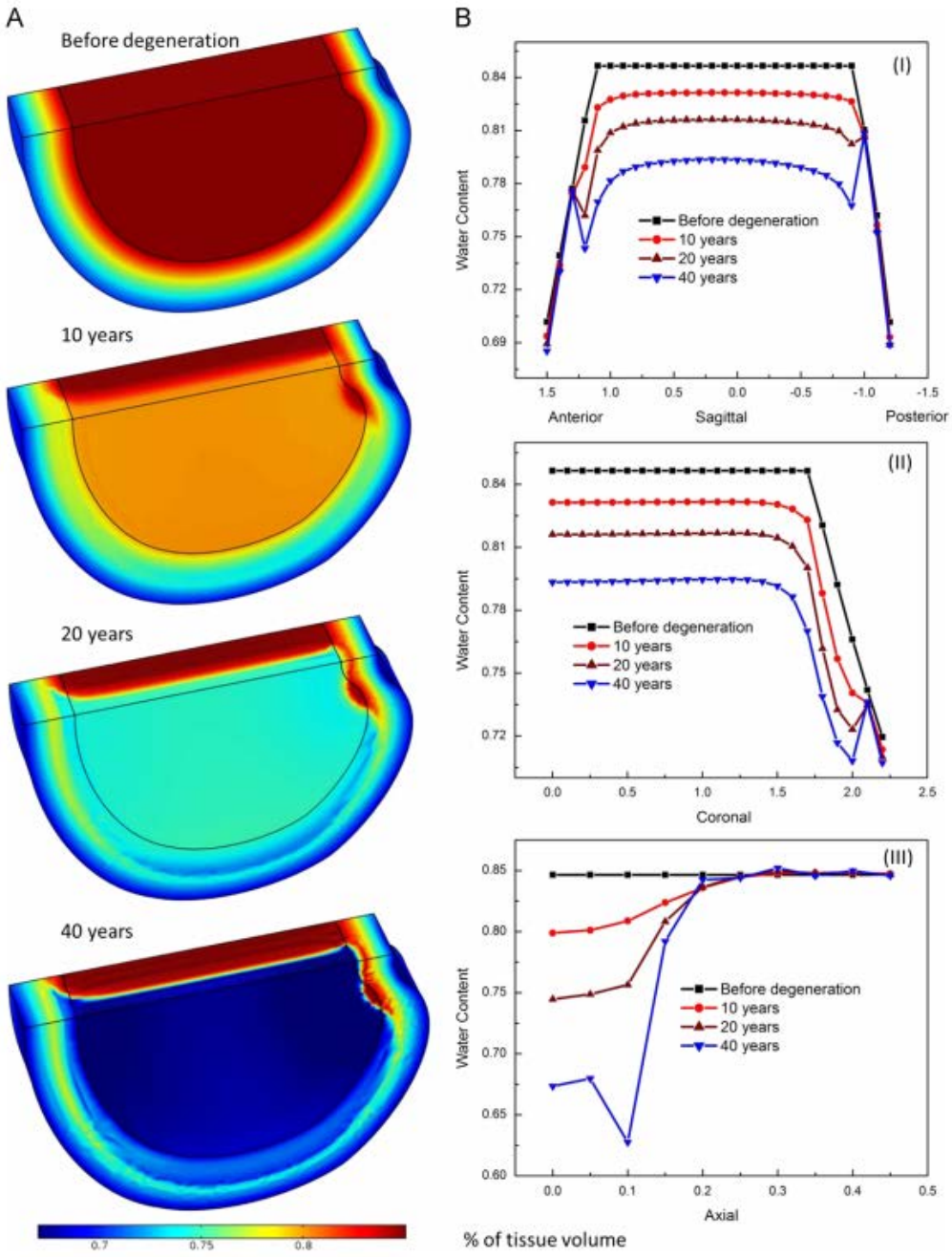

Figure 5. 7: (A) 3D distributions of water content (volume fraction) within the disc before degeneration and after 10, 20, 40 years of degeneration. (B) The variations of water content (volume fraction) with the progression of degeneration: (I) in the sagittal direction (averaged over the disc thickness) at x=0; (II) in the coronal direction (averaged over the disc thickness) at y=0; and (III) in the axial direction (averaged over the x-y plane in the NP).

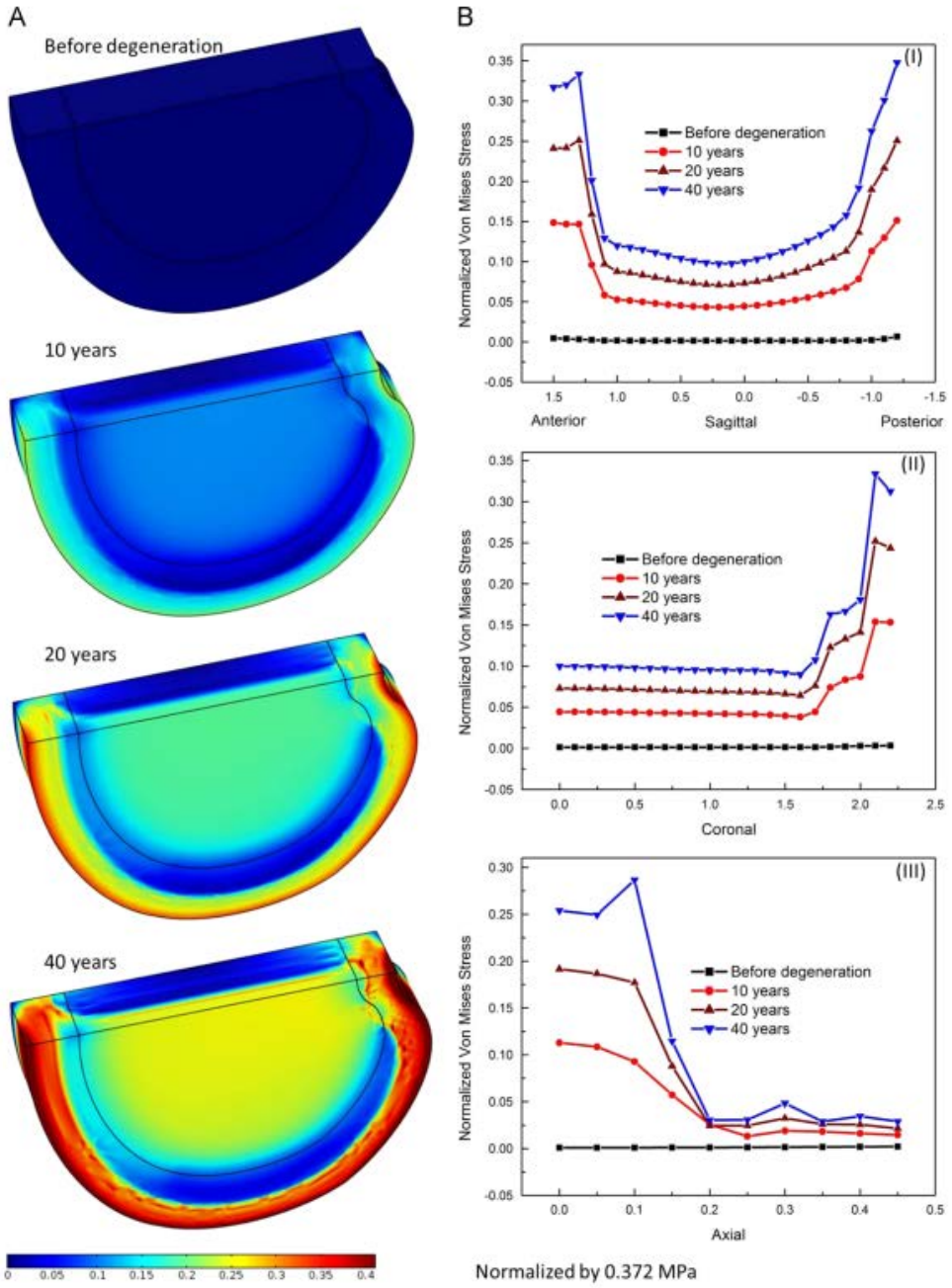

Figure 5. 8: (A) 3D distributions of Von Mises stress within the disc (normalized by 0.372 MPa) before degeneration and after degeneration for 10, 20, and 40 years. (B) Variation of Von Mises stress (normalized by 0.372 MPa) with the progression of disc degeneration: (I) in the sagittal direction (averaged over the disc thickness) at x=0; (II) in the coronal direction (averaged over the disc thickness) at y=0; and (III) in the axial direction (averaged over the x-y plane in the NP).

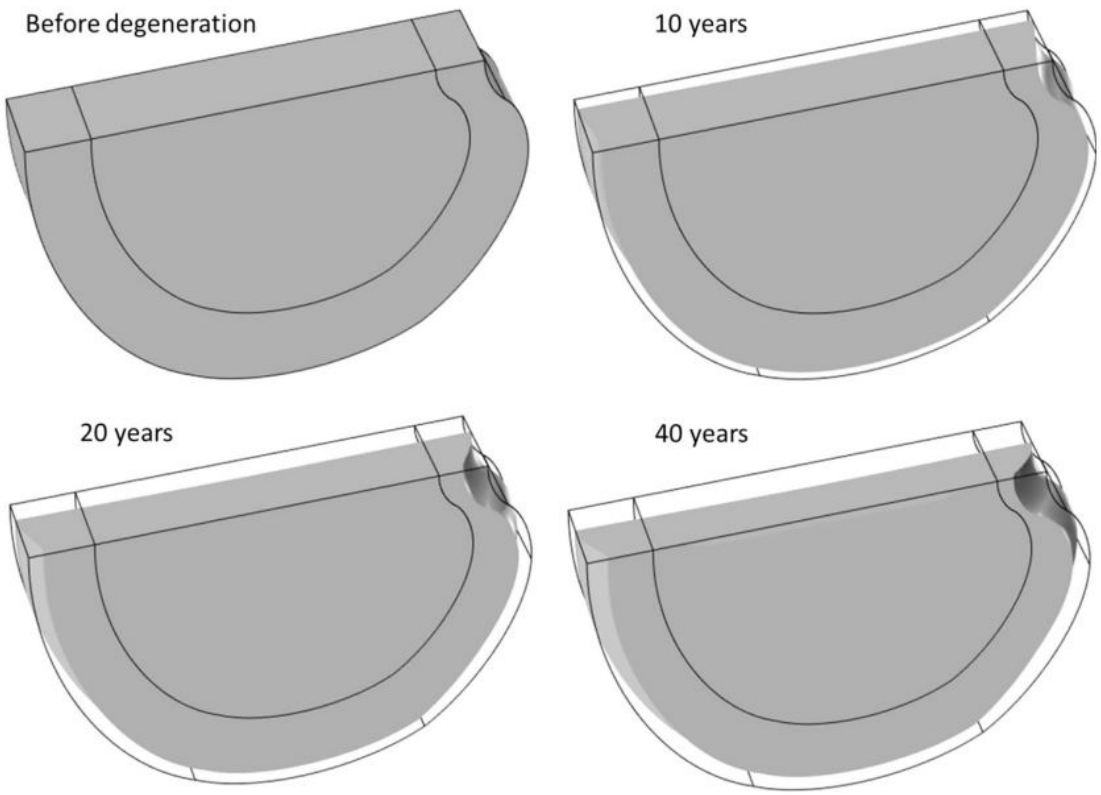

Figure 5. 9: Disc deformation (magnified by 3 times) before degeneration and after degeneration for 10, 20, and 40 years.

5.4 Discussion

In this study, the disc degeneration was initiated by decreased nutrition supply, one of the primary factors causing disc degeneration [7]. Decreased nutrition supply causes cell death [20, 168] (Figs. 5.2 and 5.3), and reduces the cellular metabolic and biosynthetic rates [37]. The decrease in PG content (Figs. 5.2 and 5.3) concomitantly reduces the amount of fixed charge density attached to its GAG chains within the disc (Fig 5.5). This leads to the reduction of the counter-ion (e.g., sodium ion) concentration and the osmolarity in the disc. Consequently, the fluid pressure is decreased (Fig. 5.6), causing less swelling of the disc and lower water content in the disc (Figs. 5.2, 5.3, and 5.7), eventually causing the uneven stress distributions (Fig. 5.8) and decreased disc height (Fig 5.9).

PG is a significant matrix component that plays a crucial role in the disc matric integrity and mechanical functions [24, 169]. As PG content decreases with time in the disc, associated fixed charge density decreases in the disc, resulting in a loss of swelling pressure and loss of water content [24, 169]. The reduction of water content (or disc volume, Fig. 5.2D and Fig. 5.3) results in a smaller tissue pore size for transport of fluids, ions, nutrients, and metabolic wastes, leading to lower values of solute diffusivity, hydraulic permeability, and electrical conductivity [67, 110, 111, 150]. Reduced tissue diffusivity would reduce the rate of nutrition supply to the cells. The balance between the rate of nutrients supply and nutrients consumption would be disturbed and tilt toward the consumption side, thus the concentration of nutrients around the cells decreases, leading to lower metabolic and synthetic activities and lower number of cells in the disc. The change in water content in the disc lags behind the change in PG content because it takes time for the water to diffuse out the disc due to that the hydraulic permeability is very small even in healthy discs (e.g.,

[0.9 ±0.43] $\times 10^{-15}$ $m^4/N \cdot s$ in the human NP [151] and 0.17×10^{-15} $m^4/N \cdot s$ in the human AF [170]). The decrease of the hydraulic permeability further decreases the rate of water flow out thus slowing the water loss.

The experimental results for the rate of GAG synthesis in the NP, inner AF, and outer AF were reported to be (mean ±SD): (2.6 ±3.5) $\times 10^{-5}$, (2.9 ±4.2) $\times 10^{-5}$, and (1.1 ±0.9) $\times 10^{-5}$ mmol/g dry weight/hr, respectively [117]. In our simulations, the rate of GAG synthesis varied from outer AF to the inner AF region [Eq. (3.17), Chapter 3]. Our calculated rates of GAG synthesis [Eq. (3.17), Chapter 3] averaged over the NP, inner AF, and outer AF regions are 0.91×10^{-5}, 0.66×10^{-5}, 0.35×10^{-5} mmol/g dry weight/hr, respectively. These values are within the range of the experimental results [117].

Glucose concentration was found to be the limiting factor for survival of cells [20]. It was also reported that pH lower than 6.8 would have a negative effect on the cell viability [20, 35, 171]. In this study, the minimum pH in the disc over time was found to be 7.08, located within the most severely degenerated area (i.e., on the mid-plane in the inner AF region, Fig. 5.10A). The minimum pH value in the case where both glucose and the oxygen levels were reduced was also higher than 6.8 (Fig. 5.10B). Thus, no direct relationship between cell viability and the pH was included in our model. It was also found that the pH value (within the degenerated area) increases with the progression of disc degeneration. This is caused by the reduction of the lactate concentration within this area. Because the cell numbers within this region decreased significantly, both the production rate and the concentration of the lactate within this region decreased correspondingly (Figs. 5.10 C and D).

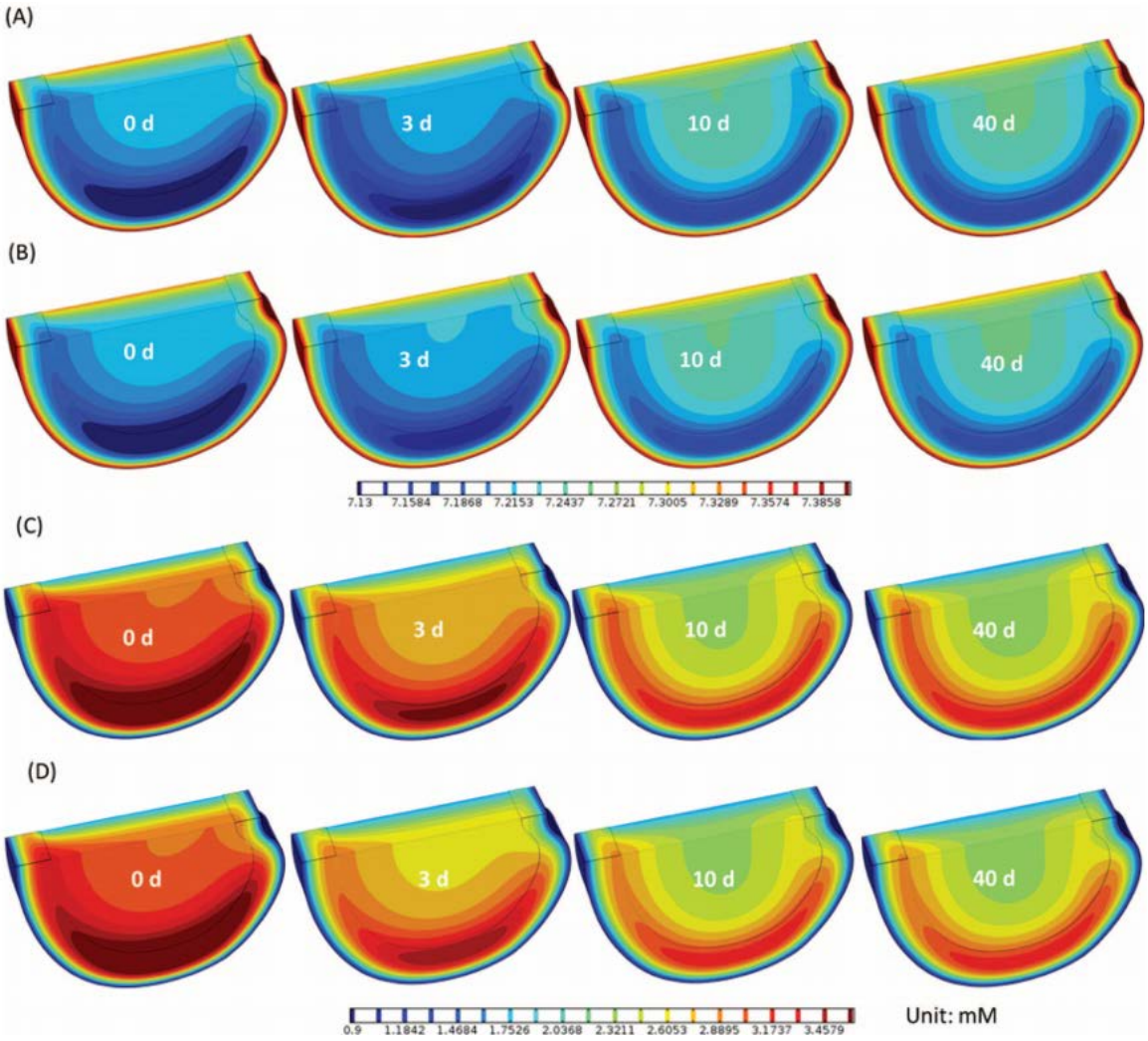

Figure 5. 10: pH and lactate distribution in the disc. (A) pH distribution and (C) lactate distribution in the disc for the case where the glucose concentration was reduced alone by 70% on NP-CEP boundary and 40% on AF periphery. (B) pH distribution and (D) lactate distribution in the disc for the case where both glucose and oxygen concentrations were reduced by 70% on NP-CEP boundary and 40% on AF periphery.

The fluid pressure is highest in the NP region at healthy condition [27, 85, 172], and decreases gradually with the disc degeneration [27, 151, 173]. The largest fluid pressure was seen shifted from the NP region toward the inner and middle AF regions, especially in the region posterior to the NP in the degenerated discs [27, 172]. Such variation of pressure distribution from healthy to degenerative state were well predicted in this study.

The results of Von Mises stress distributions indicate that the shear stress increases significantly in the AF region with the progression of disc degeneration (Fig. 5.8), this high shear stresses may be a reason for the AF delamination commonly reported in literature [174-176].

In our study, both the volume and disc height decreased with the disc degeneration progression, this is consistent with the experimental findings [177-179]. The volume decrease was mainly caused by the reduction in the swelling pressure and the loss of water in the disc, especially in the NP region and the inner AF region (Fig. 5.2), causing the disc to shrink inwards.

Since little quantitative information on nutrition boundary conditions in human discs in vivo is available in the literature, thus, in our current study, a case of reduced nutrition supply was chosen, as an example, to simulate disc degeneration process and to investigate the coupled biophysical events in the disc during the degeneration progress. The effects of different rate of nutrition reduction on the process of disc degeneration were also investigated (Fig. 5.11). The predicted results indicate that the rate of nutrition reduction has a significant effect on the onset of cell death (Fig. 5.11B), but not the long-term GAG and water contents in the disc (Fig. 5.11 C and D).

This was the first numerical study of the complicated nonlinear interactions among biological, chemical, electrical, and mechanical events occurred in the human disc during the progression of degeneration. The lack of nutrition supply to the disc could have a long term effect (e.g., up to 55 years) on disc degeneration.

The results and findings from this study are useful for developing new diagnostic techniques for detecting early disc degeneration. When combined with patient-specific magnetic resonance imaging data for disc geometry and water content distribution, this numerical model can be used to evaluate disc degeneration status, to predict long term disc degeneration, and to design effective treatment strategies for disc repair on a patient-specific basis. For instance, an injection of growth factors into the disc has been proposed as a method for treatment of disc degeneration (see review [180]), our model can be used to quantitatively analyze and simulate the outcomes of this treatment and to optimize the parameters (such as growth factor concentration, injection flow rate, duration) used in this method.

Both the GAG synthesis rate (λ_1) and degradation rate (λ_2) in human discs vary with degenerative progress [116, 181]. In our simulations, the values of λ_1 and λ_2 were assumed to be constant over time. This simplification may overestimate the time period needed for disc to reach new equilibrium after the reduction of nutrition supply at disc boundary.

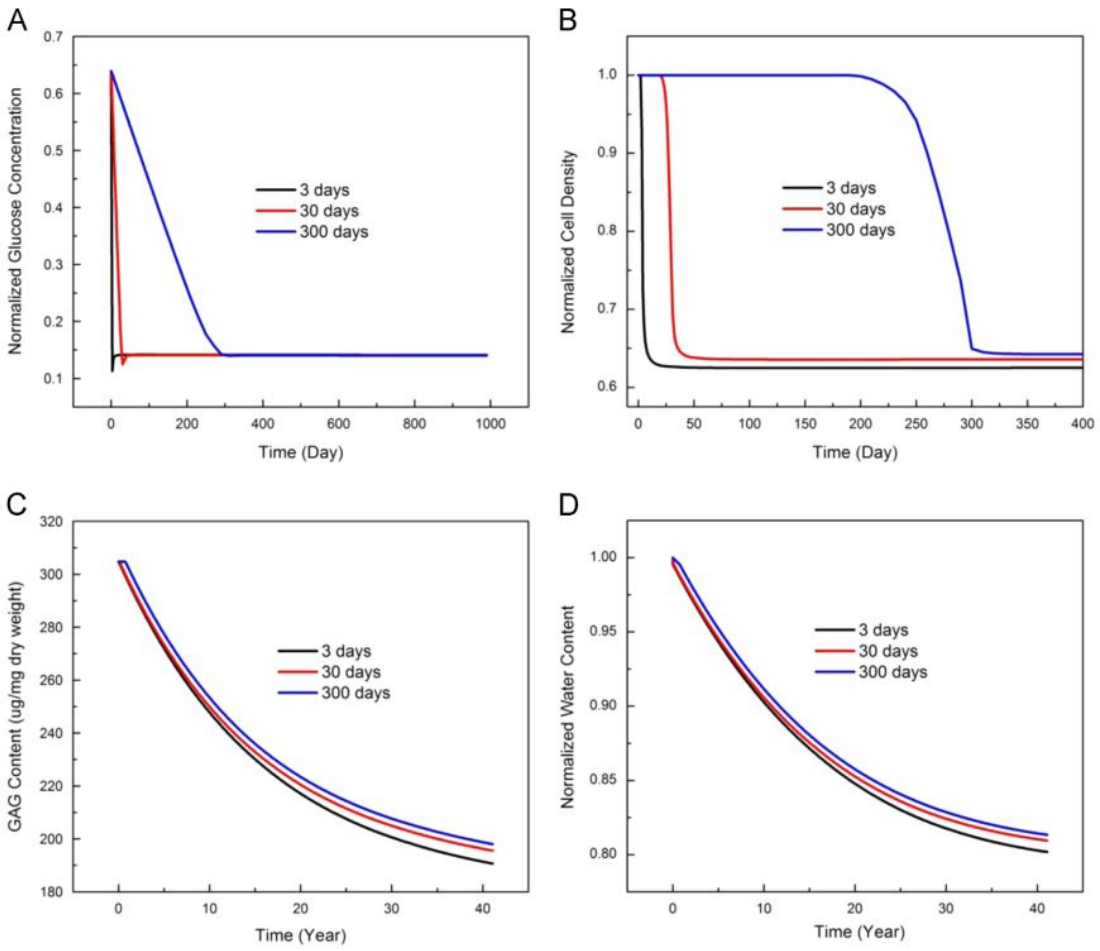

Figure 5. 11: Effect of rate of nutrition reduction at disc boundary on the temporal variation of (A) overall glucose concentration (normalized by 0.5 mM), (B) overall cell density (normalized by the value at healthy state), (C) overall GAG content, and (D) overall water content (normalized by the value at healthy state) in the disc (per unit of tissue volume at the reference configuration). Nutrition levels are reduced to the same targeted level in 3, 30, and 300 days.

Another limitation is the change of the mechanical properties with the alteration of disc composition along disc degeneration was not considered in this model. In the current simulations, mechanical properties of degenerated discs were used. This assumption on the mechanical properties may have an influence on the rate of the degeneration process and signals in the disc. The limitation may be overcome in our future studies by incorporating the tissue matrix dependent mechanical properties in soft biological tissues [182].

The anisotropy of the mechanical behavior and transport properties were not considered in this study. These simplifications may influence the distributions of the fluid pressure, deformation, and stresses within the AF region.

Moreover, in this study, the mechanical loading on the disc is assumed to be constant over time (equal to the mechanical loading on the disc at the healthy state). This does not truly reflect the real situation in human discs because the mechanical loading on disc could vary with aging or degeneration. These effects will be taken into consideration in the future studies.

In conclusion, the progression of human disc degeneration in response to a reduced glucose level have been simulated. The temporal and spatial distributions of cell viability, PG content, fixed charge density, fluid pressure, water content, Von Mises stress, and disc deformation in the human disc were numerically simulated with a 3D finite element model developed based on the cell activity coupled mechano-electrochemical multiphase mixture theory. The predicted results showed how the nutrition deprivation affects the cell viability, the tissue components (GAG and water contents), the tissue swelling pressure,

the mechanical stress (e.g., Von Mises stress), and deformation. The results of predicted PG and water content distributions are consistent with experimental results reported in the literature. This study has provided new insight into complicated interactions among biological, chemical, electrical, and mechanical events in the disc over time with progression of degeneration, and a powerful tool for developing and optimizing new diagnostic and treatment strategies for disc degeneration.

Chapter 6 Influences of Nutrition Supply and Pathways on the Degenerative Patterns in Human Intervertebral Discs

6.1 Introductory Remarks

Many spinal disorders (such as neck and low back pain) are associated with the degeneration of the intervertebral disc (IVD) [2], which may be initiated or accelerated by a nutritional deficiency [35, 119]. Due to avascular nature of the IVDs, small molecules (like the nutrients) have to reach the cells through the extracellular matrix mainly by diffusion[30], from the blood vessels at disc margins via two pathways: the cartilaginous endplate-nucleus pulposus (CEP-NP) pathway and the annulus fibrosus (AF) periphery pathway[29]. Several researchers have reported that the CEP-NP nutritional pathway is primarily responsible for nurturing cells in the NP and inner AF regions while AF periphery mainly for cells in the outer AF region [29, 32-34]. These findings clearly indicate that the nutritional pathway plays a significant role in regulating the spatial distribution of cell density within the IVD.

The disc cells are crucial for maintaining the integrity of tissue structure which is important for its mechanical functions. Loss of cell numbers and resulting extracellular matrix within the disc would trigger a cascade of biochemical and mechanical changes within the tissue, resulting in a tissue failure [3, 25, 168]. In this chapter, we are interested in whether impairment of different nutritional pathways affects the degenerative patterns (e.g., spatial distribution of cell density, glycosaminoglycan (GAG) content, and water content, etc.) in human lumbar discs. Thus, the objective of this chapter is to investigate the effects of variation of nutritional supply and pathways on degenerative patterns in human lumbar

discs. We hypothesize that variation of nutrition supply or pathways would result in different degenerative patterns in human lumbar discs. The distributions of cell density, GAG content, and water content in the disc with different nutritional supplies and pathways are studied numerically [25, 168].

6.2 Methods

The effect of impairment of nutritional pathway on disc degeneration patterns was numerically studied with a finite element method developed based on the cell-activity-coupled mechano-electrochemical mixture theory [25, 161, 168]. In this model, the disc is considered as an inhomogeneous, porous mixture consisting of the following phases: a charged solid phase with cells and GAG fixed to it, a fluid phase, a solute phase with multiple species of ions, glucose, oxygen, and lactate. The cell metabolic activities were dependent on glucose, oxygen and lactate (pH value). The cell viability was assumed to be dependent on glucose concentration only [161] as it has been reported that glucose is the most crucial nutrients for disc cell survival [20, 35, 120]. The rate of GAG content change (Q^{GAG}) was determined by the GAG synthesis rate per tissue volume (Q^{syn}) and the GAG degradation rate per tissue volume ($Q^{\deg}$) by: $Q^{GAG} = Q^{syn} - Q^{\deg}$. The GAG synthesis rate was assumed to be proportional to the value of local cell density (ρ^{cell}): $Q^{syn} = \lambda_1 \rho^{cell}$, while the GAG degradation rate was proportional to the value of local GAG content (C^{GAG}): $Q^{\deg} = \lambda_2 C^{GAG}$ [168]. The information on how GAG synthesis rate per cell (i.e., the value of λ_1) and the rate of GAG degradation (i.e., the value of λ_2) vary with disc degeneration is very limited. It is expected these values will change during the progression of disc degeneration. However, we do not know when these values start to change as disc

degeneration progresses. So in this study, we assumed that both proportional constants (i.e., λ_1 and λ_2) in GAG synthesis and degradation were invariant with time. The value of GAG synthesis rate per cell (i.e., λ_1) could be calculated by the values of local cell density, GAG content, and λ_2 (which is related to the half-life of GAG turnover [116]) in the disc at mature, healthy state because the rate of GAG content change in the mature, healthy disc is assumed to be zero [168]. The transport of water and solutes were coupled with hydration (or tissue porosity) which depends on tissue deformation in the model [110, 150].

A realistic three-dimensional disc model was generated based on an L2-3 human lumbar disc (41 years old male, non-degenerated [104]), see Fig. 6.1A. The disc was modeled with two distinct regions: NP and AF. Because of symmetry, only the upper-right quarter of the disc was simulated (Fig. 6.1B). The finite element model of the disc was developed with COMSOL (COMSOL 4.3b, COMSOL Inc. MA) based on the method developed by Sun et al. (1999) [142]. Disc at the healthy state before degeneration was chosen as the reference configuration.

The information for cell density in the mature, healthy disc was obtained from experimental data in literature[18]: 4000 cells/mm^3 in NP and 9000 cells/mm^3 in AF. Information for distributions of fixed charge density (FCD) and water content (i.e., volume fraction of water) in the mature, healthy disc were extracted from experimental data in literature [15]: fixed charge density in NP was assumed to be homogeneous, with a value of 0.3425 M, and linearly decreased from 0.3425 to 0.1634 M from the innermost AF region to the outermost AF region. Water content was 0.85 in the NP, and linearly decreased from 0.85

to 0.7 from the innermost AF region to the outermost AF region. More information on material properties, initial and boundary conditions can be found in literature [25, 161, 168].

The concentrations of nutrients and metabolic wastes in the blood were reported to be: 5.6 mM for glucose concentration, 6.4 kPa for oxygen tension, and 1mM for lactate concentration [147, 166, 167]. The effect of cartilage endplate (CEP) on nutrition supply was considered by adjusting the boundary conditions at the interface between NP and CEP [25]. Values for glucose concentration, oxygen tension, and lactate concentration at the CEP-NP boundary were 3.2 mM, 3.6 kPa, and 2.15 mM on the NP surface adjacent to the endplate; respectively; and at the AF periphery boundary were 5 mM, 5.8 kPa, and 0.9 mM, respectively [25, 147, 168]. These values were used as the reference values in this study. The equilibrium distributions of glucose, oxygen, lactate, and other signals in the healthy disc with the reference values were calculated and used as the initial condition for the following simulations. The impaired nutrition supply was simulated by lowering the level of nutrients (glucose and oxygen) at the inner side of the disc boundaries. Since the flux is proportional to the difference in nutrient concentration between blood and inner side of the disc boundaries, varying the nutrient concentration at the inner side of the disc boundaries is equivalent to change the permeability of the tissues, according to Fick's law. Three cases were investigated in this study: glucose and oxygen concentrations reduced at CEP-NP boundary only (Case 1), at AF periphery only (Case 2), and at both CEP-NP and AF periphery boundaries simultaneously (Case 3). In Case 1, discs with nutrition level at the CEP-NP boundary ranged from 100% to 0% of the corresponding reference values (while the nutrition level on the AF periphery boundary was kept at the reference level)

were simulated. In Case 2, discs with the nutrition level at the AF periphery boundary ranged from 100% to 0% of the corresponding reference values (while the nutrition level on the CEP-NP boundary was kept at the reference level) were simulated. In Case 3, discs with the nutrition level at both the CEP-NP and AF periphery boundaries ranged from 100% to 0% of the corresponding reference values were simulated.

Distribution of cell density in the disc at 40 days after reducing the level of nutrients at the boundary was analyzed to investigate the degenerative pattern in discs at the initial stage of degeneration. Forty days was chosen as a time point for the early stage of disc degeneration because the cell density and nutrient distributions in the disc were predicted to reach new equilibrium in about 30 days and 40 days, respectively, after a nutrition level has dropped on disc boundaries [168].

Variations of GAG and water contents with time were also calculated. Distributions of GAG and water contents in discs after 10 years of disc degeneration (starting from the time when the nutrient level at disc boundary starts to decrease) were analyzed to elucidate the degenerative patterns in discs at the developed stage, because disc degeneration is a slow process [116, 183].

6.3 Results

Effect of Impairment of Different Nutritional Supply and Pathways on Cell Density Distribution

The extent of decrease in the nutrition level at disc boundaries greatly affected the distribution and magnitude of the cell density. After nutrition level decreased to specified values, distribution of the cell density in the disc reached equilibrium state in about 30 days [168], and was reported in Figs. 6.2, 6.3, and 6.4. The equilibrium state for cell density

distribution was defined at when the maximum change of the relative cell density at a location is less than 0.1% /day.

Case 1: Impairment of CEP-NP Pathway Only

With the reference values of nutrition concentrations at the AF periphery boundary, the nutrition level around 30% of the reference values at the CEP-NP boundary (i.e., glucose concentration of 1.2 mM and oxygen tension of 1.53 kPa) were predicted to be sufficient for the disc to maintain viability of all the cells (i.e., 4000 cells/mm^3 in NP and 9000 cells/mm^3 in AF) within the disc (Fig. 6.2). This level is defined as the critical level for cells survival in the disc. Below this level cell death began to occur.

It was predicted that cells started to die from the center of the NP region in this case. When cell density distribution reached an equilibrium state, the cell death occurred mostly in the NP region, while the AF region was not affected (Fig. 6.2). The affected region (defined as the region where cell density decreased by more than 10%) was larger in disc with lower nutrition level at the CEP-NP boundary (Figs. 6.2 and 6.5A). For example, at the equilibrium state, 54% of the disc volume was affected and the normalized cell density (averaged over whole disc) was 48% when the nutritional level at CEP-NP boundary was 0%, compared to no region was affected (or no cell death) when the nutrition level at CEP-NP boundary was 30% or higher (Fig. 6.5 A and B).

Case 2: Impairment of AF Pathway Only

With nutrition level at the CEP-NP boundary kept at reference values, it was predicted that nutrition level around 20% of the reference values at the AF periphery boundary (i.e.,

glucose concentration of 1 mM and oxygen tension of 1.16 kPa) were sufficient for the disc (Fig. 6.3) to maintain viability of all the cells within the disc. Below this level, cell death began to occur (Fig. 6.3), mostly in the outer AF region. The affected region was larger with lower nutrition level at AF periphery (Figs. 6.3 and 6.5A). The NP region was not affected in this case (Fig. 6.3). When the nutritional level on this boundary was 0%, at the equilibrium state, 26% of the disc volume was affected (Fig. 6.5A), and the normalized cell density reduced to 76% (Fig. 6.5B), compared to no degenerative region (i.e., 0% of affected volume) or no cell death (i.e., 100% of normalized cell density) were predicted at 20% or above of the reference values on AF periphery boundary (Fig. 6.5).

Case 3: Impairment of Both CEP-NP and AF Periphery Pathways

It was predicted that the nutrition level around 50% of the reference values at both CEP-NP boundary (i.e., 2 mM for glucose concentration and 2.55 kPa for oxygen tension) and AF periphery boundary (i.e., 2.5 mM for glucose concentration and 2.9 kPa for oxygen tension) were sufficient to maintain cell viability everywhere within the disc. Below this level the cell death began to occur in the lateral regions (Fig. 6.4). When the nutrition level reduced to 10% or lower (of the reference values) at both CEP-NP and AF periphery boundaries, at equilibrium, all cells within the disc were dead (Figs. 6.4 and 6.5).

Effect of Impairment of Different Nutritional Supply and Pathways on GAG and Water Contents

The changes of GAG content (Fig. 6.6) and water content (Figs. 6.7 and 6.8) distributions within the disc in the three cases were analyzed. Results of GAG content and water content after 10 years of degeneration (starting from the time when the nutrient level at disc boundary starts to decrease) were presented here. It was predicted that the spatial

distributions of GAG and water content distributions were similar (Figs. 6.6 and 6.7). The degenerative patterns seen in Figs. 6.6 and 6.7 were related to the cell density distributions in Figs. 6.2-6.4. For Case 3, there was a zone (on the middle plane in the posterior region) with much higher water content than that in the surrounding areas (Fig. 6.7D), this phenomenon was only observed in Case 3.

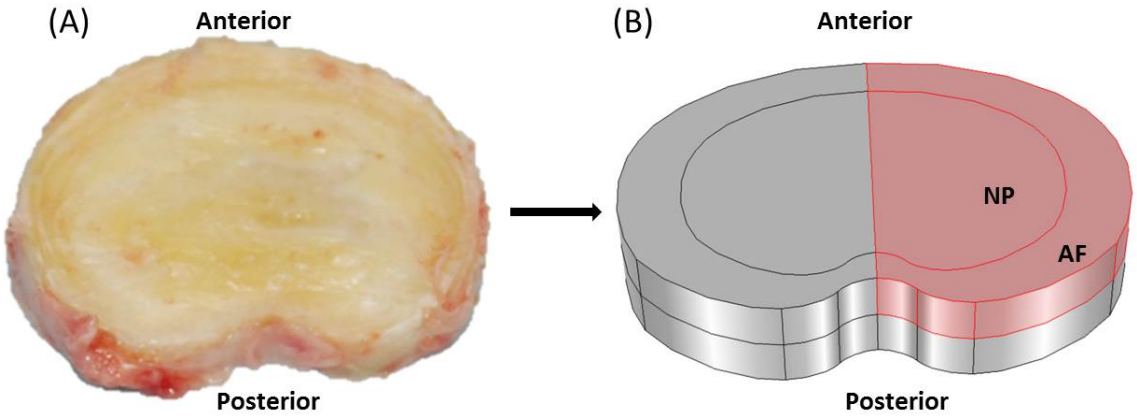

Figure 6. 1: (A) Geometry and size of the disc from human lumbar spine (L2-3, male, non-degenerated [141]) and (B) Schematic of the right–upper quarter of the disc used in the simulations. The cell density in the healthy disc was assumed to be 4000 cells/mm3 in NP and 9000 cells/mm3 in AF [18].

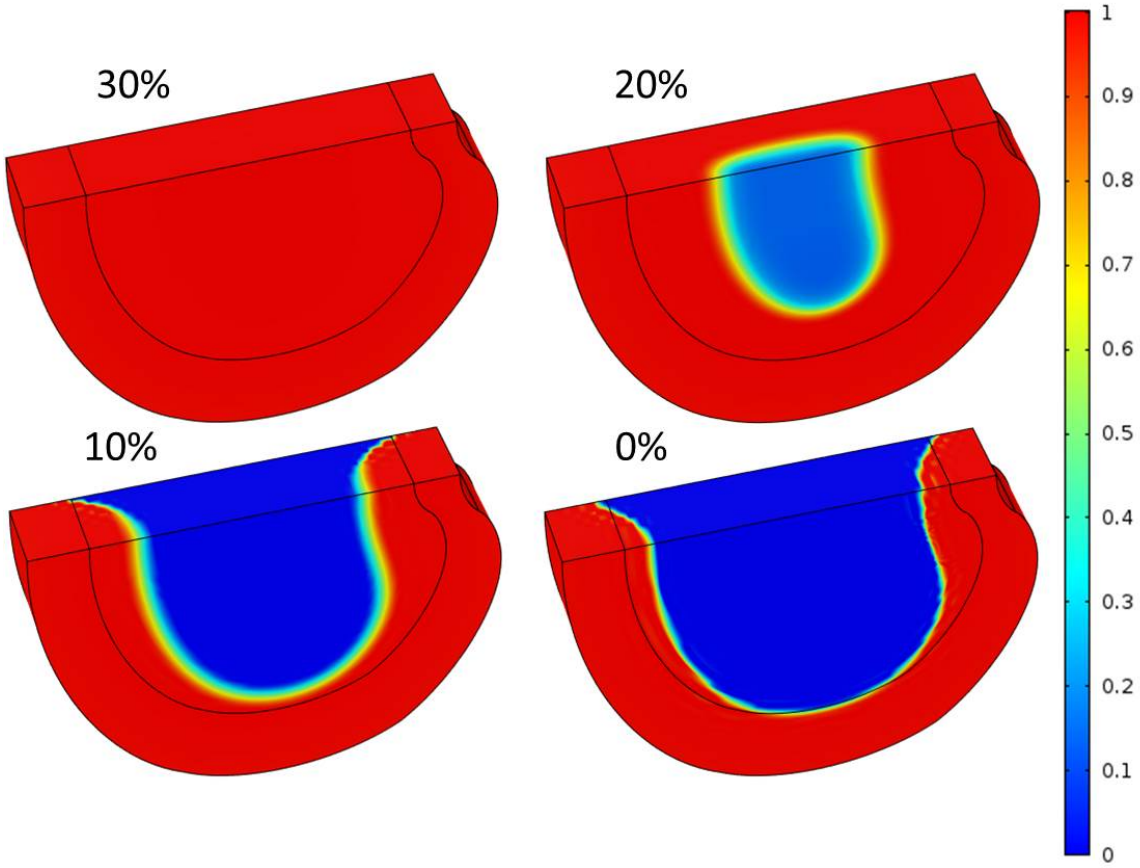

Figure 6. 2: Three-dimensional distributions of normalized cell density at steady state after nutrient concentrations on CEP-NP boundary decreased to 30%, 20%, 10%, and 0% of the corresponding reference values.

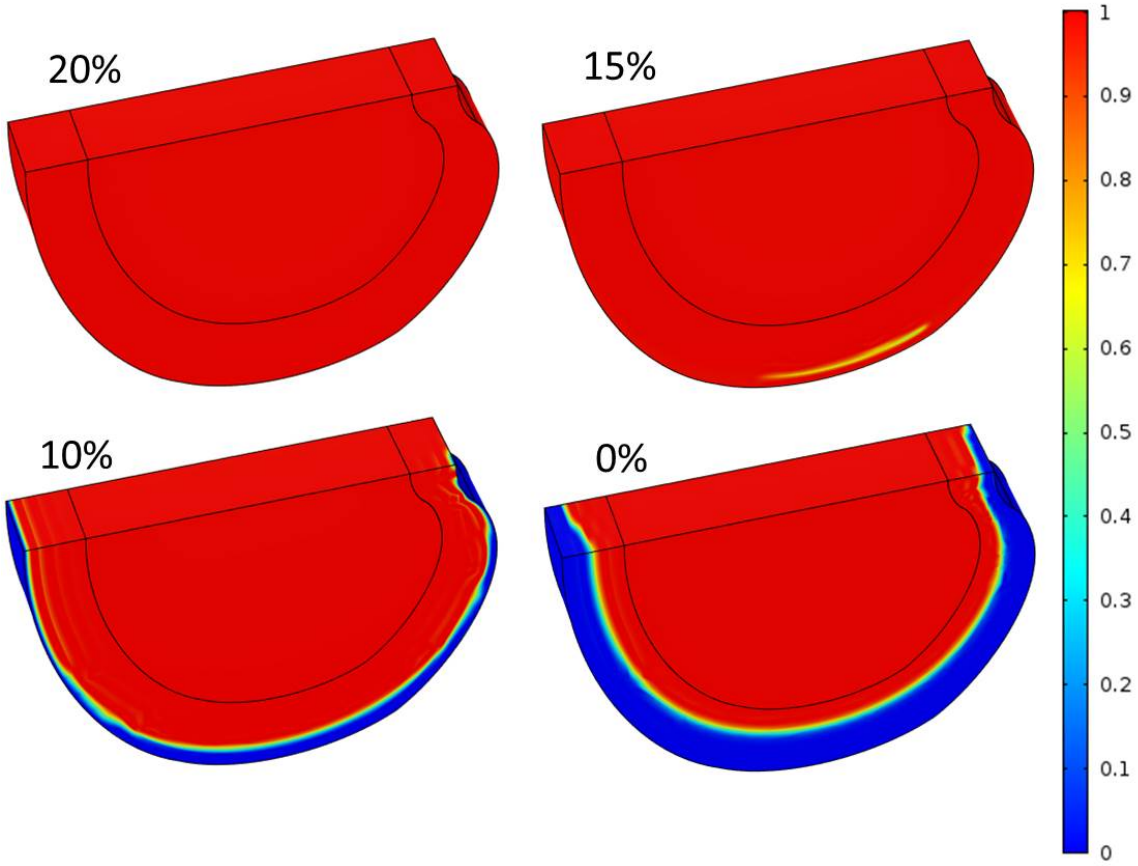

Figure 6. 3: Three-dimensional distributions of normalized cell density at steady state after nutrient concentrations on AF periphery decreased to 20%, 15%, 10%, and 0% of the corresponding reference values.

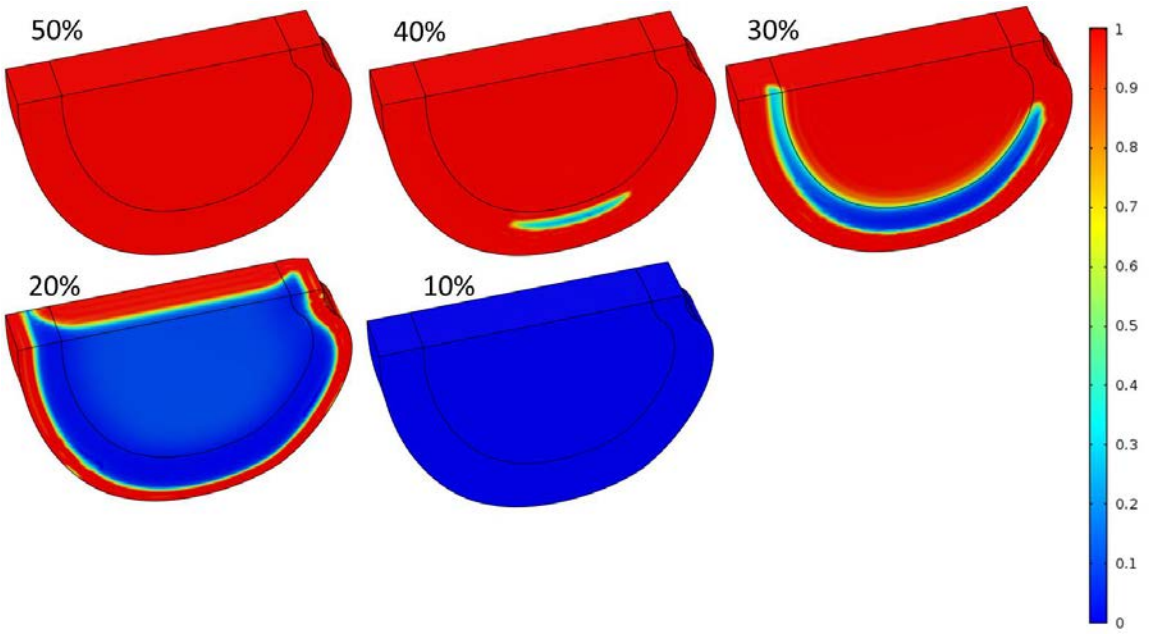

Figure 6. 4: Three-dimensional distributions of normalized cell density at steady state after nutrient concentrations on both NP and AF boundaries decreased to 50%, 40%, 30%, 20% and 10% of the corresponding reference values.

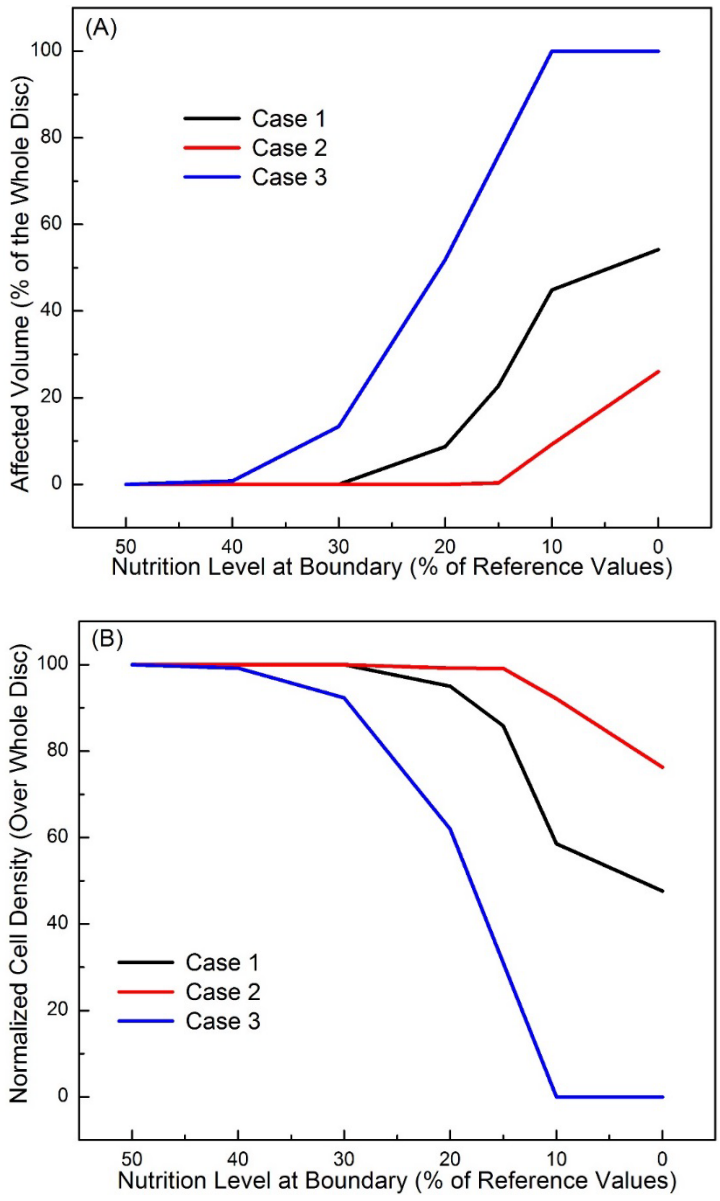

Figure 6. 5: (A) Percent of the affected regions (relative to the whole disc volume) where cell death is greater than 10% of the corresponding value at healthy state for Case 1 (black line), Case 2 (red line), and Case 3 (blue line). (B) Changes in normalized cell density (averaged over the whole disc volume) for Case 1 (black line), Case 2 (red line), and Case 3 (blue line). All the results presented in this figure were values at steady state.

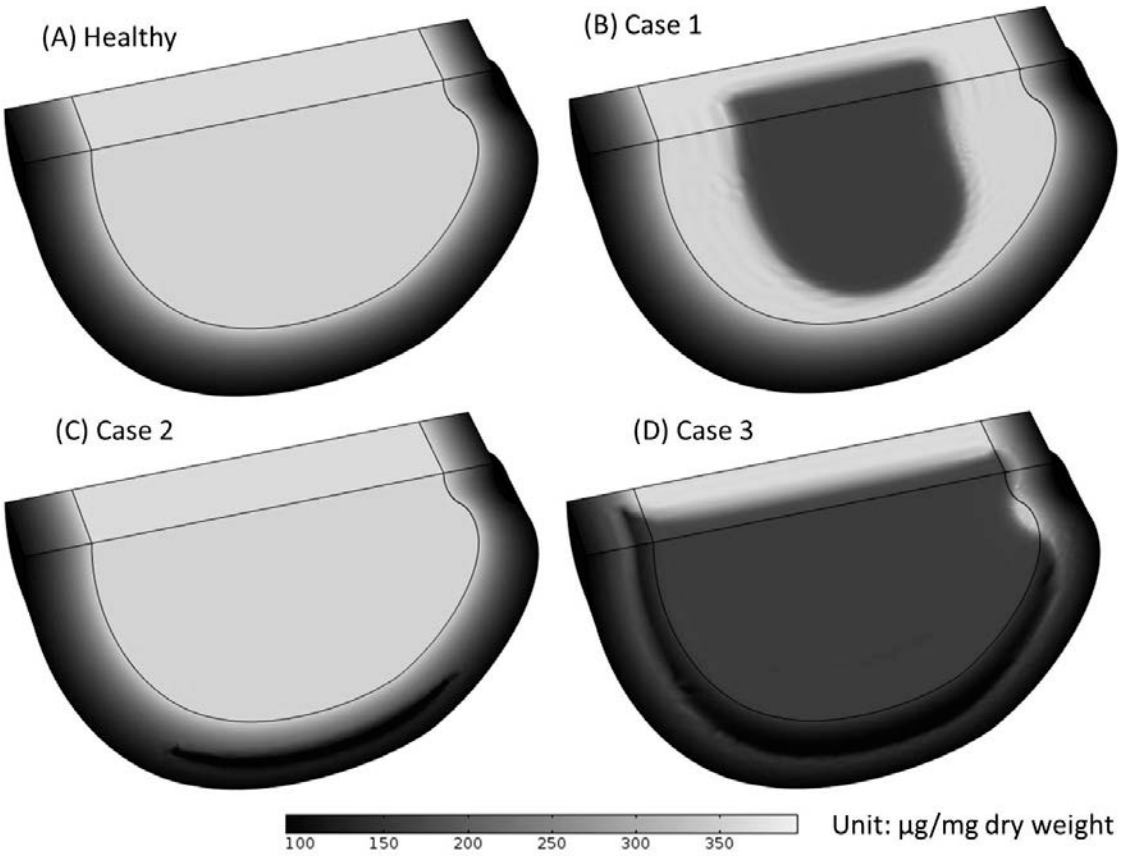

Figure 6. 6: Comparison of the GAG content distributions (A) in the healthy disc with reference values of nutrition level, (B) in Case 1 where nutrition level was decreased in CEP-NP pathway only, (C) in Case 2 where nutrition level was decreased in AF pathway only, and (D) in Case 3 where nutrition level was reduced in both pathways. The results shown in (B-D) are GAG distributions at 10 years after cell density reached steady state as nutrition level reduced to 15% of the reference values.

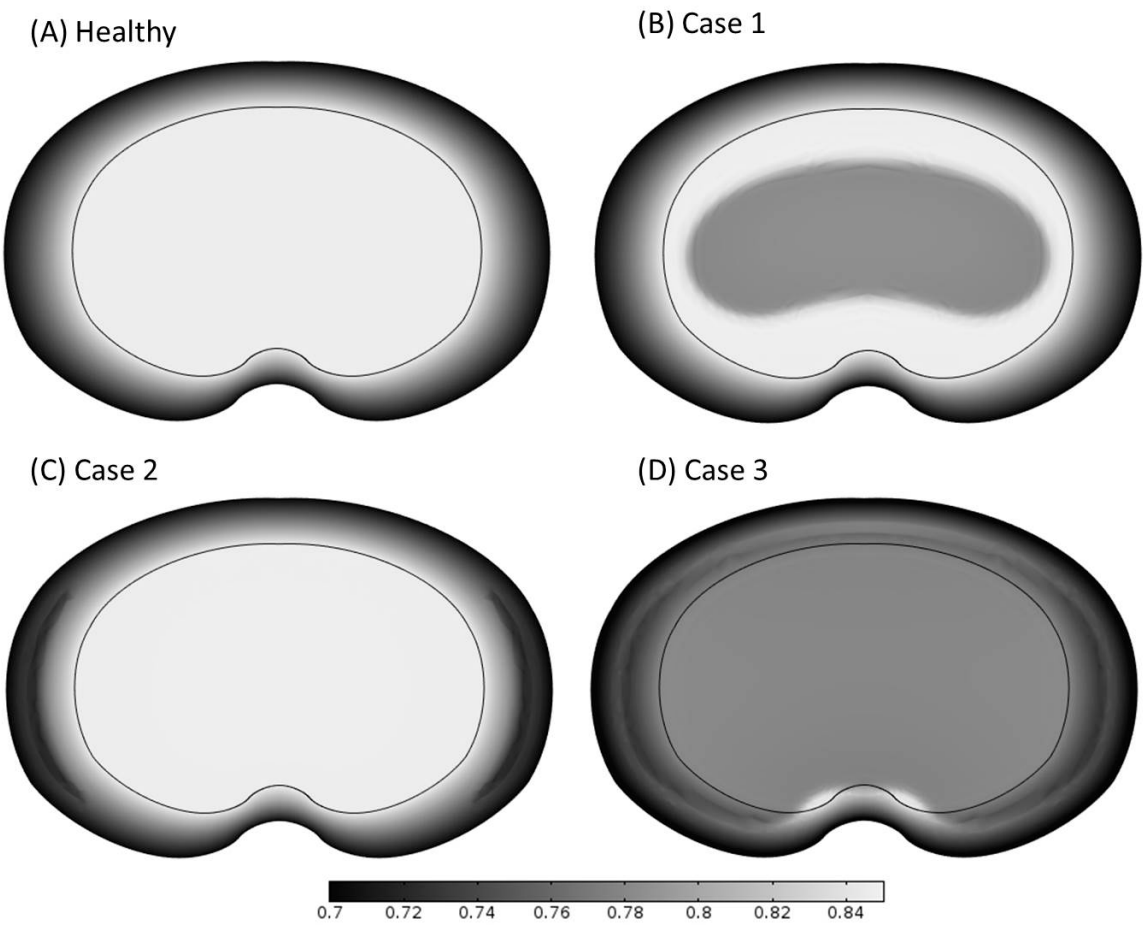

Figure 6. 7: Comparison of the water content distributions on the disc mid-axial plane (A) in the healthy disc with reference values of nutrition level, (B) in Case 1 where nutrition level was decreased in CEP-NP pathway only, (C) in Case 2 where nutrition level was decreased in AF pathway only, and (D) in Case 3 where nutrition level was decreased in both pathways. The high water content zone is clearly shown in the posterior region in the disc for Case 3. The results shown in (B-D) are water content distributions at 10 years after cell density reached steady state as nutrition level reduced to 15% of the corresponding reference values.

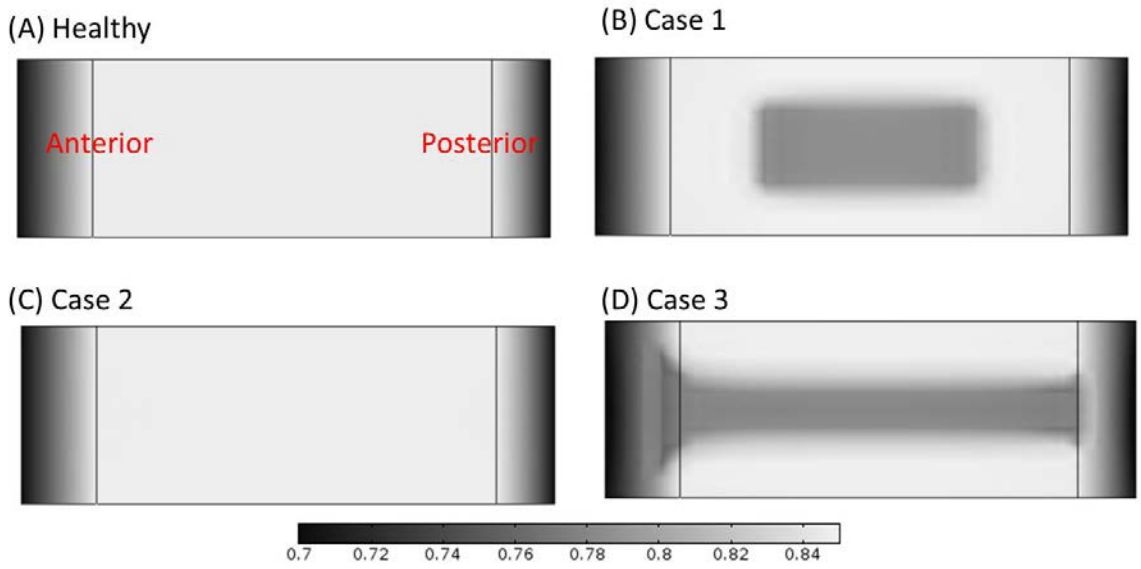

Figure 6. 8: Comparison of the water content distributions on the mid-sagittal plane (A) in the healthy disc with reference values of nutrition level, (B) in Case 1 where nutritional level was decreased in CEP-NP pathway only, (C) in Case 2 where nutrition level was decreased in AF pathway only, and (D) in Case 3 where nutrition level was decreased in both pathways. The results shown in (B-D) are water content distributions at 10 years after cell density reached steady state as nutrition level reduced to 15% of the corresponding reference values.

6.4 Discussion

It is well known that impairment of different nutritional pathways affects the cell density distribution within the disc [29, 32-34], however, little is known on the degenerative pattern (spatial distributions of cell density, GAG content, water content, etc.) of disc in relation to nutritional supplies and pathways. Results from present study indicate that impartment of the CEP-NP nutritional pathway would cause tissue degeneration mostly in the NP region, while impartment of the AF periphery nutritional pathway is primary responsible for the tissue degeneration in the outer AF region.

When the nutrition level to disc is decreased to a critical level, cell death initiates at the location where the local nutrition concentration is the lowest [and below the threshold value for cell survival (e.g., 0.5 mM) [20, 35, 105, 120, 161]]. This location depends on many factors, such as disc shape and size, the level of nutrition supply at disc boundary, and the transport properties of disc tissues. Note that the effects of disc shape and size or transport properties on degenerative patters were not simulated in current study. As the local glucose concentration decreased below the threshold value for cell survival, cell death occurs and the cell density distribution would reach a new equilibrium (where the demand and supply of nutrients are balanced) in about 30 days [168]. At this early state (around 30 days), the integrity of the extracellular matrix is close to intact because the change of extracellular composition is a much slower process [116, 168]. Thus, the reduction of cell number is the earliest degenerative sign in the disc caused by poor nutrition supply.

In the healthy, adult human lumbar discs before degeneration, we assumed that the GAG synthesis and degradation rates are balanced and the net GAG content does not change with time. When the cell death occurs, the overall GAG synthesis rate within the disc decreases, causing a decrease in the total GAG content over time until a new equilibrium is reached [168]. The slow decrease in GAG content gradually reduces the swelling pressure in the disc, resulting in the lower water content within the disc [24, 25, 169]. This explains why the pattern for the distribution of cell density in the disc is similar to the patterns of GAG and water content distributions in the disc at much later stages (e.g., 10 years later), see Figs. 6.1-6.3 and 6.5-6.6. It also explains that different nutritional supplies and pathways would result in distinctive patterns of disc degeneration. Knowledge of these patterns may help to diagnose disc degeneration in relation to poor nutrition supply. Quantitative imaging techniques like the T2-weighted magnetic resonance imaging (MRI) can be used to identify a decrease in disc height and a loss of water content in the disc, both suggestive of a loss of mass in the disc. Our predicted results in cases in which there has been a loss of nutrition supplies through the CEP-NP and/or AF periphery pathway (Fig. 6.5 B and D) are similar to those seen on MRI [184-187]. Likely, poor-nutrition-related disc degeneration in the clinical patient falls on the spectrum between these two cases (i.e., Case 1 and Case 3). For these two cases, the poor-nutrition-related disc degeneration was predicted to start at the middle axial plane of the disc, where the water content was lower than the surrounding regions, see Fig. 6.7. This is consistent with the horizontal gray band seen in T2-weighted MRI images for degenerated discs.[184] In addition, the higher water content zone predicted in Case 3 (in Fig. 6.6D) is consistent with the High Intensity Zone (HIZ) seen in T2-weighted MRI images [188-191]. The HIZ was initially proposed as a

marker to diagnose low back pain [190, 192], whereas it was also found in asymptomatic subjects later [191]. Nevertheless, the results in this study clearly indicate that this zone is related to the disc degeneration in Case 3, which could be a radiographic marker for disc degeneration [188-191]. Although the nature of the HIZ is still not clear, we speculate that the HIZ might be related to the geometry of degenerated discs. More studies are needed in order to understand this phenomenon.

The limitations of this study are similar to those described in Chapter 5. Briefly, the first limitation is that the GAG synthesis rate per cell (i.e., the value of λ_1) in the present model was assumed to be uncoupled with cell metabolism. Assuming the synthesis of one disaccharide unit of the GAG molecule requires two glucose molecules, it is expected the consumption rate of glucose by cells should be greater than twice the rate of the GAG synthesis. In this study, this condition is satisfied with the value of λ_1 from the literature [168] (data not shown). The second limitation is that the mechanical loading in this study was assumed to be constant over time (i.e., the diurnal activity was not considered). Based on the study of the effect of dynamic loading on cell viability in the disc [161], consideration of diurnal activity would not affect the distinct patterns of cell density, and GAG content and water content distributions in relation to decreased nutrition supply. Other limitations of this study include the lack of a thin layer of CEP in the model; instead, its effect on nutrition transport was simulated by varying the nutrition level at the CEP-NP interface. Another limitation is that the intrinsic mechanical properties of the disc (Lame constants λ and μ) were assumed not to change with disc degeneration. This simplification would affect the value of water content, however, its effect on degenerative patterns are not expected to be significant, because the spatial distributions of GAG and water contents

are mainly determined by the spatial distribution of cell density, while the spatial distribution of cell density is determined by the nutrition environment. Thus, the simplifications on the mechanical properties are not significant on the spatial distributions of the cell density, GAG and water contents.

In summary, the effects of different nutritional supplies and pathways on the disc degeneration patterns (in terms of distributions of cell viability, GAG content, and water content) were quantitatively studied using a three-dimensional finite element model developed based on the cell-activity-coupled mechano-electrochemical multiphase mixture theory [25, 168]. The disc degenerative patterns were quantitatively predicted and linked to the levels and pathways of the nutrition supply. This study provides a better understanding of the mechanisms of poor nutrition related disc degeneration as well as new knowledge on the diagnosis of early disc degeneration.

Chapter 7 Simulation of Disc Repair with Biological Therapies

7.1 Introductory Remarks

Low back pain is a prevalent health problem which affects more than 600 million people worldwide [4, 94, 95]. The cause of the low back pain is still not definitive, however, the intervertebral disc (IVD) degeneration is strongly associated with it [1, 193]. IVD degeneration is generally described as a cascade of progressive changes in biological, chemical, electrical, and mechanical events, which eventually leads to disc failure [1, 7, 26, 65, 119, 156, 194].

Traditional treatment methods for IVD degeneration involve conservative treatments (e.g., physiotherapy, core strengthening and other exercise modalities) and surgical interventions (such as spinal fusion or prosthetic disc replacement) [65]. Although these treatments alleviate some symptoms, they cannot stop the degenerative progression, nor restore the structure or function of the IVD [65]. The long-term efficacy of these treatments is not promising either, as many treated patients experience recurrent pain, reduced spinal mobility, and/or adjacent segment degeneration [65]. New therapies aiming to halt and/or regenerate the IVD degeneration are of crucial significance in treating the IVD degeneration-related spinal disorders. Regenerative therapies such as the biological therapy have been intensively studied in recent years. The idea of the biological therapy is to restore disc structure and function through implanting functional cells, stimulating the matrix synthesis, and/or inhibiting the matrix degradation activities in the disc [66, 67].

Cell implantation has been applied to a few clinical trials (a detailed review can be found in Benneker et al [67] and Sakai and Andersson [66]). These clinical trials showed positive treatment outcomes, including increases in tissue water content and disc height in the patients under therapy [68-72], except one study in which no improvement in pain relief after one-year follow-up was reported [73]. These studies showed a great potential of the cell therapy in retarding and/or reversing disc degeneration. Nonetheless, many critical issues in relation to the therapies are unaddressed, such as the number of cells needed, the time required for repair, the nutrients demanded by the implanted cells, and the long-term (such as 5, 10, or more years) efficacy of biological therapies. These issues are challenging and costly to address experimentally.

Numerical simulations are an alternative means to investigate the process of disc degeneration or regeneration quantitatively and can provide insights into the complicated biological, chemical, electrical, and mechanical events in discs under pathophysiological conditions, which might be difficult to measure directly or simultaneously in vivo. Recently, a numerical model for human discs has been developed based on the finite element method and cell-activity-coupled mechano-electrochemical theory [161, 168]. This model can be used to predict not only the distributions of cell density, water content, glycosaminoglycan (GAG) content, glucose concentration, oxygen concentration, lactate concentration, pH value, mechanical stresses and strains in the disc, but also the variations of disc height, GAG content, and water content with the progression of disc degeneration [25, 161, 168]. This model is unique in the sense that not only the transport of nutrients and metabolic wastes as well as fluid flow are coupled with tissue deformation (or

hydration), but also the tissue deformation, GAG content, and water content are coupled with cell density [25, 161, 168].

This model was validated by simulating the degenerative progression in the IVD with initial GAG and water distributions from a 27-year old healthy lumbar disc [15, 168]. The predicted distributions of GAG and water contents in the disc with reduced nutrition supply for 27 years (i.e., at age of 54 years) were calculated and compared with the experimental data measured in human cadaveric discs of average age of 54 years, reported in the literature [155]. It was found that model predictions were consistent with the results in the literature [168].

In this study, we attempt to use this model to numerically investigate the repair processes in the degenerated discs treated with biological therapies and to analyze the long-term efficacy of these therapies.

7.2 Methods

The details of the finite element model for human lumbar discs used in the current study can be found in Chapter 5. Briefly, the model took into account of the cell viability and metabolism, transport of interstitial fluid, ions, glucose, oxygen and lactate, GAG synthesis/degradation, tissue swelling, and mechanical stresses and strains in the disc. The coupling of transport properties of fluid and solutes with tissue deformation (or hydration) was considered. The cell viability was assumed to depend on the local glucose concentration only and the cells were assumed not to proliferate in the disc. The cell metabolisms (consumptions of glucose and oxygen, and production of lactate) were related to local glucose, oxygen, and lactate (or pH value) concentrations in the tissue according

to Bibby et al. [37]. The rate of GAG content change (Q^{GAG}) was related to the GAG synthesis rate (Q^{syn}) and the GAG degradation rate ($Q^{\deg}$) by: $Q^{GAG} = Q^{syn} - Q^{\deg}$, where Q^{syn} was a function of local cell density (ρ^{cell}) with $Q^{syn} = \lambda_1 \rho^{cell}$, and $Q^{\deg}$ was assumed to be proportional to the value of local GAG content (C^{GAG}) by $Q^{\deg} = \lambda_2 C^{GAG}$. In the current study, the value for GAG synthesis rate per cell (i.e., λ_1) was assumed to be an invariant with time (its value may vary from region to region[168]) and it does not directly correlated with the cell metabolism. The value of λ_1 at the healthy state was used in this study [168], see below. The value of λ_2 was assumed to be constant, and calculated from the half-life time of GAG turnover in the disc [116, 168]. More information on the model can be found in Table 7.1.

In this study, three types of biological therapies were simulated: Case I - increasing cell density, Case II - increasing GAG synthesis rate, and Case III - decreasing GAG degradation rate. Two degenerative discs were treated with each of the three types of therapies; one was a mildly degenerated disc (20% loss in cell number, 7% decrease in GAG content, 5% decrease in water content in the NP, and 2.2% decrease in disc height, see Figs. 7.1 C and D. All are relative to the healthy state), and the other was a severely degenerated disc (70% loss in cell number, 30% decrease in GAG content, 15% decrease in water content in the NP, and 8% decrease in disc height, Figs. 7.1 E and F). Examples for the distributions of cell density, oxygen concentration, glucose concentration, lactate concentration, and mechanical stresses in the degenerated discs can be found in Chapter 5.

Only the NP region of the discs was treated, as the NP undergoes major compositional and morphological changes with disc degeneration. For Case I, three cell density values (4000 cells/mm^3, 8000 cells/mm^3, and 12000 cells/mm^3) were investigated. In Case II, the GAG synthesis rate (i.e., λ_1) in the NP was increased by 100% (from 0.911×10^{-5} mmol/g dry weight/hr to 1.822×10^{-5} mmol/g dry weight/hr). In Case III, the relative GAG degradation rate in the NP (i.e., the value of λ_2) was decreased by 50%, i.e., 1.997×10^{-9}/s to 0.9986×10^{-9}/s [168]. For comparison, a control case (without treatment) was also simulated.

Effects of the nutrition supply on the therapy outcomes were also studied by adjusting the nutrition (i.e., glucose, oxygen) level at disc boundaries. Glucose and oxygen concentrations on the IVD boundary at the healthy state were set as: 3.2 mM, and 3.6 kPa on the NP surface adjacent to the endplate; 5.0 mM and 5.8 kPa on the AF periphery [25, 147, 168]. These values were defined as the normal nutrition level on IVD boundaries. Therapies at various nutrition levels at the NP surface (0%, 15%, 30%, 50%, and 100% of the normal nutrition level mentioned above), while nutrition level at the AF boundary remained the same as normal nutrition level, were simulated in the severely degenerated discs for Case I. For Cases II and III, the normal nutrition level at the disc boundary was used.

Table 7. 1: List of Variables and Assumptions used in the Model

Constituent	Variable	Diffusion/ Convection*	Bio-reaction	Comment
Solid matrix	Displacement vector	No	No (excluding cells & proteoglycan)	Deformation is coupled with swelling pressure (or fixed charge density) and fluid flow [6, 102].
Cell	Cell density	No	Yes	Cells start to die when local glucose concentration is below the threshold (0.5 mM) [20]. No proliferation is assumed. Cells are fixed to solid matrix.
Proteoglycan (GAG)	GAG content	No	Yes	It depends on cell density, GAG synthesis rate per cell, and GAG degradation rate. GAG content is assumed to be proportional to fixed charge density [168]. Proteoglycan is a part of solid matrix.
Water	Chemical potential of water	Yes	No	Hydraulic permeability is tissue deformation (or hydration) dependent [150].
Cation (Na^+)	Electrochemical potential of cation	Yes	See comment	Its concentration depends on GAG content (or fixed charge density) [168]. Diffusivity is tissue deformation (or hydration) dependent [110].
Anion (Cl^-)	Electrochemical potential of anion	Yes	See comment	Its concentration depends on GAG content (or fixed charge density) [168]. Its diffusivity is tissue deformation (or hydration) dependent [110].
Glucose	Chemical potential of glucose	Yes	Yes	The rate of consumption by cells is a function of local glucose and oxygen concentrations and pH [37]. Its diffusivity is tissue deformation (or hydration) dependent [110].

Oxygen	Chemical potential of oxygen	Yes	Yes	The rate of consumption by cells is a function of local oxygen concentration and pH [37]. Its diffusivity is tissue deformation (or hydration) dependent [110].
Lactate	Chemical potential of lactate	Yes	Yes	The rate of production by cells is a function of local glucose and oxygen concentrations and pH [37]. Its concentration is related to pH value [37]. Its diffusivity is tissue deformation (or hydration) dependent [110].

*All fluxes are relative to solid matrix

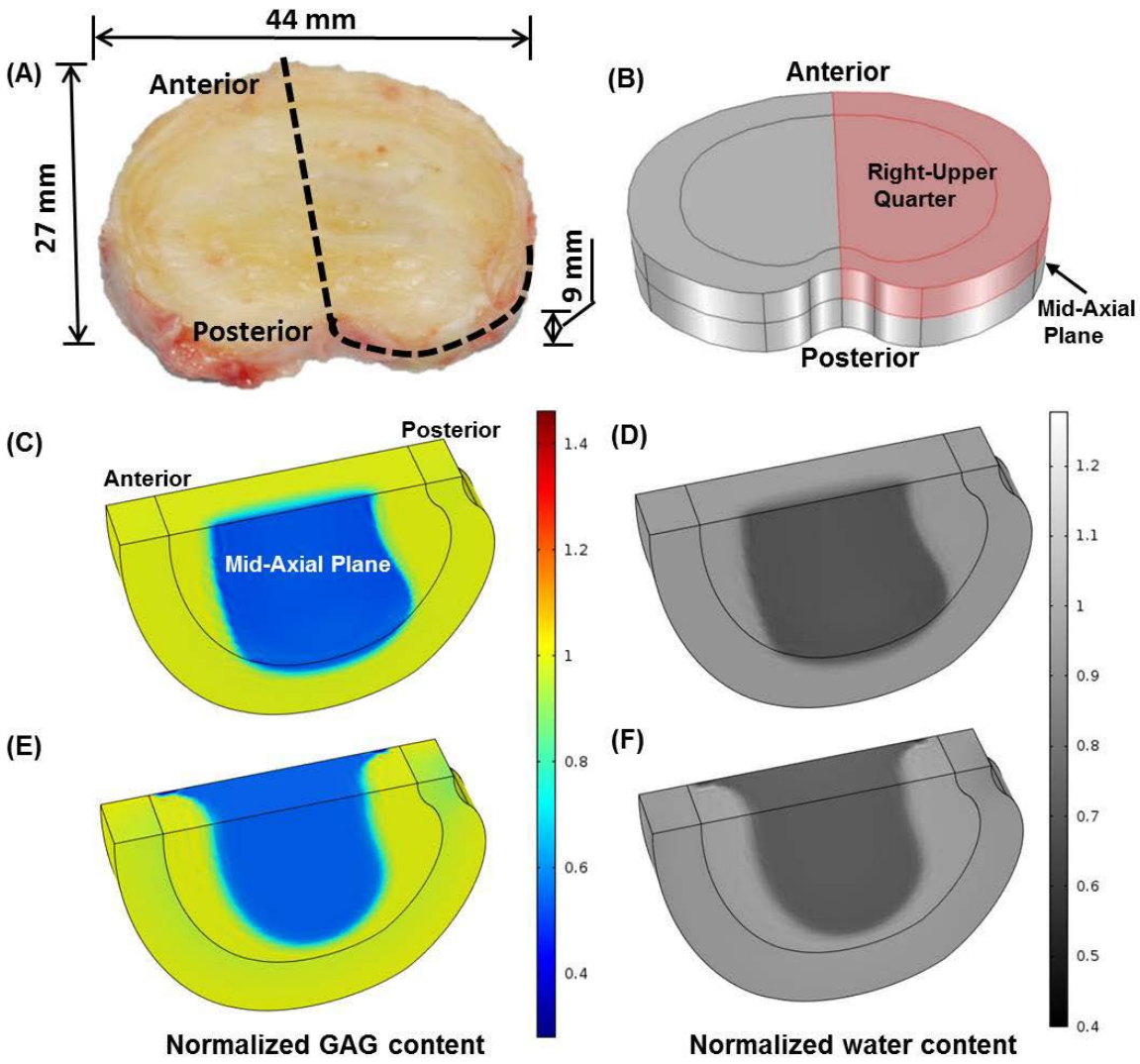

Figure 7. 1: (A) A picture of a human lumbar disc (L2-3, male, non-degenerated) [105]. (B) The upper-right quarter of the disc for simulation. (C) GAG content and (D) water content distributions in the mildly degenerated disc before treatment. (E) GAG content and (F) water content distributions in the severely degenerated disc before treatment. All values are normalized to that at the healthy state.

7.3 Results

Treatments with Increasing Cell Density in the NP (Case I)

The treatment outcomes were predicted to be cell density dependent. The higher the cell density, the more rapid the repair process would occur. For example, in the severely degenerated disc after treatments with a cell density of 12000 cells/mm^3 and 8000 cells/mm^3, the normalized GAG content (averaged over the NP) increased from the initial value of 70.0% to 100% (i.e., the value at healthy state) in 2.57 years and 4.56 years, respectively; the normalized water content (averaged over the NP) elevated from the initial value of 85% to 100% (i.e., the value at healthy state) in 2.44 years and 4.29 years, respectively; and disc height returned (from the initial value of 91.9%) to 100% (i.e., the value at healthy state) in 2.4 years and 4.3 years, respectively, see Figs. 7.2-7.4. In contrast, the repair process was much slower for the same disc treated with a cell density of 4000 cells/mm^3. The GAG content, water content, and disc height returned to 84.3%, 92.5%, and 96.2% of the corresponding values at healthy state, respectively, at the end of 10 years, see Fig. 7.4.

The treatment outcomes were also predicted to be nutrition level dependent, see Fig. 7.5. A critical nutrition level (defined as the minimum nutrition level at the NP-CEP boundary) to maintain the viability of all the cells within the treated NP were determined (Fig. 7.6). It was found that the higher the cell density is used for the treatment, the higher the critical nutrition level is required.

Treatment with A 100% Increase in the GAG Synthesis Rate in the NP (Case II)

The treatment outcomes were dependent on the disc degeneration stage. For the mildly degenerated disc, it was predicted that overall GAG and water contents increased (Fig. 7.7 A, B, E and F), and disc height returned back to the value at healthy state (i.e., 100%) after 1.88 years (Fig. 7.7G). For the severally degenerated disc, however, it was predicted that there was no significant improvement in the GAG content (Fig. 7.7 C and E) or water content (Fig. 7.7 D and F) in the NP. The normalized GAG content (averaged over the NP) elevated slightly (from initially 70.0% to 71.6%) after 10 years of treatment (Fig. 7.7E). The normalized water content (averaged over the NP) and the disc height continued to decrease with time following the treatment (Fig. 7.7 F and G). It was predicted that normal nutrition level at the disc boundary was sufficient for this treatment, and there was no change in cell density in the disc.

Treatment with a 50% Decrease in the GAG Degradation Rate in the NP (Case III)

It was predicted that the outcomes of this therapy were similar to those in Case II. After treatment, the GAG content (Fig. 7.8 A and I) and water content (Fig. 7.8 E and J) in the NP as well as the disc height (Fig. 7.8K) increased in the mildly degenerated disc, but not in the severely degenerated disc (Fig. 7.8 C, G-K).

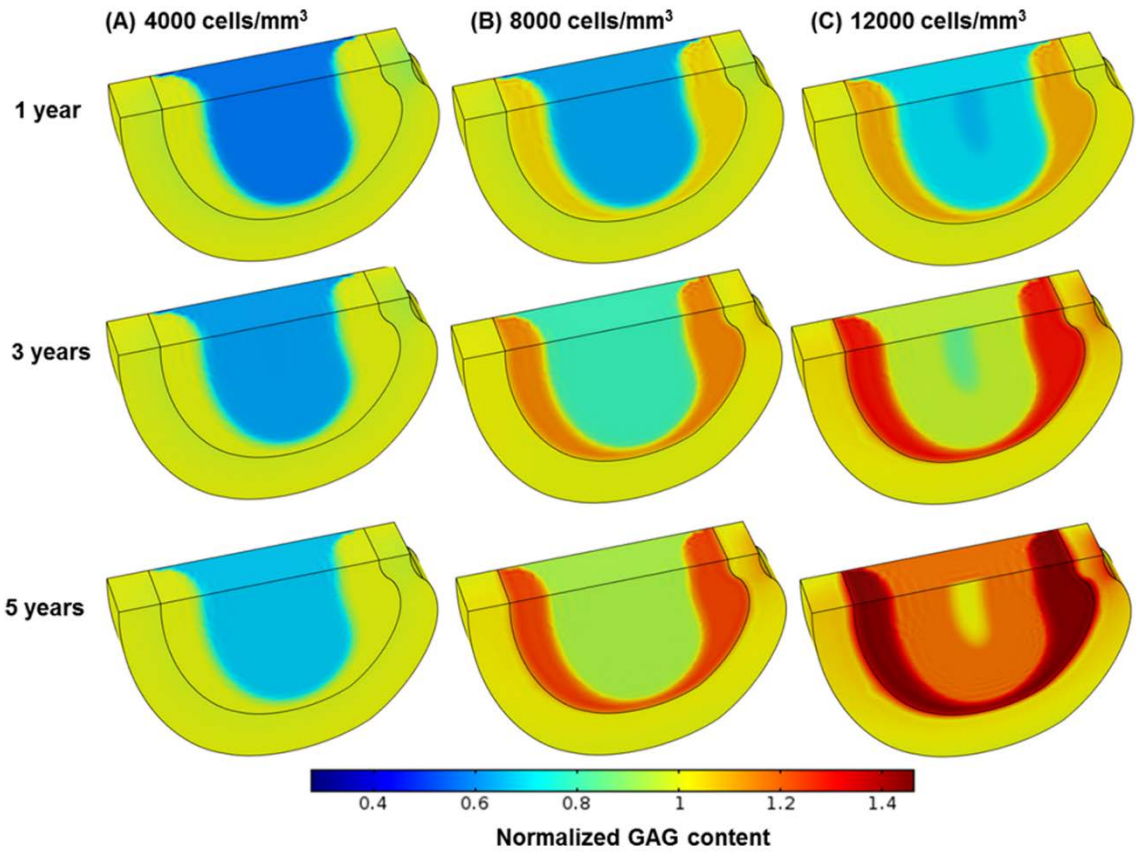

Figure 7. 2: Comparisons of GAG content (normalized to that at the healthy state) in the severely degenerated disc treated with various cell densities in Case I: (A) 4000 cells/mm3, (B) 8000 cells/mm3, and (C) 12000 cells/mm3. The treatment is under normal nutrition level at the disc boundary.

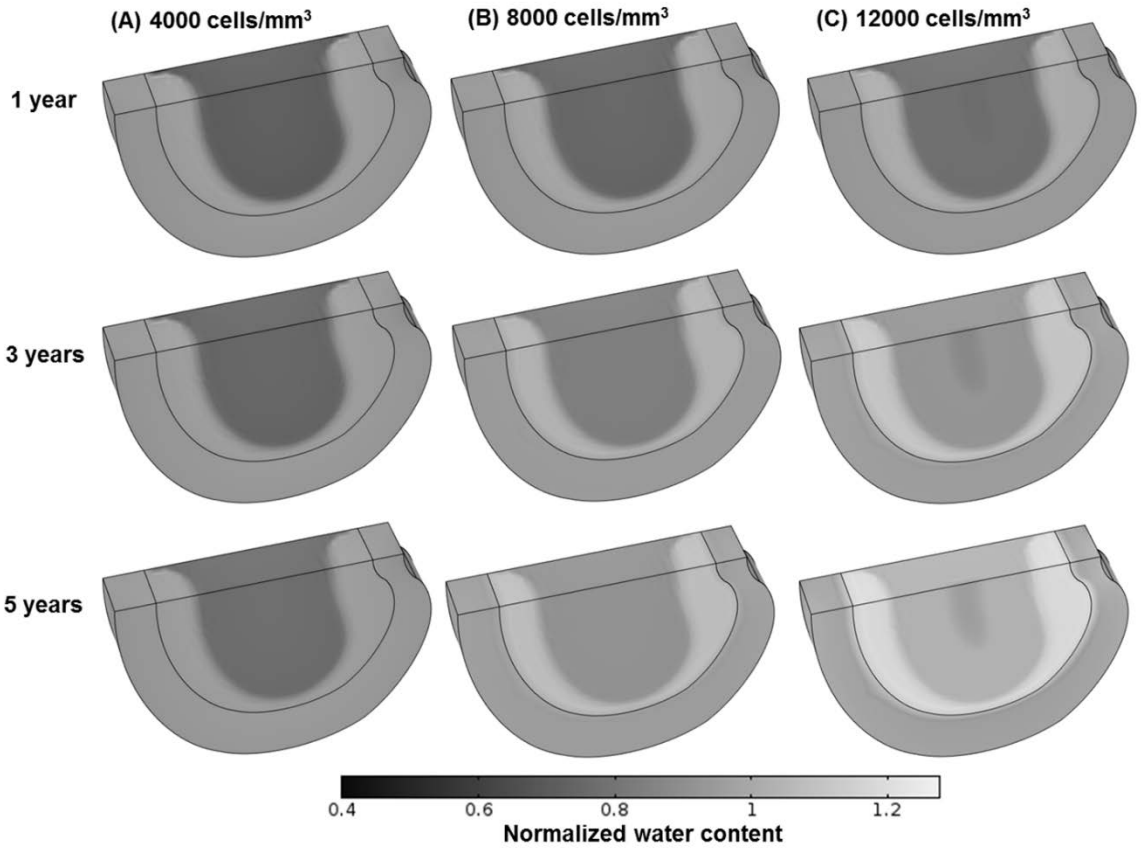

Figure 7. 3: Comparisons of water content (normalized to that at the healthy state) in the severely degenerated disc treated with various cell densities in Case I: (A) 4000 cells/mm3, (B) 8000 cells/mm3, and (C) 12000 cells/mm3. The treatment is under normal nutrition level at the disc boundary.

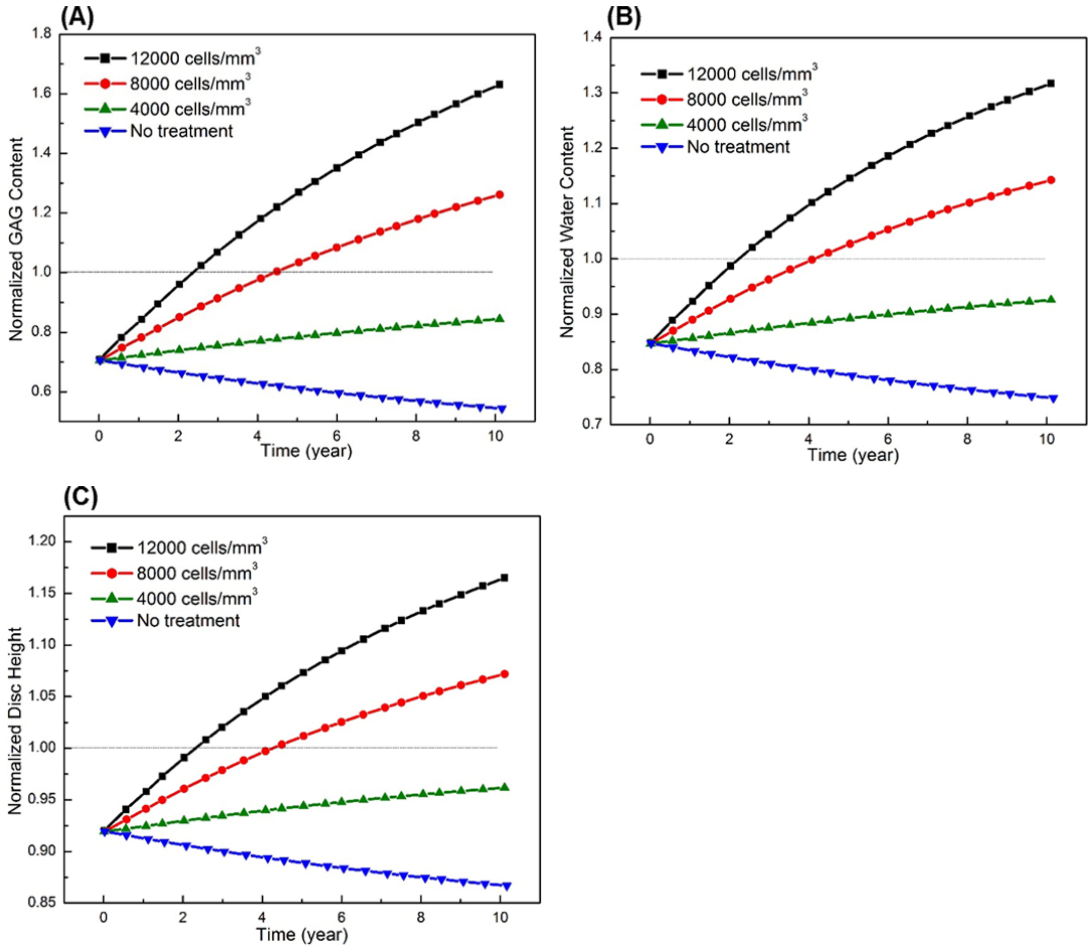

Figure 7. 4: Comparisons of treatment outcomes in the severely degenerated disc treated with various cell densities in Case I: (A) GAG content, (B) water content, and (C) disc height. The treatment is under normal nutrition level at the disc boundary. Values in (A) and (B) are averaged over NP.

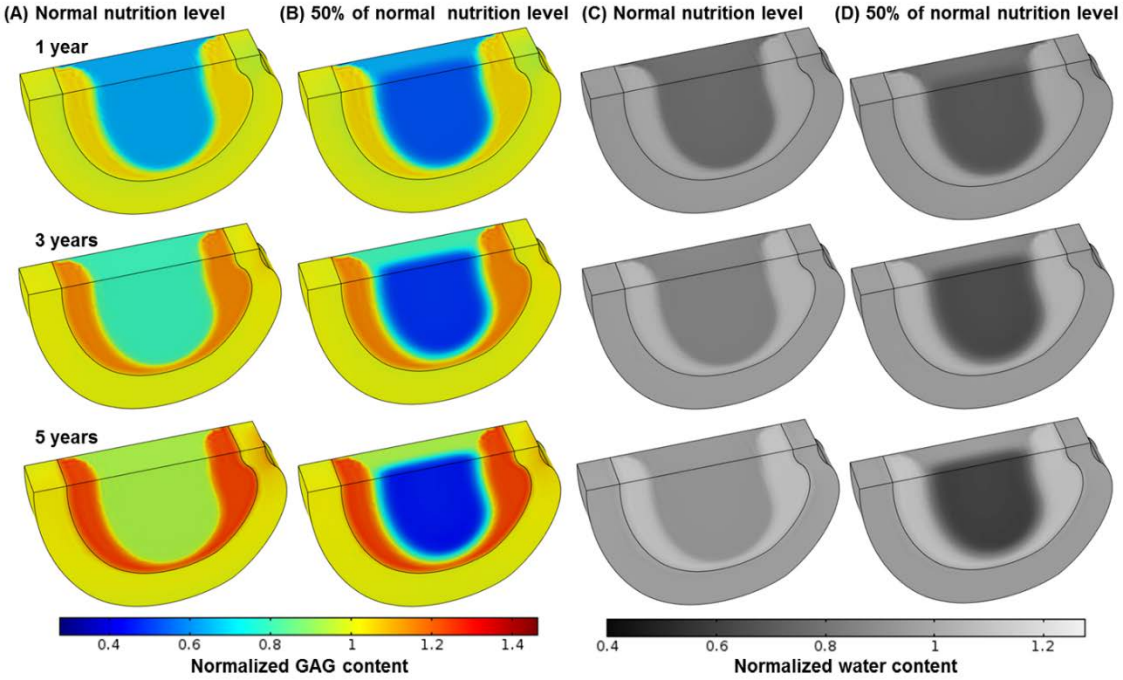

Figure 7. 5: Comparisons of treatment outcomes in the severely degenerated disc treated with a cell density of 8000 cells/mm3 in Case I between normal nutrition level and lower nutrition level (e.g., 1.6 mM for glucose, and 1.8 kPa for oxygen on the NP surface, while normal level remains on AF periphery): (A-B) GAG content, (C-D) water content.

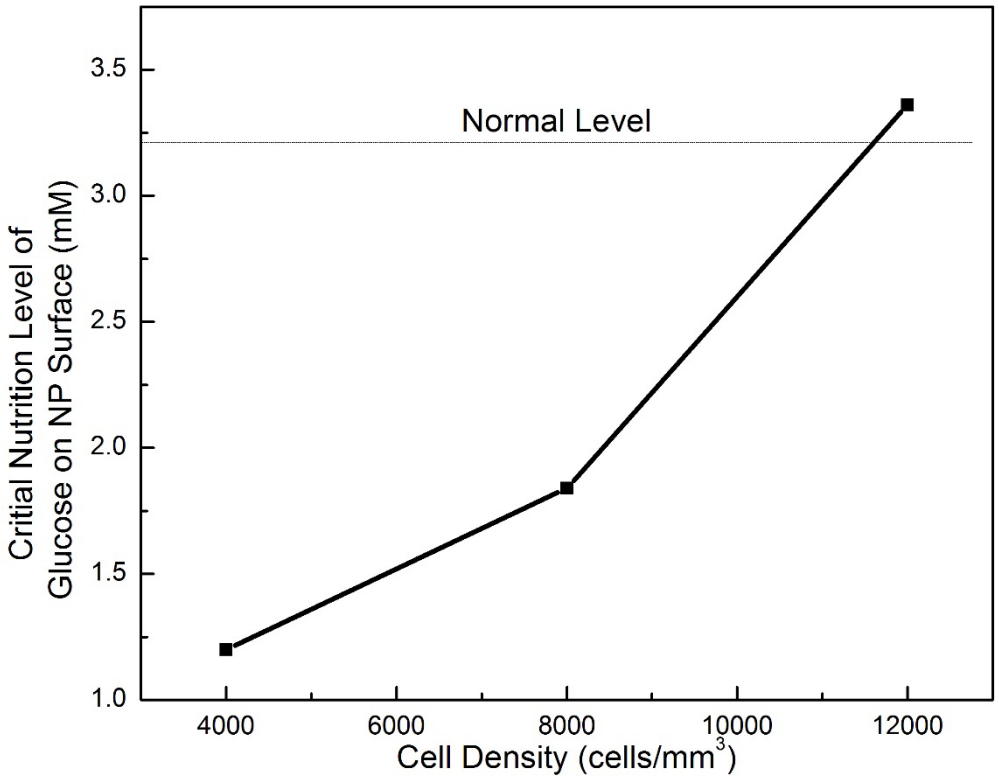

Figure 7. 6: The critical nutrition level (minimum level of glucose at the NP surface for cell survival) versus the cell density in the NP in severely degenerated disc treated with various cell densities in Case I.

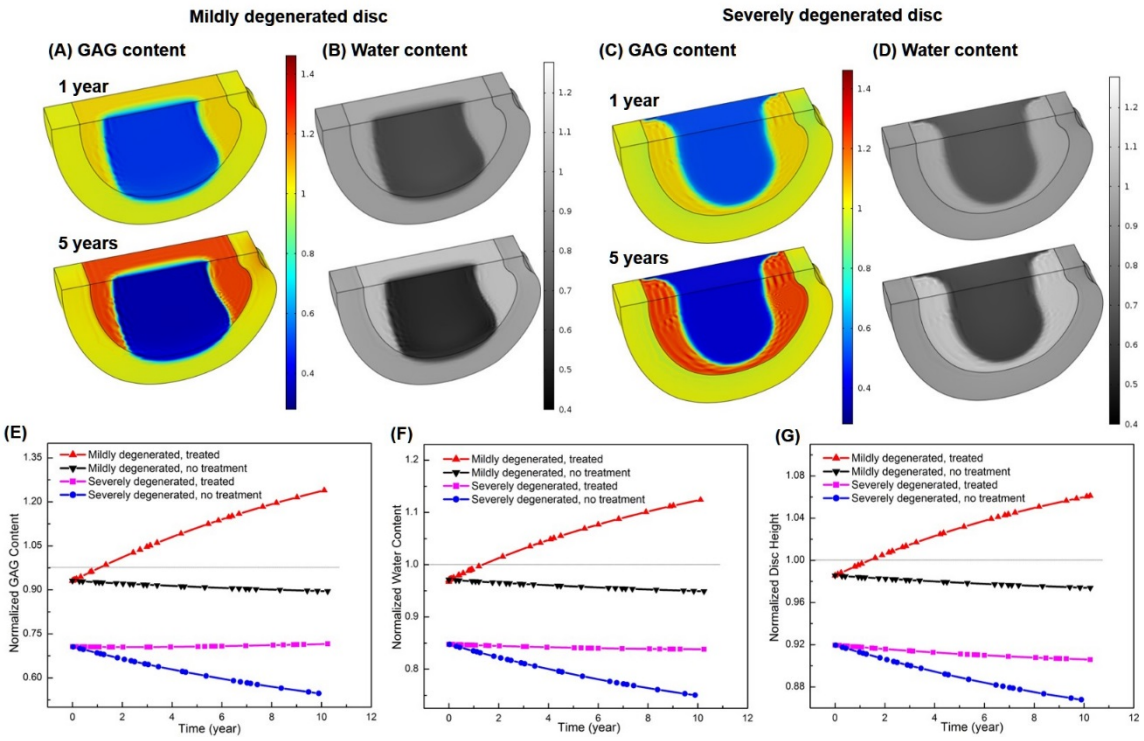

Figure 7. 7: Comparison of treatment outcomes between mildly and severely degenerated discs and between non-treated (control) and treated discs in Case II (i.e., increasing GAG synthesis rate in the NP): spatial distributions of GAG content (A, C) and water content (B, D), and temporal variations of GAG content (E), water content (F), and disc height (G). The treatment is under normal nutrition level at the disc boundary. All the values are normalized to that at the healthy state. Values in (E) and (F) are averaged over NP.

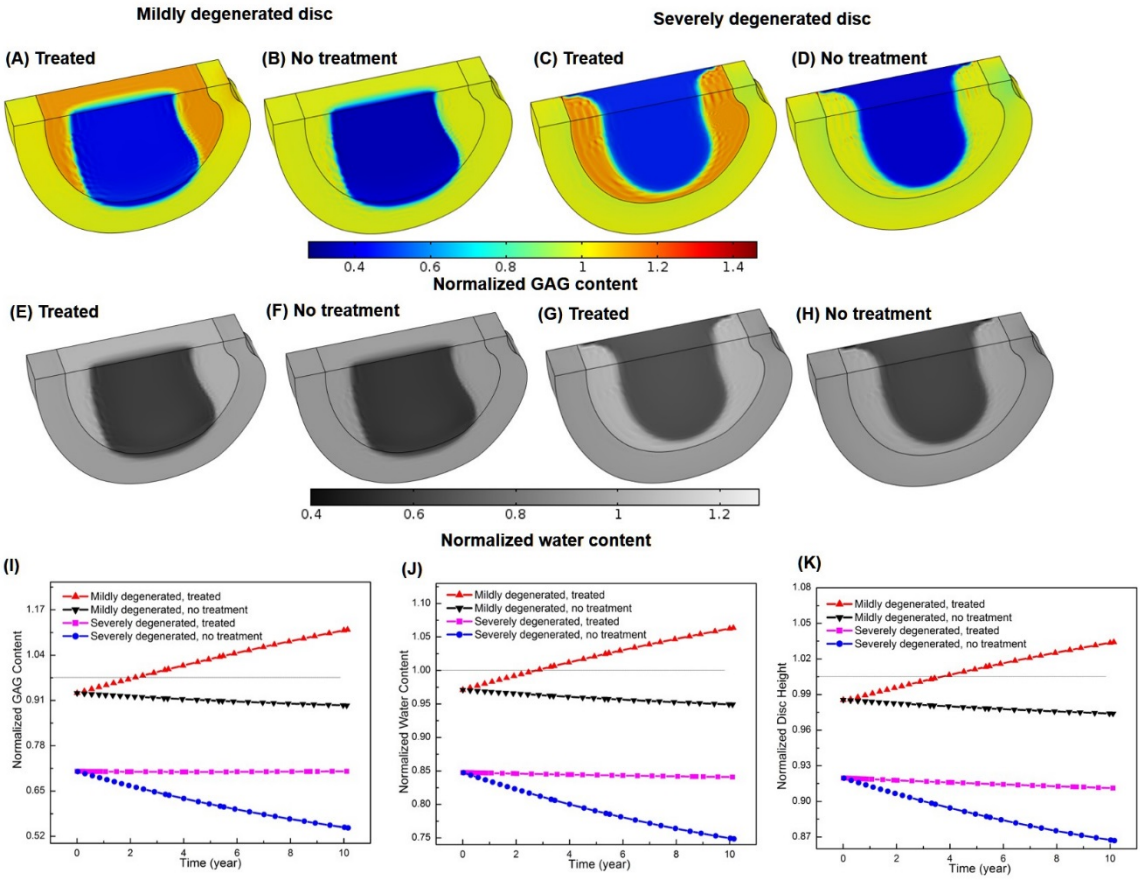

Figure 7. 8: Comparison of treatment outcomes between mildly and severely degenerated discs and between non-treated (control) and treaded discs in Case III (decreasing GAG degradation rate in the NP): spatial distributions of GAG content (A-D) and water content (E-H) after 5 years, and temporal variations of GAG content (I), water content (J), and disc height (K). The treatment is under normal nutrition level at the disc boundary. All values are normalized to that at the healthy state. Values in (I) and (J) are averaged over NP.

7.4 Discussion

Three types of biological therapies for disc repair were simulated in this study. The predicted results indicate that therapy with increasing cell density in the NP (i.e., Case I) is effective for both mildly and severely degenerated discs. Our simulated results for water content and disc height in Case I are qualitatively consistent with those reported in the clinical trials and in an animal model treated with cell implantation [68-73, 195, 196].

For instance, intervertebral disc repair using autologous chondrocyte transplantation has been investigated in a dog model for up to 12 months [196]. Results from this study indicate that cell implantation improves disc height retention and leads to increased matrix components [196]. Similar studies have also been conducted in human intervertebral discs [68, 72, 195]. For example, one study showed that fluid content in the treated group of human patients was considerably higher than that in the control group at a 2-year follow-up [68].

Note that this therapy requires higher nutrition supply to the disc in order for the newly implanted cells to survive and function. The level of nutrition supply to the disc in this therapy depends on the number of implanted cells. When treating discs with implanting a large number of cells, or discs with poor nutrition supply from the nearby blood vessels, it is crucial to improve the nutrition condition within the disc for successful treatment outcomes.

Our analysis indicates that the therapies with a cell density of 4000 and 8000 cells/mm^3 in the NP (Case I) do not exceed the nutrition supply when the normal nutrition level is applied on disc boundaries (Fig. 7.6). In the therapy with a cell density of 12000 cells/mm^3,

however, there is a small amount of cell death in a tiny region (0.34% of total NP volume) near the NP center (Fig. 7.6). Cell density in the NP is dependent primarily on the glucose concentration at the boundary, glucose diffusivity, glucose consumption rate per cell, and disc thickness [18]. Using the approach by Maroudas et al (1975) [18], we have re-derived their Equation 2 in Appendix of their paper and used it to estimate cell density in the NP. Assuming the glucose consumption rate was $5x10^{-11}$ mmol/cell/hour [18], one could estimate the maximum cell density in the NP in the disc (with 9 mm thickness) being ~15,000 cells/mm^3 for a glucose diffusivity of $5.2x10^{-6}$ cm^2/s, an average value for NP used in our study. Note that the glucose diffusivity in water at 37 ^{o}C is around 9.4×10^{-10} m^2/s [197], the value of glucose diffusivity for NP used in our study reflects 55% of the value in the water, which is consistent with the values in cartilaginous tissues reported in the literature [18, 198, 199].

Degenerative progression in the discs with reduced nutrition supply is a very slow process [183]. For example, in Chapter 5, the predicted results indicated that a 5% decrease in water content in the NP would take about 10 years. This is because matrix turnover is very slow [116]. In adults, disc height and volume do not increase with time, indicating the GAG synthesis rate (per cell) is also slow in order to balance the slow rate of GAG degradation. This is why the repairing process in the disc with implanting normal cell density (i.e., 4000 cells/mm^3) takes a long period of time (Figs. 7.2-7.4).

In the current study, the implanted cells for Case I were assumed to have the same properties as those for adult human NP cells. Disc repair with implanting different types of cells can also be simulated if information on these cells (e.g., nutrient threshold for cell viability, cell metabolism, and GAG synthesis rate) is available.

Therapies with increasing the GAG synthesis rate (Case II) and decreasing the GAG degradation rate (Case III) are predicted to be effective primarily for mildly degenerated discs, and not effective for severely degenerated disc. This may be because the number of viable cells in the NP of the severely degenerated disc is low, e.g., only 30% of the normal value (compared to 80% in the mildly degenerated disc simulated). The amount of GAG synthesized by the viable cells could not exceed the amount of GAG breakdown in this simulated disc, even though the GAG synthesis rate (per cell) for the remaining cells in the NP is doubled (Case II), or the GAG degradation rate is reduced by half (Case III), thus resulting in no improvement in GAG content or water content or disc height within the treated disc. Thus, the number of viable cells in degenerated discs is crucial for the success of therapies in Case II and Case III.

One of the differences between Case II and Case III is the demand of nutrients for the synthesis of GAG, that is, more nutrients are expected for the therapy in Case II than in Case III because of the increase in GAG synthesis rate in Case II. From this point of view, the therapy with decreasing GAG degradation rate (Case III) may be more attractive for the mildly degenerated discs, especially for the degenerated discs with a deficiency in nutrition supply.

Nutrition supply is also important for the therapy in Case II (i.e., increasing the GAG synthesis rate). In this study, the GAG synthesis rate by the cells is not directly correlated with the cell metabolism. This is a limitation of the current study. However, this limitation may not have significant influences on the results in this work because the total nutrition supply to the disc is sufficient to maintain the elevated cellular synthetic activities. In our model, the total influx of the glucose into the disc from all the boundaries at the mildly

degenerated disc in Case II (i.e., 7.0×10^{-10} mmol/s) is about 90 times larger than the rate of glucose required for the synthesis of disaccharide units of GAG (7.4×10^{-12} mmol/s), assuming two glucose molecules are required to synthesize one disaccharide unit of a GAG molecule [200].

Another limitation of this study is that the GAG synthesis rate per cell in the NP is assumed to be constant during the repair process. This assumption leaded to the overestimate of the GAG and water contents as well as the disc height in all three types of therapies (Figs. 7.4, 7.7, and 7.8) because the GAG synthesis rate (per cell) would decrease when the cell volume (or cellular environment) deviates from its optimal value [133, 201-204]. One more limitation is that the intrinsic mechanical properties of the matrix (Lame constants λ and μ) were assumed to be constant during degeneration and repair processes (did not change with tissue compositional changes). This assumption would have an effect on the estimation of tissue height change. These issues will be considered in our future studies.

In conclusion, this study has simulated and predicted the effects of three types of biological therapies for disc repair using a finite element method. The predicted results indicate that while all three types of therapies are effective for mildly degenerated discs, only the therapy with increasing cell density is effective for severely degenerated discs. This study provides not only additional insights into disc degeneration and repair processes, but also a quantitative guide for choosing proper treatment strategies for disc repair.

Chapter 8 Simulation of Antibiotics Penetration into the Disc

8.1 Introductory Remarks

Antibiotics are used in the perioperative prophylaxis and treatment of intervertebral disc (IVD) infections. Due to avascular nature of the IVD, antibiotics have to transport (mainly by diffusion) into the IVD from blood vessels at disc boundaries. Penetration of antibiotics into IVD has been studied in animals [205-211] and humans [212-215]. These studies have suggested that the ability of antibiotics to penetrate into IVDs depends on several factors, such as IVD porosity, antibiotic molecular weight (or size), antibiotic charge, etc. [205, 208-210, 212, 216].

It is known that the cartilaginous end-plate (CEP) becomes less permeable with age and degeneration [29, 41] before it disappears [217], and thus affects the penetration of antibiotics into the disc [218]. If the antibiotics are relatively insoluble or have a short metabolic half-life, they may be metabolized before it reaches the minimum inhibitory concentration (MIC) in the disc to inhibit the growth of infecting organism. Another concern is the binding of antibiotics to serum proteins. An antibiotic which binds strongly to serum proteins would result in lower levels of free antibiotic in serum, reducing the concentration gradient for diffusion into the disc [219, 220].

A number of experimental studies have indicated that electrical charge plays a significant role in penetration of antibiotics into discs [207, 209, 210, 212, 215, 221]. Gibson et al (1987) reported that despite high levels of flucloxacillin and cephadrine in serum, little antibiotic could be detected in AF or NP harvested 30 minutes to 4 hours after intravenous (IV) administration in the 12 adolescent patients [212]. Tai et al (2002) examined the

penetration of negatively charged cefuroxime and positively charged gentamicin into patients and they found that gentamicin diffused into discs much easier than cefuroxime [215]. Conaughty et al (2006) found that bacterial growth in disc treated with positively charged vancomycin was slower than that treated with negatively charged linezolid. They stated that differences in the electrical charge between the two molecules may affect the penetration of the molecules into the discs [221]. Riley et al (1994) studied the penetration of positively charged gentamicin and negatively charged penicillin into a rabbit IVD model and reported that penicillin has less ability than gentamicin to penetrate into the negatively charged nucleus pulposus (NP) [209]. Thomas et al (1995) found that uptake of positively charged aminoglycosides was higher than that of the negatively charged penicillins and cephalosporins, and the uncharged ciprofloxacin showed an intermediate degree of uptake in a mouse disc model [210]. Results from these studies either directly suggested or indicated that positively charged antibiotics have easier access to or higher uptake in the discs than the negatively charged ones.

In spite of many experimental data on antibiotic penetration into disc have reported, there is a lack of analytic tools to predict kinetics of charged antibiotic transport in the IVD. Thus, the objective of this study was to quantitatively analyze and compare the penetration of differently charged antibiotics (positively, negatively, and uncharged) into human lumbar discs with a finite element method, to understand the effect of electrical charge on the kinetics of antibiotic penetration into the IVD.

8.2 Methods

The Theoretical Framework

A multiphysics model for IVD has been developed based on the triphasic continuum mixture theory [6]. In this model, the disc was modeled as an inhomogeneous, porous, mixture consisting of a charged solid phase, a fluid phase, and a solute phase (with multiple species of solutes, e.g., Na+, Cl- , antibiotics). The material properties, such as fixed charge density, hydraulic permeability, solute diffusivities were nonlinearly coupled with tissue deformation (or tissue hydration). The interactions among tissue deformation, electrical charge, fluid and solute transport were taken into consideration in the model. The governing equations were cast in terms of displacement of solid matrix and (electro)chemical potentials of fluid and solutes. For example, the equation of mass balance for the antibiotic (A) is given as

$$\partial\left(\phi^{w}c^{A}\right)\Big/\partial t+\nabla\cdot(\mathbf{J}^{A}+\phi^{w}c^{A}\mathbf{v}^{\mathbf{s}})=0\,, \tag{8.1}$$

where ϕ^{w} is the water volume fraction (or, tissue porosity, or water content), c^{A} is the molar concentration (per unit fluid volume) of the antibiotic, J^{A} is the molar flux of the antibiotic ~~A~~ (relative to the solid phase), and v^{s} is the velocity of the solid phase. In equation (1), the binding effect was neglected because the main focus of this study was to investigate the charge effect on antibiotic penetration into charged disc tissues.

The molar flux of the antibiotic can be expressed as:

$$\mathbf{J}^{A}=H^{A}c^{A}\mathbf{J}^{\mathbf{w}}-\frac{\phi^{w}c^{A}D^{A}}{\varepsilon^{A}}\nabla\varepsilon^{A}\,, \tag{8.2}$$

where H^A is the convection coefficient (hindrance factor) of the antibiotic, J^w is the volume flux of water relative to the solid phase, D^A is the diffusivity of the antibiotic in the disc tissue which depends on the ratio of antibiotic size (hydraulic radius r^A) and the intrinsic Darcy permeability of the tissue (k): $D^A = D_0^A \cdot \exp[-\alpha(\frac{r^A}{\sqrt{k}})^\beta]$ [110], where D_0^A is the diffusivity of antibiotic in water, and α and β are two positive parameters dependent on the structure of the disc. ε^A is the modified (electro)chemical potential of the antibiotic, which is related to the molar concentration (per unit fluid volume) of the antibiotic c^A by the following equation:

$$c^A = \frac{\varepsilon^A}{\gamma_A}[\exp(z^A \frac{F_c \psi}{RT})]^{-1}, \tag{8.3}$$

where γ_A is the activity coefficient of the charged antibiotic in tissue, z^A is the valence of the net electrical charge of the antibiotic, F_c is the Faraday constant, ψ is the electrical potential within the disc, R is the gas constant, T is the absolute temperature. The electrical potential ψ can be solved with the electro-neutrality equation [222]:

$$\sum_\alpha z^\alpha c^\alpha = 0, \tag{8.4}$$

where z^α is the valence of the charged solutes or fixed charge in the disc, and c^α is the concentration of the corresponding solute or fixed charge. For the solutes considered in this study (i.e., Na^+, Cl^-, antibiotics), Eq. (8.4) reduces to,

$$c^+ - c^- + z^A c^A - c^F = 0. \tag{8.5}$$

Other governing equations for the solid deformation, fluid flow, ions and nutrients transport can be found in our recent publication [161].

Finite Element Model

A 3D finite element model for IVDs was developed based on the framework stated above. Antibiotic penetrations into a healthy IVD model were simulated in this study. The IVD height was 10 mm and the CEP thickness was 0.6 mm [based on a human L2-3 disc [104, 161], see Fig. 8.1A. The IVD was modeled as an inhomogeneous structure with three regions: nucleus pulposus (NP), annulus fibrosus (AF), and cartilage endplate (CEP). The disc was attached to a part of the vertebra (Fig. 8.1B) and the displacement boundary condition (Fig. 8.1C) was applied on the top of the vertebra surface. Since the vertebra is about 10 times stiffer than the disc, the effect of the vertebra height on disc deformation was assumed to be negligible. Thus, only a small part of the vertebra was included in the model to reduce computational cost. Due to symmetry, only the upper-right quarter of the disc-vertebra segment was modeled (Fig. 8.1B). COMSOL software (COMSOL 4.3b, COMSOL, Inc., MA) was used to solve a system of partial differential equations [161, 168].

The material properties (including the mechanical properties, transport properties, and electrochemical properties) used in this study were similar to those used in Gu et al [168] for the disc and vertebral bone, and in Zhu et al [161] for CEP. Briefly, it is assumed that these material properties were uniform in the NP and CEP, whereas varied linearly from the innermost AF to the outermost AF. The values of the mechanical properties (Lame constants λ and μ), fixed charge density, and water content were obtained from experimental results, with λ=15.6 kPa and μ=0.18 kPa in the NP; λ=100 kPa and μ=200

kPa in the CEP, and λ linearly increased from 15.6 kPa to 300 KPa for the regions from the inner most AF to the AF periphery, and μ linearly increased from 0.18 kPa to 100 kPa for the regions from the innermost AF to the AF periphery [144, 152, 223]. The vertebra was modeled as a single-phase, linear elastic solid with mechanical properties of λ=86.5 MPa, and μ=57.5 MPa [165]. The fixed charge density was 342.5 mM and water content (volume fraction) was 0.85 in the NP. The fixed charge density was 90 mM and water content was 0.6 in the CEP. Fixed charge density linearly decreased from 342.5 mM to 163.4 mM from the innermost AF to AF periphery. Water content linearly decreased from 0.85 to 0.7 from the innermost AF to the AF periphery [15].

Three groups of antibiotics were investigated: a positively charged group (Group I: antibiotics with various valences (z), e.g., z=+1, +2), a negatively charged group (Group II: antibiotics with various valences, e.g., z= -1,-2), and a neutral group (Group III, z=0). To eliminate the effects of differences in molecular characteristics (such as molecular weight, size, binding affinity to serum proteins and disc proteins, etc.) on the transport of antibiotics into discs, all the antibiotics are assumed to have the same molecular properties [e.g., molecular weight (400 g/mol), diffusivity in water at 37 ^{o}c (6.2×10^{-10} m^2/s), hydraulic radius (0.53 nm), and blood-disc partition coefficient], except electrical charge. The uptake of the antibiotics by the cells was not considered in the current study.

The serum level of antibiotics post intravenous (IV) administration generally follows such a curve as shown in Fig. 8.1C-I, as reported in the literature for several antibiotics [208, 214, 224, 225]. In this study, the antibiotic concentration in the blood was assumed to peak (i.e., 160 mg/L) at 30 seconds after a single IV administration, then decline exponentially (Fig. 8.1C-I). We assumed that the blood-disc partition coefficient is unity at both the CEP

boundary and the AF periphery for each antibiotic studied. Cases with single and multiple IV administrations of antibiotics (Fig. 8.1C) were simulated.

Our preliminary study showed that a change in electrical potential due to existing and transport of a charged antibiotic was negligible since the molar concentration of an antibiotic (< 0.4 mM) is much smaller than the molar concentration of Na^+ or Cl^- (> 60 mM). Thus, in this study, the antibiotic concentration was neglected in Eq (8.5) to facilitate the simulations.

8.3 Results

Effects of Electrical Charge on Kinetics of Antibiotics Transport into the Disc

It was predicted that concentrations of positively charged antibiotics were higher than those of negatively charged ones at each time point after the single IV administration (Fig. 8.2). The peak concentrations (averaged over the disc) were 29.4%, 16.1%, 8.3%, 4.2%, and 2.1% (of its peak concentration in the serum, i.e., 160 mg/L) for antibiotics with z=+2, z=+1, z=0, z=-1, and z=-2, respectively (Fig. 8.2A). The time to achieve peak value of overall concentration in the disc (averaged over whole disc) was found to be different (Fig. 8.2A), with 5.56 hr, 4.44 hr, 3.89 hr, 2.78 hr, 2.22 hr for antibiotics with valance z=+2, z=+1, z=0, z=-1, and z=-2, respectively. At the center of the disc, the antibiotics reached peak concentrations of 28.2%, 14.5%, 6.7%, 2.8%, and 1.1% (normalized by 160 mg/L) at 13.33 hr, 11.11 hr, 10.00 hr, 9.44 hr, 8.89 hr for valance z=+2, z=+1, z=0, z=-1, and z=-2, respectively (Fig. 8.2B). Assuming the minimum inhibitory concentration (MIC) to be the same for all antibiotics, say, 1 mg/L, the treated regions (defined as drug concentration higher than MIC) in the disc at 2 hours after IV administration was predicted to be much larger by using positively charged antibiotics than negatively ones (Fig. 8.3).

Single IV Administration vs. Multiple IV Administrations

Our simulated results showed that multiple IV administrations of the same antibiotic would effectively maintain the concentration level higher than the MIC (assumed to be 1 mg/L in this study) for a prolonged period of time (Fig. 8.4). For example, the duration of the antibiotic (negatively charged, z=-2) concentration at the levels above the MIC at the disc center increased from ~19 hours to ~37 hours after a second administration was issued at 15 hrs (Fig. 8.4). Comparison of the spatial distribution of the antibiotic (z=-2) in the disc between the single IV administration and double IV administrations were shown in Fig. 8.5.

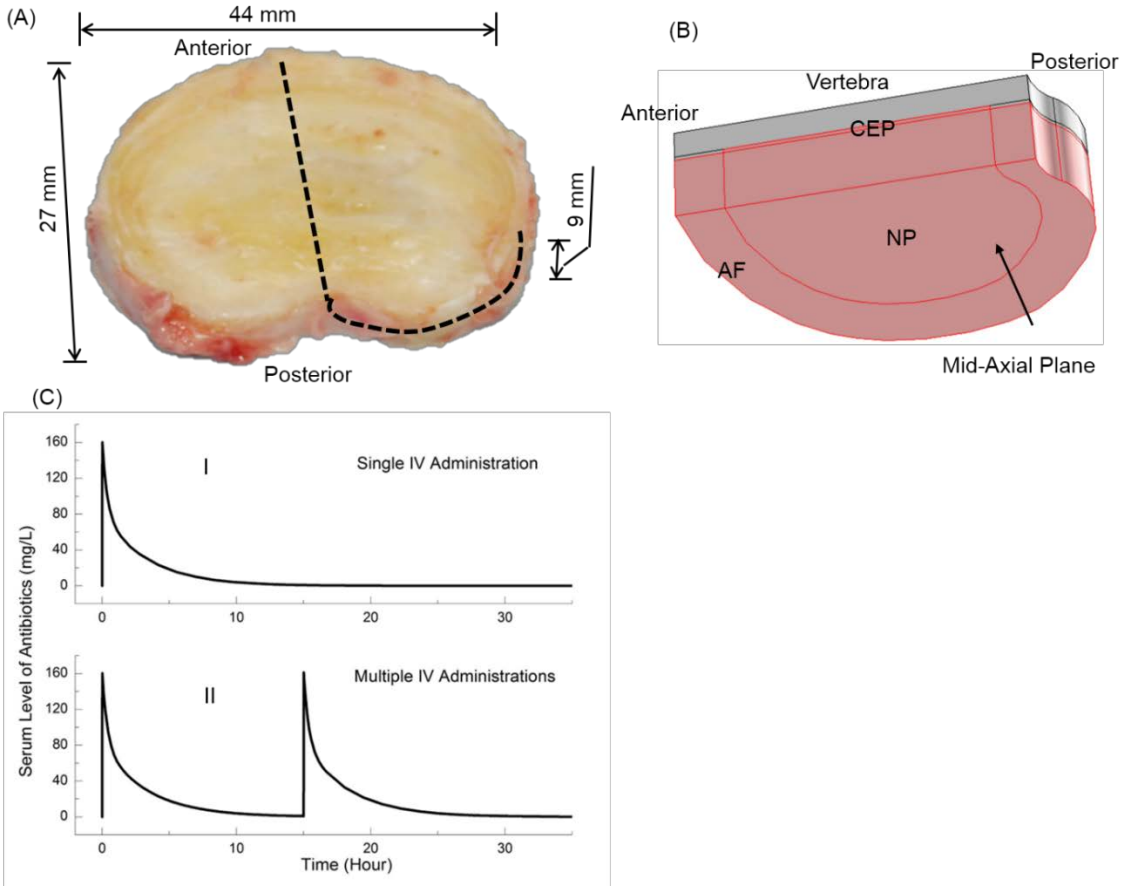

Figure 8. 1: (A) Picture of a human lumbar intervertebral disc (IVD, L2-3, non-degenerated). (B) Schematic of a quarter of the IVD-vertebra segment used in the FEM

analysis (due to symmetry). NP: Nucleus pulposus. AF: Annulus fibrosus. CEP: Cartilaginous endplate. (C) The variation of antibiotic level in serum with time: (I) post an IV administration, and (II) post multiple IV administrations.

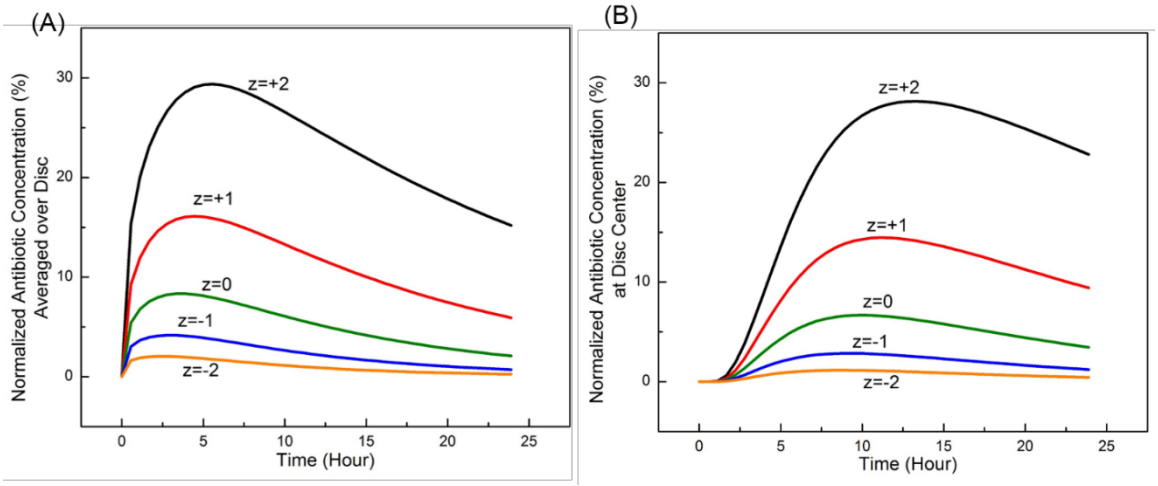

Figure 8. 2: Effect of electrical charge on antibiotic concentrations in a single IV administration: (A) over the disc, and (B) at the disc center. z is the valence of the antibiotics. All the concentrations were normalized to the peak value of the concentration in serum (i.e., 160 mg/L).

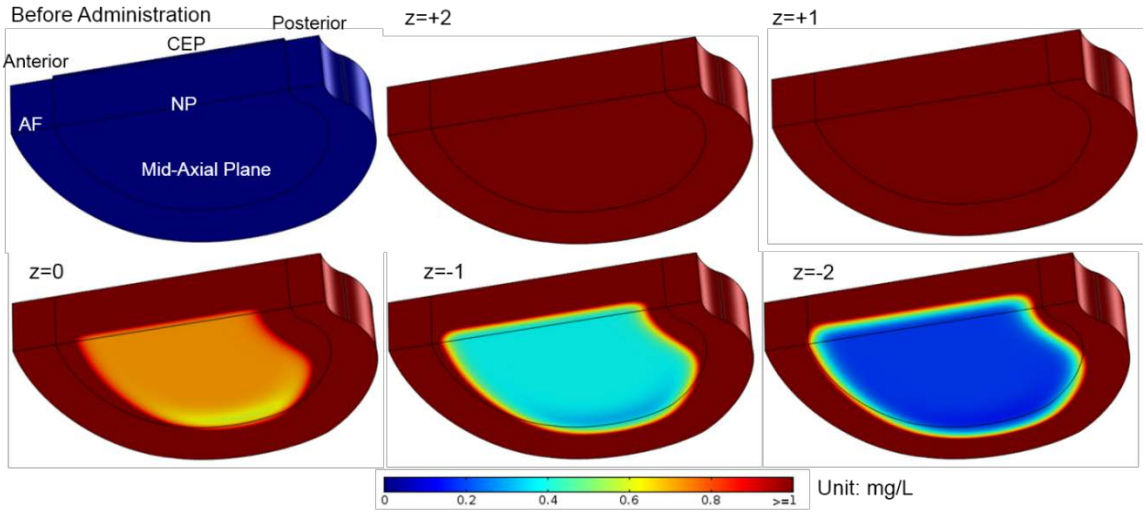

Figure 8. 3: Spatial distributions of antibiotic concentrations at 2 hours post a single IV administration. z is the valence of the antibiotics. Regions with concentration higher than the minimum inhibitory concentration (e.g., 1 mg/L) were colored in crimson.

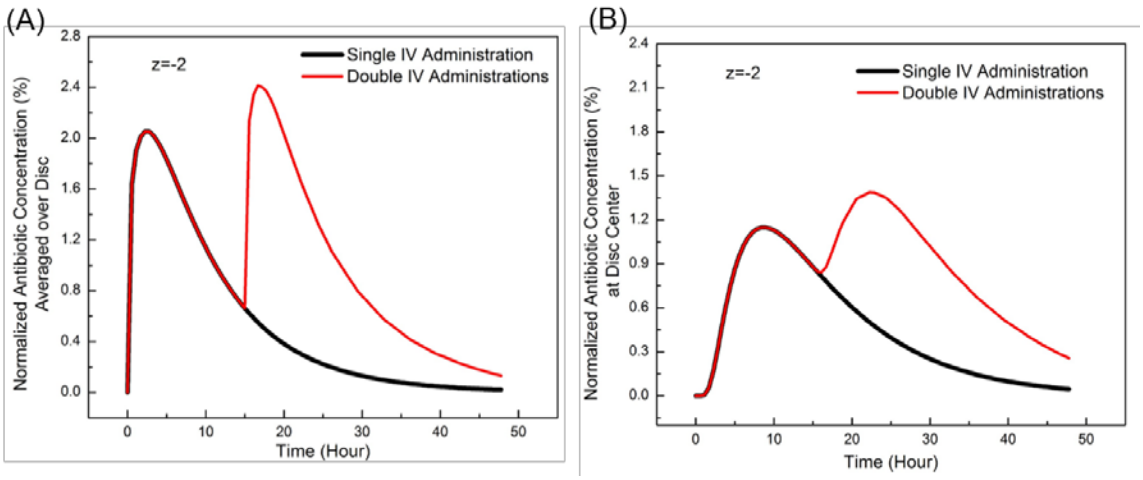

Figure 8. 4: Comparison of the antibiotic (z=-2) concentration profiles between single IV administration and double IV administration cases: (A) averaged over the disc and (B) at the disc center. The concentration was normalized to the peak value in serum (i.e., 160 mg/L).

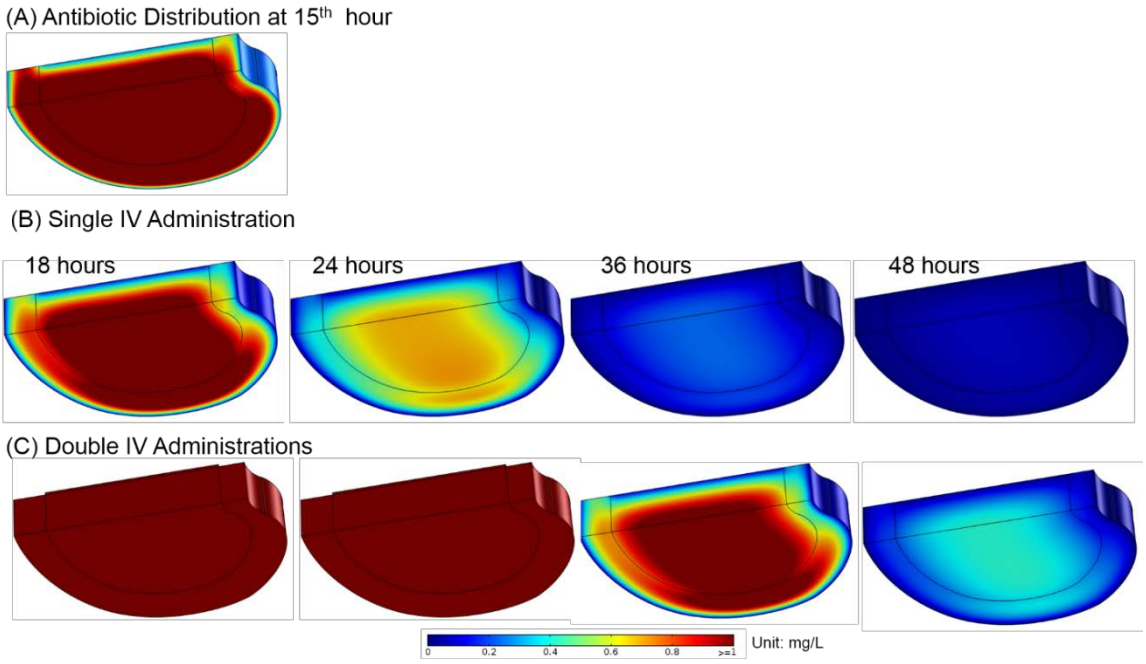

Figure 8. 5: (A) Spatial distributions of a negatively charged (z=-2) antibiotic in the disc at 15th hour after the single IV administration. Variations of spatial concentration distributions of a negatively charged (z=-2) antibiotic in the disc with (B) a single IV administration, and (C) double IV administrations. Regions with concentration higher than 1 mg/L were colored in crimson.

8.4 Discussion

The effects of electrical charge of antibiotics on the antibiotics diffusion into human IVDs were numerically investigated in this study. Our quantitative results showed that the electrical charge of antibiotics has great influences both on the concentration distribution and time to reach peak value in the disc, with higher concentration level and longer time to reach peak values in the disc for positively charged antibiotics than those for negatively charged ones.

The much lower concentration of negatively charged antibiotics within the disc is due to the Donnan's effect. The disc contains abundant negatively charged groups which are attached to the proteoglycan side chains. These negatively charged groups are fixed to the extracellular matrix and affect the concentration distribution of charged solutes within the disc. The negatively charged antibiotics are excluded from the disc whereas positively charged or uncharged ones can easily build up within the disc. This notion is consistent with experimental findings reported in the literature [209, 210, 221].

Concentrations of antibiotics in the disc reach peak values at different time points, as antibiotics inflow and outflow into and out the disc with the rise and fall of antibiotic level in the blood serum. The driving force for the transport of charged antibiotics is the combination of electrical potential gradient and concentration gradient. Due to the existence of fixed negatively charged groups in the disc, the electrical potential inside the disc is lower than that in the outside of the disc. Thus, the direction of driving force caused by electrical potential difference for negatively charged antibiotics is outward, whereas it is inward for positively charged antibiotics. The direction of driving force caused by concentration gradient varies with time, and is inward initially. When the driving force caused by electrical potential gradient is balanced by the driving force caused by concentration gradient, the antibiotic concentration within the disc reaches its peak value in time. Due to the fact that during the influx processes, the driving forces caused by electrical potential gradient and concentration gradient are in the opposite directions for negatively charged antibiotics, whereas the two driving forces are in the same direction for positively charged antibiotics, it takes a shorter time for negatively charge antibiotics to

reach the balance point (i.e., concentration reaches peak value) than for positively charged antibiotics.

The multiple IV administrations of antibiotics could effectively maintain the high antibiotic concentration in the disc for a prolonged duration (Figs. 8.4 and 8.5). The pattern of concentration change with time for the second IV administration is similar to the first one, indicating the patterns are repeatable for subsequent IV administrations. This phenomenon is useful for estimating the number of IV administrations needed in order to maintain antibiotic concentration above the therapeutic level for a period of time.

In this study, only the charge effect on transport of antibiotics in IVD was investigated. Other factors, such as binding, anisotropy, and the interaction between pH and antibiotic charge, will be considered in subsequent studies.

In conclusion, this study is primarily a parametric analysis with the focus on investigating the effect of electrical charge on antibiotics penetration into human IVD. Our results indicate that electrical charge has great influences on both the concentration level and the kinetics of antibiotics in the disc, with much higher concentration and longer time to reach the peak value for positively charged antibiotics than those for the negatively charged ones. This numerical model can be used to provide quantitative guidance on dosage to use, timing of administration, and duration of treatment for disc infection.

Chapter 9 Simulation of Water Content Distributions in Degenerated Human Intervertebral Discs

9.1 Introductory Remarks

The intervertebral disc (IVD) is the largest avascular structure in the human body and it functions to support mechanical loading and to provide flexibility to the spine system. The most common biochemical characteristics of intervertebral disc degeneration are the loss of glycosaminoglycan (GAG) and the decrease of water content [12].

The three major causes for disc degenerations are nutrition deprivation, inappropriate mechanical loading, and genetic factors [7]. How each of these causal factors leads to the various patterns (e.g., the spatial distributions of matrix components) in discs during degenerative progression remains unknown. That is, it is difficult to correlate a specific disc degeneration pattern to a certain cause. Investigation of these patterns is important for developing a new method to detect disc degeneration at its early stage, as well as for assessing outcomes of disc repair with biological therapies, including implanting cells, enhancing matrix synthesis, and inhibiting matrix degradation [66, 67, 226].

Magnetic resonance imaging (MRI) techniques (e.g., T1- and T2-weighted images) are widely used in estimating the degeneration stage of human discs. For example, Pfirrmann scoring is a scaling method to grade the disc degeneration stages based on T2-weighted MRI images [227]. It is reported that a horizontal gray band (i.e., a band with lower signal intensity near the mid-axial plane in the disc) seen in the T2-weighted MRI images of degenerated discs is an indication for degeneration stages of disc [227]. The exact

pathology for the 'band-like' pattern is unclear. A "bright spot" in the posterior region of the disc seen in T2-weighted MRI images, known as High Intensity Zone (HIZ), is another characteristic of disc degeneration [188-191]. Some researchers reported that the HIZ was a reliable marker for annular tears in painful discs [188-190, 192], whereas others found the HIZ also appeared in asymptomatic subjects without annular tears [191, 228]. The mechanisms for the occurrence of the HIZ in the degenerated discs with annular tears are generally thought to be caused by inflammation and/or neovascularization into that region [192, 229]. However, the occurrence of HIZ in the degenerated discs without annular tears is unclear.

Since the principal source of MRI-sensitive protons in the disc is water, we hypothesized that the patterns of water content distribution in the discs are related to the intensity patterns observed in T2-weighted MRI images. As a first step to test this hypothesis, in this study, we aimed to investigate variations of water content distribution in the disc during degenerative progression and repair processes. Knowledge of water content distribution is important for understanding degenerative patterns seen in MRI images and may provide guidance to develop a new quantitative method for detecting early disc degeneration.

9.2 Methods

A finite element model for human lumbar disc was used for this study [168]. This finite element method was developed based on the cell-activity-coupled mechano-electrochemical theory for intervertebral discs. The details of the finite element model can be found in our previous studies [25, 161, 168]. Briefly, the disc was modeled as an mixture of solid phase, fluid phase, and solute phase based on the triphasic continuum mixture theory [6]. The coupling phenomena among tissue deformation, transport of fluid

and solutes, and electro-osmotic effects were modeled. The cell viability was dependent on local glucose level, and the glycosaminoglycan (GAG) content was dependent on cell density, GAG synthesis rate and degradation rate (see Table 1 of Zhu et al (2015)[230] for details) [168, 230]. This model is able to predict the distributions of cell density, oxygen tension, glucose concentration, lactate concentration, pH value, GAG content, ion concentrations, fluid pressure, water content, stresses and strains of the solid matrix, and tissue deformation in the discs. Moreover, this model has been validated by comparing model predictions of water content and GAG content distributions with those from experiments [25, 168].

The geometry of the disc was generated based on a human L2-3 disc (41 years old male, non-degenerated [104, 161], Fig. 9.1A). The disc was modeled as an inhomogeneous structure with two regions: nucleus pulposus (NP) and annulus fibrosus (AF). Due to symmetry, only the upper-right quarter of the disc was simulated (Fig. 9.1B). The mesh in the model contained 7888 hexahedral elements. The finite element model of the disc was developed with COMSOL (COMSOL 4.3b, COMSOL Inc. MA) based on the method developed by Sun et al. (1999) [142]. Disc at the healthy state before degeneration was chosen as the reference configuration.

The mechanical properties (Lame constants λ and μ) used in the study were λ=0.39 MPa and μ=0.01 MPa for the NP region, and λ linearly increased from 0.39 to 1.01 MPa and μ linearly increased from 0.01 to 0.29 MPa from the innermost AF region to the outermost AF region [162-164]. Cell density was 4000 cells/mm^3 in NP and 9000 cells/mm^3 in AF, which were taken from experimental data measured in mature, healthy discs [18]. Fixed charge density (FCD) and water content (i.e., volume fraction of water) in the mature,

healthy disc were also extracted from experimental data in the literature [15], that is, fixed charge density was assumed to be homogeneous with a value of 0.34 M in the NP, and linearly decreased from 0.34 to 0.16 M from the innermost AF region to the outermost AF region. Water content (i.e., volume fraction) was 0.85 (water volume over tissue volume) in the NP, and linearly decreased from 0.85 to 0.70 from the innermost AF region to the outermost AF region. More information on material properties, initial and boundary conditions can be found in Chapter 5.

In this study, the effect of cartilage endplate (CEP) on nutrition supply was considered by adjusting the boundary conditions for nutrients at the interface between NP and CEP (to save computational time) [25], in order to account for the changes in solute diffusivity and hydraulic permeability in CEP seen in mildly and moderately degenerated discs [231, 232]. More specifically, the following nutrition boundary conditions were used for the heathy disc: 3.20 mM for the glucose concentration and 3.60 kPa for the oxygen tension on the NP surface (adjacent to the CEP), and 5.00 mM for the glucose concentration and 5.80 kPa for the oxygen tension on the AF periphery [25, 147, 168]. The degenerated disc models (without annular tears) were virtually created by reducing the nutrition levels at the disc boundary. For generating a mildly degenerated disc, the glucose concentration was reduced to 1.12 mM and oxygen tension to 1.25 kPa on the NP surface (adjacent to the CEP), and the glucose concentration was reduced to 1.40 mM, oxygen tension to 1.62 kPa on the AF periphery. For generating a moderately degenerated disc, the glucose concentration was reduced to 0.64 mM and oxygen tension to 0.71 kPa on the NP surface (adjacent to the CEP), and the glucose concentration was reduced to 1.00 mM and oxygen tension to 1.16 kPa on the AF periphery. The degeneration processes for both mildly and

moderately degenerated discs due to insufficient nutrient supply were simulated (Figs. 9.2 and 9.3).

The discs at 10^{th} year of degeneration (Fig. 9.2) were treated with biological therapies and their repair processes (for another 10 years) were simulated (Figs. 9.4-9.6). The discs without treatment (i.e., the discs with 20 years of degeneration in Fig. 9.2) were served as a control. Three types of biological therapies for disc repair were investigated numerically: increasing cell density in the NP (Case I), increasing GAG synthesis rate in the NP (Case II), and decreasing GAG degradation rate in the NP (Case III). For Case I, two different values for cell density in the NP (4000 cells/mm^3 and 8000 cells/mm^3) were investigated. In Case II, the GAG synthesis rate per cell in the NP was assumed to increase by 100%, i.e., from 0.91×10^{-5} mmol/g dry weight/hr to 1.82×10^{-5} mmol/g dry weight/hr. In Case III, the relative GAG degradation rate in the NP was assumed to decrease by 50%, i.e., from 2.00×10^{-9}/s to 1.00×10^{-9}/s [168]. Note that the nutrition level at the disc boundary during the therapy was assumed to be the same as those at the healthy condition.

9.3 Results

Change in Water Content Distribution in the Discs with Degenerative Progression

Water content distribution in the healthy disc (before degeneration) is shown in Fig. 9.2A. With the disc degeneration progression, the water content was predicted to decrease in the disc (Fig. 9.2 B and C). A horizontal region with lower water content appeared at the middle of NP (compared with the rest of the NP region). This region was defined as the degenerated region in this study. This region was wider in the disc with lower nutrition level at the disc boundary (Fig. 9.2 B and C, Mid-sagittal plane view). A spot at the posterior region with higher water content was predicted in the mildly degenerated disc

(Fig. 9.2B, mid-axial plane view). However, the spot was not distinctive in the moderately degenerated disc (Fig. 9.2C). The water content distributions along the axial direction at the center of NP were predicted and compared with an experimental measurement (Fig. 9.3) [155]. Disc height (the red line marks the original geometry of the disc before degeneration and repair) decreased slightly in the mildly degenerated disc, but noticeably in the moderately degenerated disc after 10 years of degeneration.

Changes in Water Content Distribution in the Degenerated Discs after Treatment

Before treatment, there were a 20% loss in cell number, 8% decrease in GAG content, 4% decrease in water content, and 2.3% decrease in disc height in the mildly degenerated disc. Whereas in the moderately degenerated disc, there were a 60% loss in cell number, 26% decrease in GAG content, 14% decrease in water content in the disc, and 9.3% decrease in disc height.

After treatment with increased cell density in the NP (i.e., Case I), the water content was predicted to increase in both the mildly and moderately degenerated discs after treatment (Fig. 9.4). The increase rate depended on the cell density in the NP; that is, the higher the cell density (e.g., 8000 cells/mm^3) was used, the faster the water content would increase in the treated disc. Consequently, the horizontal region with lower water content (mid-sagittal view) disappeared faster in the degenerated disc treated with a higher value of cell density. Similarly, the spot with relatively higher water content (mid-axial view) disappeared faster in the degenerated disc treated with a cell density of 8000 cells/mm^3, compared to that treated with a cell density of 4000 cells/mm^3. Disc height increased after the treatment (Fig. 9.4).

In Case II, the water content was predicted to further decrease in the degenerated region and to increase in the non-degenerated region (Fig. 9.5). The overall water content increased in the mildly degenerated disc after treatment, resulting in an increase in the disc height (Fig. 9.5A), while there was no significant increase in overall water content or disc height in the moderately degenerated disc after treatment (Fig. 9.5B). The spot with higher water content in the posterior region at mid-axial plane remained after treatment (Fig. 9.5). The results predicted by our model for Case III were similar to those for Case II (Fig. 9.6).

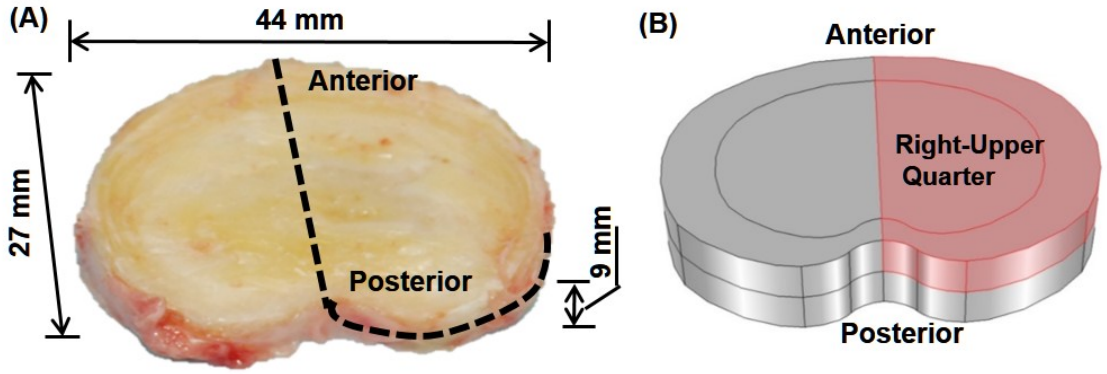

Figure 9. 1: (A) Geometry of a human lumbar disc (L2-3, male, non-degenerated) [105] and (B) its upper-right quarter were used for simulations.

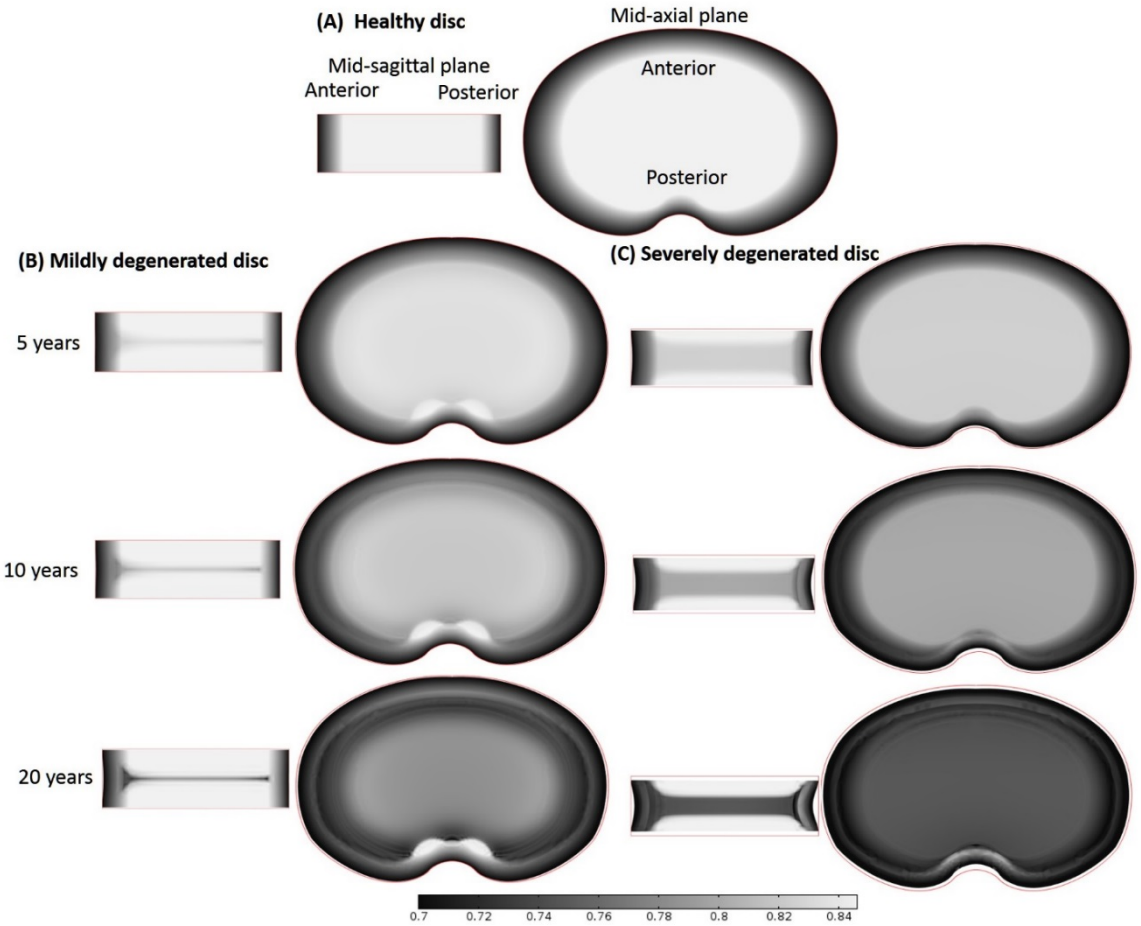

Figure 9. 2: (A) Water content (water volume over tissue volume) distribution in the healthy disc at the mid-sagittal plane (Left) and at the mid-axial plane (Right). Change of water content distribution with time (B) in the mildly degenerated disc and (C) in the moderately degenerated discs (both without therapies). Discs with 10 years of degeneration were treated with biological therapies (see Figs. 9.4-9.6) and discs with 20 years of degeneration (last row) served as a control for treated discs (see Figs. 9.4-9.6).

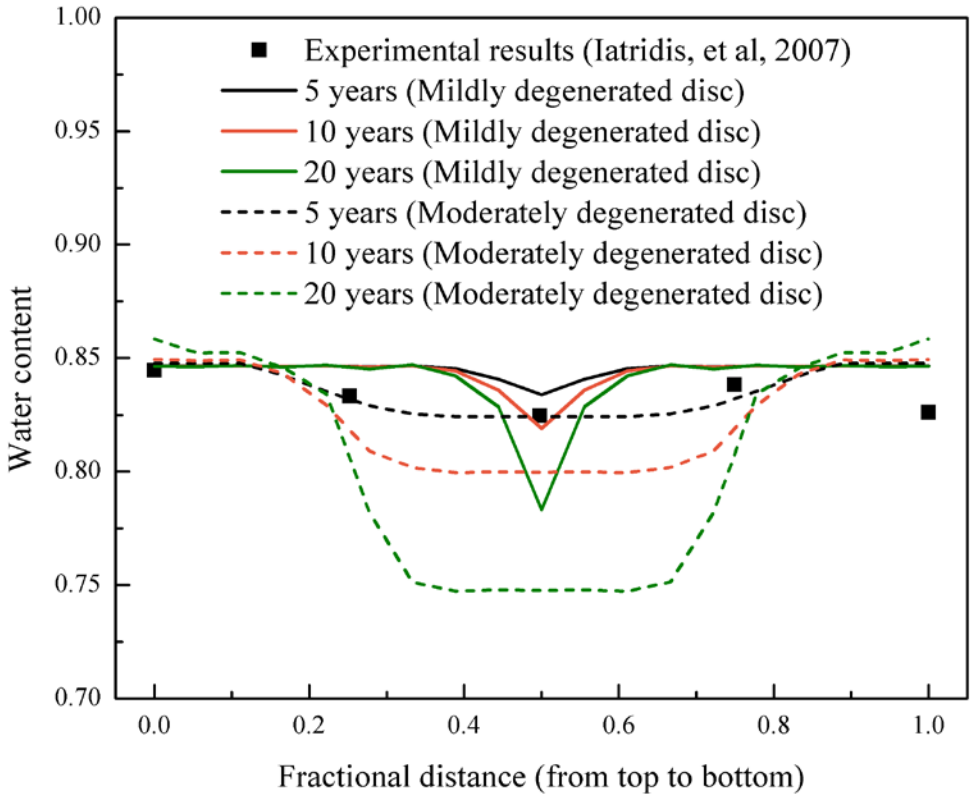

Figure 9. 3: Predicted variations of water content (water volume over tissue volume) distributions along the axial direction at the center of NP, and comparison with an experimental measurement [155].

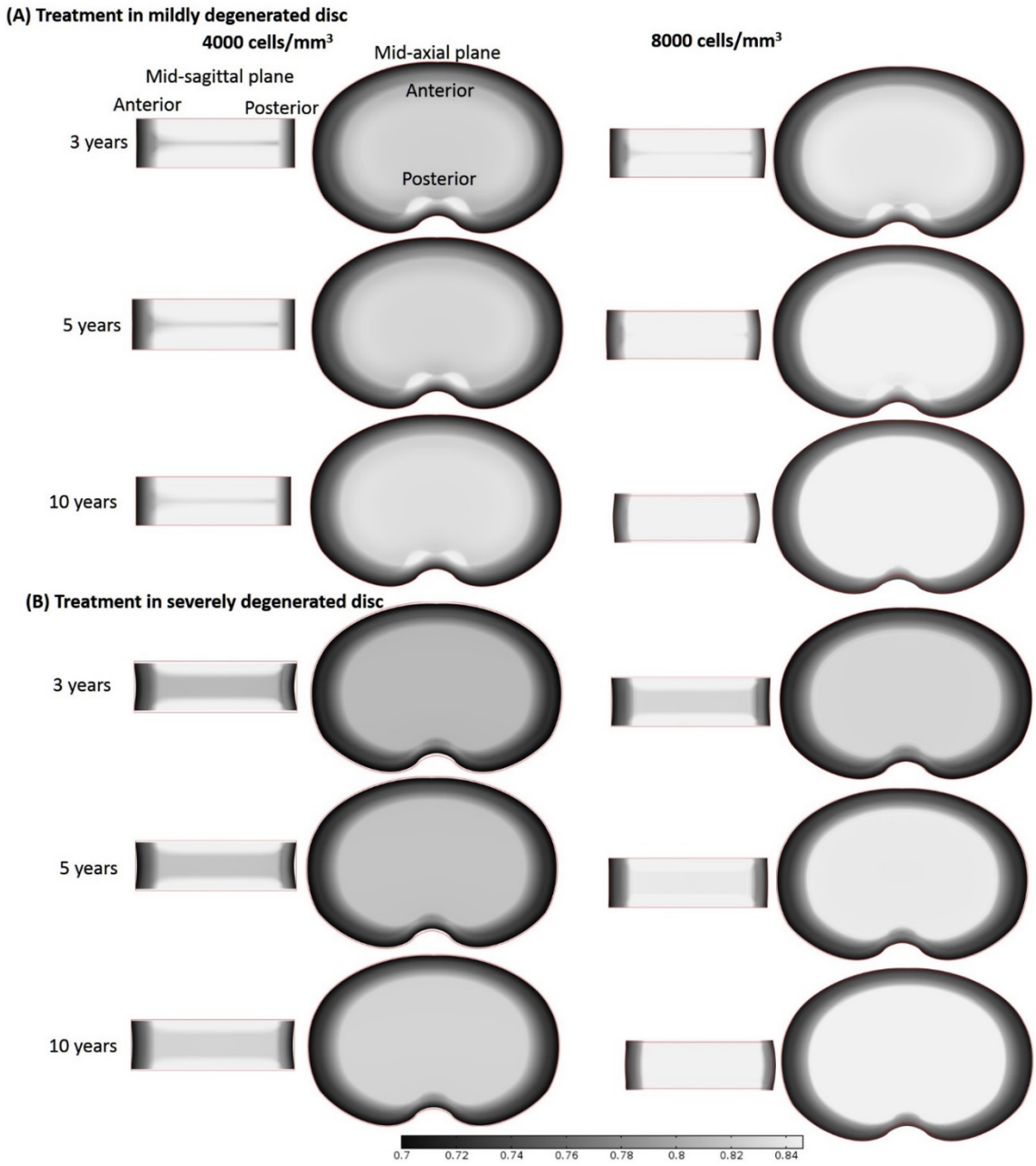

Figure 9. 4: Variation of water content (water volume over tissue volume) distribution with time in the discs treated with a cell density of 4000 or 8000 cells/mm3 (Case I): (A) in the mildly degenerated disc, and (B) in the severally degenerated disc.

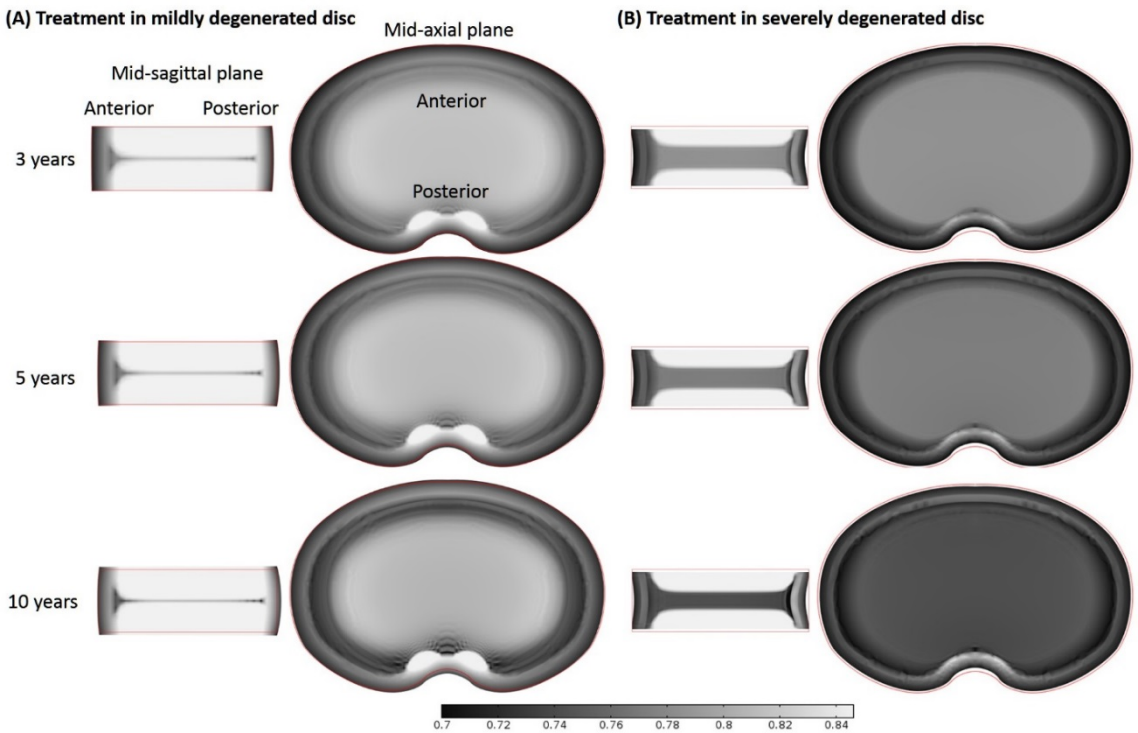

Figure 9. 5: Variation of water content (water volume over tissue volume) distribution with time in the discs treated with increased GAG synthesis rate by 100% (Case II): (A) in the mildly degenerated disc, and (B) in the severally degenerated disc.

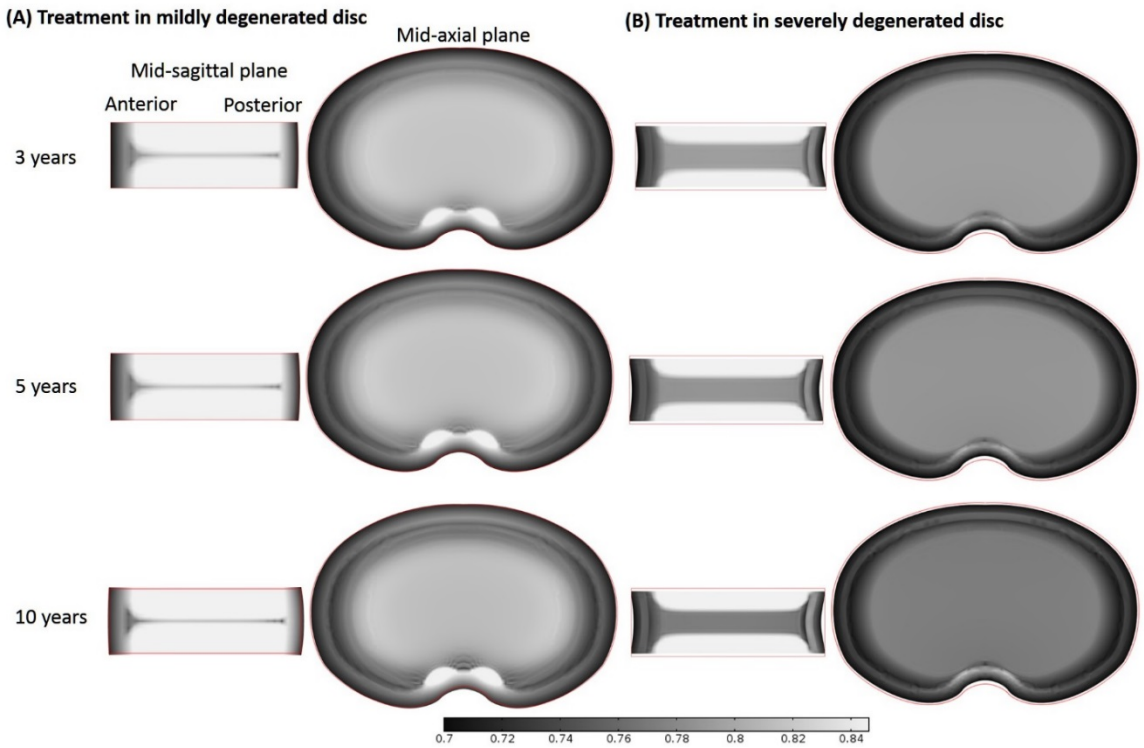

Figure 9. 6: Variation of water content (water volume over tissue volume) distribution with time in the discs treated with reduced GAG degradation by 50% (Case III): (A) in the mildly degenerated disc, and (B) in the severally degenerated disc.

9.4 Discussion

The first goal of this study was to numerically investigate the temporal and spatial variations of water content during disc degeneration process. The predicted variation of water content distribution along the axial direction at the center of NP in the degenerated discs is consistent with experimental findings reported by Iatridis et al [155], see Fig. 9.3, indicating that the water content distribution predicted by our model is realistic.

Two patterns of water content distributions, a horizontal region with lower water content and a spot with higher water content, were predicted to appear during the degenerative progression. The horizontal region with lower water content appeared at the mid-axial plane of NP is due to the fact that nutrition levels are lowest [119, 168], and more cells die in this region when nutrient concentrations at the disc boundaries reduce to a level below the critical level (defined as the minimum nutrition level at the disc boundary to maintain the viability of all the cells within the disc), resulted in a lower GAG content in the region [168]. Since lower GAG content corresponds to lower osmolarity (or swelling pressure) [24, 25], less water is retained at the mid-axial plane of NP [25]. The water content distribution in the disc is dependent not only on the GAG distribution, but also on the tissue deformation (i.e., dilation) [6] which is related to the disc geometry and tissue mechanical properties. The appearance of the bright spot in the posterior region (Fig. 9.2C) is related to disc geometry as well as the nutrition pathways [233].

The predicted patterns of water content distributions in degenerated discs were similar to those observed in T2-weighted MRI images [189, 190, 227]. It is reported that the intensity of a T2-weighted MRI images depends on three factors (a) collagen concentration, (b) tissue anisotropy (orientation of collagen), and (c) water content in the tissue [234-236];

and water is the main source of MRI-sensitive protons in the tissue [235]. During disc degeneration, variation of water content and collagen structure might occur simultaneously. Thus, it is not surprising to see a correlation in patterns between water content distribution (Fig. 9.2) and the intensity of T2-weighted MRI images [188-191, 227]. More investigation is needed to further confirm this correlation. Incidentally, our results indicate that the nutrition level at disc boundary is a factor influencing the patterns of water content distribution in the degenerated disc (Fig. 9.2 B and C), which may be used for the diagnosis of disc degeneration.

The second goal of this study was to numerically investigate the variation of water content distribution with biological therapies. Our predicted results indicate that increasing cell density (such as by cell implantation) may be the only therapy (among the three therapies investigated in this study) which is effective for eliminating the two patterns of water content distribution appeared in the degenerated discs. Therapies with increasing the GAG synthesis rate or decreasing the GAG degradation rate may be effective for increasing the overall water content and the disc height (Figs. 9.4 and 9.5), but not effective for eliminating the two patterns. This result is helpful to assess the therapy outcome with MRI techniques.

There are some limitations in this study. The solid matrix of the tissue was assumed to be isotropic and linearly elastic, which may not be able to accurately describe the large deformation of disc. This would affect the value of the water content predicted, but may not affect the patterns of water content distributions significantly, as the predict patterns in the generated discs were consistent with those experiment findings [168, 237]. For a more realistic simulation, the anisotropic and nonlinear model should be considered [238]. The

other limitation of this study is that only one disc geometry was studied. Since the shape and size of discs are important factors affecting the diffusion of nutrients and deformation, more disc geometries will be studies in the future.

In conclusion, the change in water content distribution with disc degenerative progression and repair process has been investigated with a finite element model. The horizontal region with lower water content at the mid-axial plane of NP and the spot with higher water content at the posterior region may imply the gray band and HIZ observed on T2-weighted MRI images. This study provided new guidance to develop a novel method for diagnosing disc degeneration and assessing outcomes of biological therapies with MRI techniques.

Chapter 10 Dissertation Summary

Low back pain affects millions of people each year, causing huge financial burden to the patients and the society. Degeneration of the intervertebral disc (IVD) has been found to be strongly associated with the low back pain. IVDs are the largest avascular structure in the human body and their main function is to support mechanical loading and to provide flexibility for the spine system. Poor nutrition supply and abnormal mechanical loading to the IVD are thought to be two primary external factors leading to disc degeneration.

However, how the disc degeneration progresses after the disc degeneration being triggered by these factors is largely unknown, as the biological, chemical, electrical, and mechanical events in IVDs are coupled at different levels. It is important to understand the biophysics and pathophysiology in IVD (a biological system). The major objectives of this dissertation were (1): to develop a comprehensive numerical model to study the biological, chemical, electrical, and mechanical events in the IVD during progression and repair, (2) to quantitatively simulate the changes in tissue composition, extracellular environment, and morphology change with the progression of disc degeneration, and (3) to quantitatively simulate the changes in tissue composition and morphology change during the process of disc repair. In order to achieve these aims, a cell-activity coupled multiphasic mixture theory was developed, and a finite element model based on this theory framework was developed to study the issues in the objectives.

A cell-activity coupled multiphasic mixture theory which coupled the biology (cell viability, metabolic activities, synthetic activities) and mechanics [including the solid

deformation, fluid flow, and solutes transport (diffusion, convection, and binding)] to characterize intervertebral disc degeneration and repair was developed in this project, based on the framework of multiphasic mechano-electrochemical continuum mixture theory [5, 6, 102]. A constitutive model on the nutrition dependent cell viability was developed, a constitutive model for the proteoglycan (PG) synthesis/degradation was developed.

A 3D multi-physics finite element model was developed based on the cell-activity coupled mixture theory. In this model, the phenomena at a solute (or solvent) level (e.g., diffusion and/or reaction of ions, nutrients, growth factors, and interstitial fluid), cellular level (e.g., cell metabolism and viability), and tissue level (e.g., disc volume and shape) are accounted for. The model also includes the interactions among biological (cell activity), chemical (osmolarity, pH, ECM synthesis and degradation), electrical (charges on ECM and solutes), and mechanical (loading and tissue swelling) events in the IVD. Numerical results were obtained by solving a dozen of partial differential equations using a finite element method.

Effects of nutrition supply and dynamic loading on cell viability (for preventing degeneration) were numerically investigated. It is found that poor nutrition leads to cell death, and dynamic compression has less detrimental effects on the cell viability compared to static compression.

The initiation and progression of disc degeneration (up to 55 years) related to poor nutrition supply were simulated and investigated. The mechanical, chemical, electrical, and biological events in human lumbar discs under degenerative changes were predicted and

analyzed. The predicted distributions of water content in the IVD are consistent with those from direct measurements published in the literature.

The effect of nutritional pathway on disc degeneration patterns (spatial distributions of cell density, GAG content, water content, etc.) was numerically investigated. Results indicate that impairment of the CEP-NP nutritional pathway would cause tissue degeneration mostly in the NP region, while impairment of the AF periphery nutritional pathway primarily leads to tissue degeneration in the outer AF region.

The long-term efficacy (up to 10 years) of biological therapies (e.g., cell implantation, biosynthetic activities stimulation, biodegradation activities inhibition) for disc repair was simulated and analyzed. The predicted results indicate that while all three types of biological therapies (i.e., cell implantation, biosynthetic activities stimulation, biodegradation activities inhibition) are effective for mildly degenerated discs, only the therapy with increasing cell density is effective for severely degenerated discs. This study provides not only additional insights into disc degeneration and repair processes, but also a quantitative guide for choosing proper treatment strategies for disc repair.

The model was also used to study kinetics of charged antibiotics (for treating disc infections). Our results indicate that electrical charge has great influences on both the concentration level and the kinetics of antibiotics in the disc, with a much higher concentration and a longer time to reach the peak value for positively charged antibiotics than those for the negatively charged ones. This study (in Chapter 8) shows that this numerical model can be used to provide quantitative guidance on dosage to use, timing of administration, and duration of treatment for disc infection.

This numerical model also show a promising application in helping diagnosis of the disc degeneration in clinical when combined with MRI. This model can be used to predict the water content distributions in the degenerated discs. Our predicted patterns of water content distributions in degenerated discs are similar to those observed in T2-weighted MRI images. The horizontal region with lower water content at the mid-axial plane of NP and the spot with higher water content at the posterior region predicted with this model may imply the gray band and HIZ observed on T2-weighted MRI images. This study shows that this numerical model may be a powerful tool for diagnosing disc degeneration and assessing outcomes of biological therapies with MRI techniques.

References

1. Freemont, A.J., The cellular pathobiology of the degenerate intervertebral disc and discogenic back pain. Rheumatology, 2009. 48(1): p. 5-10.

2. Luoma, K., et al., Low back pain in relation to lumbar disc degeneration. Spine, 2000. 25(4): p. 487-492.

3. Buckwalter, J.A., Spine update-aging and degeneration of the human intervertebrald disc. Spine, 1995. 20(11): p. 1307-1314.

4. Vos, T., et al., Years lived with disability (YLDs) for 1160 sequelae of 289 diseases and injuries 1990-2010: a systematic analysis for the Global Burden of Disease Study 2010. Lancet, 2012. 380(9859): p. 2163-96.

5. Gu, W.Y., W.M. Lai, and V.C. Mow, A mixture theory for charged-hydrated soft tissues containing multi-electrolytes: passive transport and swelling behaviors. J Biomech Eng, 1998. 120(2): p. 169-80.

6. Lai, W.M., J.S. Hou, and V.C. Mow, A triphasic theory for the swelling and deformation behaviors of articular cartilage. J Biomech Eng, 1991. 113(3): p. 245-58.

7. Urban, J.P. and S. Roberts, Degeneration of the intervertebral disc. Arthritis Res Ther, 2003. 5(3): p. 120-30.

8. Sztrolovics, R., et al., Aggrecan degradation in human intervertebral disc and articular cartilage. Biochem J, 1997. 326 (Pt 1): p. 235-41.

9. Roberts, S., et al., Matrix metalloproteinases and aggrecanase - Their role in disorders of the human intervertebral disc. Spine, 2000. 25(23): p. 3005-3013.

10. Weiler, C., et al., 2002 SSE Award Competition in Basic Science: expression of major matrix metalloproteinases is associated with intervertebral disc degradation and resorption. Eur Spine J, 2002. 11(4): p. 308-20.

11. Hendry, N.G., The hydration of the nucleus pulposus and its relation to intervertebral disc derangement. J Bone Joint Surg Br, 1958. 40-B(1): p. 132-44.

12. Lyons, G., S.M. Eisenstein, and M.B. Sweet, Biochemical changes in intervertebral disc degeneration. Biochim Biophys Acta, 1981. 673(4): p. 443-53.

13. Adams, P., D.R. Eyre, and H. Muir, Biochemical aspects of development and ageing of human lumbar intervertebral discs. Rheumatol Rehabil, 1977. 16(1): p. 22-9.

14. Johnstone, B. and M.T. Bayliss, The large proteoglycans of the human intervertebral disc - changes in their biosynthesis and structure with age, topography, and pathology. Spine, 1995. 20(6): p. 674-684.

15. Urban, J.P.G. and A. Maroudas, The measurement of fixed charge density in the intervertebral disc. Biochim Biophys Acta, 1979. 586: p. 166-178.

16. Eyre, D.R. and H. Muir, Quantitative analysis of types I and II collagens in human intervertebral discs at various ages. Biochim Biophys Acta, 1977. 492(1): p. 13.

17. Raj, P.P., Intervertebral disc: anatomy-physiology-pathophysiology-treatment. Pain Pract, 2008. 8(1): p. 18-44.

18. Maroudas, A., et al., Factors involved in the nutrition of the human lumbar intervertebral disc: cellularity and diffusion of glucose in vitro. J Anat, 1975. 120(Pt 1): p. 113-30.

19. Holm, S., G. Selstam, and A. Nachemson, Carbohydrate metabolism and concentration profiles of solutes in the canine lumbar intervertebral disc. Acta Physiol Scand, 1982. 115(1): p. 147-56.

20. Bibby, S.R. and J.P. Urban, Effect of nutrient deprivation on the viability of intervertebral disc cells. Eur Spine J, 2004. 13(8): p. 695-701.

21. Roberts, S., et al., Mechanoreceptors in intervertebral discs. Morphology, distribution, and neuropeptides. Spine (Phila Pa 1976), 1995. 20(24): p. 2645-51.

22. Trout, J.J., J.A. Buckwalter, and K.C. Moore, Ultrastructure of the human intervertebral disc: II. Cells of the nucleus pulposus. Anat Rec, 1982. 204(4): p. 307-14.

23. Boos, N., et al., Classification of age-related changes in lumbar intervertebral discs: 2002 Volvo Award in basic science. Spine (Phila Pa 1976), 2002. 27(23): p. 2631-44.

24. Urban, J.P.G. and J.F. Mcmullin, Swelling pressure of the lumbar intervertebral disks - influence of age, spinal level, composition, and degeneration. Spine, 1988. 13(2): p. 179-187.

25. Zhu, Q., X. Gao, and W. Gu, Temporal changes of mechanical signals and extracellular composition in human intervertebral disc during degenerative progression. J Biomech, 2014. 47(15): p. 3734-43.

26. Adams, M.A. and P.J. Roughley, What is intervertebral disc degeneration, and what causes it? Spine, 2006. 31(18): p. 2151-2161.

27. Adams, M.A., D.S. McNally, and P. Dolan, 'Stress' distributions inside intervertebral discs - The effects of age and degeneration. J Bone Joint Surg Br, 1996. 78b(6): p. 965-972.

28. Zhao, C.Q., et al., The cell biology of intervertebral disc aging and degeneration. Ageing Res Rev, 2007. 6(3): p. 247-61.

29. Nachemson, A., et al., In vitro diffusion of dye through the end-plates and the annulus fibrosus of human lumbar inter-vertebral discs. Acta orthop. Scandinav, 1970. 41: p. 8.

30. Urban, J., S. Holm, and A. Maroudas, Diffusion of small solutes into the intervertebral disc: as in vivo study. Biorheology, 1978. 15: p. 203-221.

31. Brodin, H., Paths of nutrition in articular cartilage and intervertebral discs. Acta Orthop Scand, 1955. 24(3): p. 177-83.

32. van der Werf, M., et al., Inhibition of vertebral endplate perfusion results in decreased intervertebral disc intranuclear diffusive transport. J Anat, 2007. 211(6): p. 769-74.

33. Ogata, K. and L.A. Whiteside, 1980 Volvo award winner in basic science. Nutritional pathways of the intervertebral disc. An experimental study using hydrogen washout technique. Spine (Phila Pa 1976), 1981. 6(3): p. 211-6.

34. Rajasekaran, S., et al., ISSLS prize winner: A study of diffusion in human lumbar discs: a serial magnetic resonance imaging study documenting the influence of the endplate on diffusion in normal and degenerate discs. Spine (Phila Pa 1976), 2004. 29(23): p. 2654-67.

35. Horner, H.A. and J.P.G. Urban, 2001 Volvo Award winner in basic science studies: Effect of nutrient supply on the viability of cells from the nucleus pulposus of the intervertebral disc. Spine (Phila Pa 1976), 2001. 26(23): p. 2543-2549.

36. Holm, S., et al., Nutrition of the intervertebral disc: solute transport and metabolism. Connect Tissue Res, 1981. 8(2): p. 101-19.

37. Bibby, S.R.S., et al., Metabolism of the intervertebral disc: Effects of low levels of oxygen, glucose, and pH on rates of energy metabolism of bovine nucleus pulposus cells. Spine, 2005. 30(5): p. 487-496.

38. Ishihara, H. and J.P. Urban, Effects of low oxygen concentrations and metabolic inhibitors on proteoglycan and protein synthesis rates in the intervertebral disc. J Orthop Res, 1999. 17(6): p. 829-35.

39. Ohshima, H. and J.P. Urban, The effect of lactate and pH on proteoglycan and protein synthesis rates in the intervertebral disc. Spine (Phila Pa 1976), 1992. 17(9): p. 1079-82.

40. Roberts, S., et al., Transport properties of the human cartilage endplate in relation to its composition and calcification. Spine (Phila Pa 1976), 1996. 21(4): p. 415-20.

41. Benneker, L.M., et al., 2004 Young Investigator Award Winner: vertebral endplate marrow contact channel occlusions and intervertebral disc degeneration. Spine (Phila Pa 1976), 2005. 30(2): p. 167-73.

42. Hristova, G.I., et al., Calcification in human intervertebral disc degeneration and scoliosis. J Orthop Res, 2011. 29(12): p. 1888-95.

43. Wang, Y., T. Videman, and M.C. Battie, Lumbar vertebral endplate lesions: prevalence, classification, and association with age. Spine (Phila Pa 1976), 2012. 37(17): p. 1432-9.

44. Kurunlahti, M., et al., Association of atherosclerosis with low back pain and the degree of disc degeneration. Spine (Phila Pa 1976), 1999. 24(20): p. 2080-4.

45. Kauppila, L.I., Prevalence of stenotic changes in arteries supplying the lumbar spine. A postmortem angiographic study on 140 subjects. Ann Rheum Dis, 1997. 56(10): p. 591-5.

46. Lotz, J.C. and J.R. Chin, Intervertebral disc cell death is dependent on the magnitude and duration of spinal loading. Spine, 2000. 25(12): p. 1477-1482.

47. Iatridis, J.C., et al., Effects of mechanical loading on intervertebral disc metabolism in vivo. J Bone Joint Surg Am, 2006. 88 Suppl 2: p. 41-6.

48. Iatridis, J.C., et al., Compression-induced changes in intervertebral disc properties in a rat tail model. Spine (Phila Pa 1976), 1999. 24(10): p. 996-1002.

49. Rannou, F., et al., Intervertebral disc degeneration: the role of the mitochondrial pathway in annulus fibrosus cell apoptosis induced by overload. Am J Pathol, 2004. 164(3): p. 915-24.

50. Walsh, A.J. and J.C. Lotz, Biological response of the intervertebral disc to dynamic loading. J Biomech, 2004. 37(3): p. 329-37.

51. Lotz, J.C., et al., Compression-induced degeneration of the intervertebral disc: an in vivo mouse model and finite-element study. Spine (Phila Pa 1976), 1998. 23(23): p. 2493-506.

52. Setton, L.A. and J. Chen, Mechanobiology of the intervertebral disc and relevance to disc degeneration. J Bone Joint Surg Am, 2006. 88 Suppl 2: p. 52-7.

53. Matsui, H., et al., Familial predisposition for lumbar degenerative disc disease. A case-control study. Spine (Phila Pa 1976), 1998. 23(9): p. 1029-34.

54. Simmons, E.D., Jr., et al., Familial predisposition for degenerative disc disease. A case-control study. Spine (Phila Pa 1976), 1996. 21(13): p. 1527-9.

55. Sambrook, P.N., A.J. MacGregor, and T.D. Spector, Genetic influences on cervical and lumbar disc degeneration: a magnetic resonance imaging study in twins. Arthritis Rheum, 1999. 42(2): p. 366-72.

56. Battie, M.C., et al., 1995 Volvo Award in clinical sciences. Determinants of lumbar disc degeneration. A study relating lifetime exposures and magnetic resonance imaging findings in identical twins. Spine (Phila Pa 1976), 1995. 20(24): p. 2601-12.

57. Battie, M.C., et al., Similarities in degenerative findings on magnetic resonance images of the lumbar spines of identical twins. J Bone Joint Surg Am, 1995. 77(11): p. 1662-70.

58. Annunen, S., et al., An allele of COL9A2 associated with intervertebral disc disease. Science, 1999. 285(5426): p. 409-12.

59. Paassilta, P., et al., Identification of a novel common genetic risk factor for lumbar disk disease. JAMA, 2001. 285(14): p. 1843-9.

60. Kawaguchi, Y., et al., Association between an aggrecan gene polymorphism and lumbar disc degeneration. Spine, 1999. 24(23): p. 2456-2460.

61. Watanabe, H., et al., Dwarfism and age-associated spinal degeneration of heterozygote cmd mice defective in aggrecan. Proc Natl Acad Sci USA, 1997. 94(13): p. 6943-7.

62. Li, S.W., et al., Transgenic mice with targeted inactivation of the Col2a1 gene for collagen-Ii develop a skeleton with membranous and periosteal bone but no endochondral bone. Genes & Development, 1995. 9(22): p. 2821-2830.

63. Kimura, T., et al., Progressive degeneration of articular cartilage and intervertebral discs. An experimental study in transgenic mice bearing a type IX collagen mutation. Int Orthop, 1996. 20(3): p. 177-81.

64. Takahashi, M., et al., The association of degeneration of the intervertebral disc with 5a/6a polymorphism in the promoter of the human matrix metalloproteinase-3 gene. J Bone Joint Surg Br, 2001. 83(4): p. 491-5.

65. Smith, L.J., et al., Degeneration and regeneration of the intervertebral disc: lessons from development. Dis Model Mech, 2011. 4(1): p. 31-41.

66. Sakai, D. and G.B. Andersson, Stem cell therapy for intervertebral disc regeneration: obstacles and solutions. Nat Rev Rheumatol, 2015. 11(4): p. 243-56.

67. Benneker, L.M., et al., Cell therapy for intervertebral disc repair: advancing cell therapy from bench to clinics. Eur Cell Mater, 2014. 27: p. 5-11.

68. Meisel, H.J., et al., Clinical experience in cell-based therapeutics: intervention and outcome. Eur Spine J, 2006. 15 (Suppl 3): p. 397-405.

69. Hohaus, C., et al., Cell transplantation in lumbar spine disc degeneration disease. Eur Spine J, 2008. 17 (Suppl 4): p. 492-503.

70. Yoshikawa, T., et al., Disc regeneration therapy using marrow mesenchymal cell transplantation: a peport of two case studies. Spine, 2010. 35(11): p. E475-E480.

71. Orozco, L., et al., Intervertebral disc repair by autologous mesenchymal bone marrow cells: a pilot study. Transplantation, 2011. 92(7): p. 822-8.

72. Coric, D., et al., Prospective study of disc repair with allogeneic chondrocytes presented at the 2012 Joint Spine Section Meeting. J Neurosurg Spine, 2013. 18(1): p. 85-95.

73. Haufe, S.M. and A.R. Mork, Intradiscal injection of hematopoietic stem cells in an attempt to rejuvenate the intervertebral discs. Stem Cells Dev, 2006. 15(1): p. 136-7.

74. Schmidt, H., et al., What have we learned from finite element model studies of lumbar intervertebral discs in the past four decades? J Biomech, 2013. 46(14): p. 2342-55.

75. Belytschko, T., et al., Finite element stress analysis of an intervertebral disc. J Biomech, 1974. 7(3): p. 277-85.

76. Schmidt, H., et al., Application of a calibration method provides more realistic results for a finite element model of a lumbar spinal segment. Clin Biomech (Bristol, Avon), 2007. 22(4): p. 377-84.

77. Eberlein, R., G.A. Holzapfel, and C.A. Schulze-Bauer, An anisotropic model for annulus tissue and enhanced finite element analyses of intact lumbar disc bodies. Comput Method Biomec, 2001. 4(3): p. 20.

78. Laible, J.P., et al., A poroelastic-swelling finite element model with application to the intervertebral disc. Spine (Phila Pa 1976), 1993. 18(5): p. 659-70.

79. Argoubi, M. and A. Shirazi-Adl, Poroelastic creep response analysis of a lumbar motion segment in compression. J Biomech, 1996. 29(10): p. 1331-9.

80. Schroeder, Y., et al., A biochemical/biophysical 3D FE intervertebral disc model. Biomech Model Mechanobiol, 2010. 9(5): p. 641-50.

81. Karajan, N., Multiphasic intervertebral disc mechanics: theory and application. Archives of Computational Methods in Engineering, 2012. 19(2): p. 261-339.

82. Jacobs, N.T., et al., Validation and application of an intervertebral disc finite element model utilizing independently constructed tissue-level constitutive formulations that are nonlinear, anisotropic, and time-dependent. J Biomech, 2014. 47(11): p. 2540-6.

83. Ehlers, W., N. Karajan, and B. Markert, An extended biphasic model for charged hydrated tissues with application to the intervertebral disc. Biomech Model Mechanobiol, 2009. 8(3): p. 233-51.

84. Yao, H. and W.Y. Gu, Physical signals and solute transport in human intervertebral disc during compressive stress relaxation: 3D finite element analysis. Biorheology, 2006. 43(3-4): p. 323-35.

85. Iatridis, J.C., J.P. Laible, and M.H. Krag, Influence of fixed charge density magnitude and distribution on the intervertebral disc: applications of a poroelastic and chemical electric (PEACE) model. J Biomech Eng, 2003. 125(1): p. 12-24.

86. Sun, D.D. and K.W. Leong, A nonlinear hyperelastic mixture theory model for anisotropy, transport, and swelling of annulus fibrosus. Ann Biomed Eng, 2004. 32(1): p. 92-102.

87. Lin, H.S., Y.K. Liu, and K.H. Adams, Mechanical response of the lumbar intervertebral joint under physiological (complex) loading. J Bone Joint Surg Am, 1978. 60(1): p. 41-55.

88. Spilker, R.L., D.M. Daugirda, and A.B. Schultz, Mechanical response of a simple finite element model of the intervertebral disc under complex loading. J Biomech, 1984. 17(2): p. 103-12.

89. Kulak, R.F., T.B. Belytschko, and A.B. Schultz, Nonlinear behavior of the human intervertebral disc under axial load. J Biomech, 1976. 9(6): p. 377-86.

90. Shirazi-Adl, S.A., S.C. Shrivastava, and A.M. Ahmed, Stress analysis of the lumbar disc-body unit in compression. A three-dimensional nonlinear finite element study. Spine (Phila Pa 1976), 1984. 9(2): p. 120-34.

91. Shiraziadl, A., Finite-element simulation of changes in the fluid content of human lumbar disks-mechanical and clinical implications. Spine, 1992. 17(2): p. 206-212.

92. Lanir, Y., Biorheology and fluid flux in swelling tissues. I. Bicomponent theory for small deformations, including concentration effects. Biorheology, 1987. 24(2): p. 173-87.

93. Wilson, W., C.C. van Donkelaar, and J.M. Huyghe, A comparison between mechano-electrochemical and biphasic swelling theories for soft hydrated tissues.

Journal of Biomechanical Engineering-Transactions of the Asme, 2005. 127(1): p. 158-165.

94. Hoy, D., et al., The global burden of low back pain: estimates from the Global Burden of Disease 2010 study. Ann Rheum Dis, 2014. 73(6): p. 968-74.

95. Hoy, D., et al., A systematic review of the global prevalence of low back pain. Arthritis Rheum, 2012. 64(6): p. 2028-37.

96. Macfarlane, G.J., et al., Predictors of early improvement in low back pain amongst consulters to general practice: the influence of pre-morbid and episode-related factors. Pain, 1999. 80(1-2): p. 113-9.

97. Lidgren, L., The bone and joint decade 2000-2010. Bull World Health Organ, 2003. 81(9): p. 629.

98. Steenstra, I.A., et al., Prognostic factors for duration of sick leave in patients sick listed with acute low back pain: a systematic review of the literature. Occup Environ Med, 2005. 62(12): p. 851-60.

99. Kent, P.M. and J.L. Keating, The epidemiology of low back pain in primary care. Chiropr Osteopat, 2005. 13: p. 13.

100. Thelin, A., S. Holmberg, and N. Thelin, Functioning in neck and low back pain from a 12-year perspective: a prospective population-based study. J Rehabil Med, 2008. 40(7): p. 555-61.

101. Katz, J.N., Lumbar disc disorders and low-back pain: socioeconomic factors and consequences. J Bone Joint Surg Am, 2006. 88 Suppl 2: p. 21-4.

102. Mow, V.C., et al., Biphasic creep and stress relaxation of articular cartilage in compression? Theory and experiments. J Biomech Eng, 1980. 102(1): p. 73-84.

103. Huang, C.Y. and W.Y. Gu, Effects of mechanical compression on metabolism and distribution of oxygen and lactate in intervertebral disc. J Biomech, 2008. 41(6): p. 1184-96.

104. Jackson, A.R., et al., 3D finite element analysis of nutrient distributions and cell viability in the intervertebral disc: effects of deformation and degeneration. J Biomech Eng, 2011. 133(9): p. 091006.

105. Shirazi-Adl, A., M. Taheri, and J.P. Urban, Analysis of cell viability in intervertebral disc: Effect of endplate permeability on cell population. J Biomech, 2010. 43(7): p. 1330-6.

106. Bibby, S.R., et al., Metabolism of the intervertebral disc: Effects of low levels of oxygen, glucose, and pH on rates of energy metabolism of bovine nucleus pulposus cells. Spine, 2005. 30(5): p. 487-496.

107. Huang, C.Y., F. Travascio, and W.Y. Gu, Quantitative analysis of exogenous IGF-1 administration of intervertebral disc through intradiscal injection. J Biomech, 2012. 45(7): p. 1149-55.

108. Gu, W.Y., W.M. Lai, and V.C. Mow, Transport of multi-electrolytes in charged hydrated biological soft tissues. Transport Porous Med, 1999. 34(1-3): p. 143-157.

109. Yao, H. and W.Y. Gu, Three-dimensional inhomogeneous triphasic finite-element analysis of physical signals and solute transport in human intervertebral disc under axial compression. J Biomech, 2007. 40(9): p. 2071-7.

110. Gu, W.Y., et al., Diffusivity of ions in agarose gels and intervertebral disc: effect of porosity. Ann Biomed Eng, 2004. 32(12): p. 1710-7.

111. Gu, W.Y. and H. Yao, Effects of hydration and fixed charge density on fluid transport in charged hydrated soft tissues. Ann Biomed Eng, 2003. 31(10): p. 1162-70.

112. Lin, J., et al., Modeling of typical microbial cell growth in batch culture Biotechnol Bioprocess Eng, 2000. 5(5): p. 382-385

113. Horner, H.A. and J.P.G. Urban, 2001 Volvo Award winner in basic science studies: Effect of nutrient supply on the viability of cells from the nucleus pulposus of the intervertebral disc. Spine, 2001. 26(23): p. 2543-2549.

114. Bibby, S.R., et al., Cell viability in scoliotic discs in relation to disc deformity and nutrient levels. Spine, 2002. 27(20): p. 2220-2227.

115. Bibby, S.R. and J.P. Urban, Effect of nutrient deprivation on the viability of intervertebral disc cells. European Spine Journal, 2004. 13(8): p. 695-701.

116. Sivan, S.S., et al., Aggrecan turnover in human intervertebral disc as determined by the racemization of aspartic acid. J Biol Chem, 2006. 281(19): p. 13009-14.

117. Handa, T., et al., Effects of hydrostatic pressure on matrix synthesis and matrix metalloproteinase production in the human lumbar intervertebral disc. Spine (Phila Pa 1976), 1997. 22(10): p. 1085-91.

118. Bashir, A., et al., Nondestructive imaging of human cartilage glycosaminoglycan concentration by MRI. Magn Reson Med, 1999. 41(5): p. 857-65.

119. Urban, J.P., S. Smith, and J.C. Fairbank, Nutrition of the intervertebral disc. Spine, 2004. 29(23): p. 2700-9.

120. Bibby, S.R.S., Cell metabolism and viability in the intervertebral disc. 2002, University of Oxford.

121. Roberts, S., J. Menage, and J.P. Urban, Biochemical and structural properties of the cartilage end-plate and its relation to the intervertebral disc. Spine (Phila Pa 1976), 1989. 14(2): p. 166-74.

122. Urban, J.P.G., S. Roberts, and J.R. Ralphs, The nucleus of the intervertebral disc from development to degeneration. Am Zool, 2000. 40(1): p. 53-61.

123. Oegema, T.R., Jr., Biochemistry of the intervertebral disc. Clin Sports Med, 1993. 12(3): p. 419-39.

124. Gyntelbe.F, One year incidence of low-back pain among male residents of copenhagen aged 40-59. Dan Med Bull, 1974. 21(1): p. 30-36.

125. Frymoyer, J.W., et al., Risk factors in low-back pain. An epidemiological survey. J Bone Joint Surg Am, 1983. 65(2): p. 213-8.

126. Holm, S. and A. Nachemson, Nutrition of the intervertebral disc: acute effects of cigarette smoking. An experimental animal study. Ups J Med Sci, 1988. 93(1): p. 91-9.

127. Wuertz, K., et al., In vivo remodeling of intervertebral discs in response to short- and long-term dynamic compression. J Orthop Res, 2009. 27(9): p. 1235-42.

128. Wang, D.L., S.D. Jiang, and L.Y. Dai, Biologic response of the intervertebral disc to static and dynamic compression in vitro. Spine (Phila Pa 1976), 2007. 32(23): p. 2521-8.

129. Kroeber, M., et al., Effects of controlled dynamic disc distraction on degenerated intervertebral discs: an in vivo study on the rabbit lumbar spine model. Spine (Phila Pa 1976), 2005. 30(2): p. 181-7.

130. Maclean, J.J., et al., Anabolic and catabolic mRNA levels of the intervertebral disc vary with the magnitude and frequency of in vivo dynamic compression. J Orthop Res, 2004. 22(6): p. 1193-200.

131. Huang, C.Y.C., et al., Effects of cyclic compressive loading on chondrogenesis of rabbit bone-marrow derived mesenchymal stem cells. Stem Cells, 2004. 22(3): p. 313-323.

132. Kasra, M., et al., Effect of dynamic hydrostatic pressure on rabbit intervertebral disc cells. J Orthop Res, 2003. 21(4): p. 597-603.

133. Ohshima, H., J.P. Urban, and D.H. Bergel, Effect of static load on matrix synthesis rates in the intervertebral disc measured in vitro by a new perfusion technique. J Orthop Res, 1995. 13(1): p. 22-9.

134. Ariga, K., et al., Mechanical stress-induced apoptosis of endplate chondrocytes in organ-cultured mouse intervertebral discs: an ex vivo study. Spine (Phila Pa 1976), 2003. 28(14): p. 1528-33.

135. Jackson, A.R., et al., Effect of compression and anisotropy on the diffusion of glucose in annulus fibrosus. Spine 2008. 33(1): p. 1-7.

136. Malandrino, A., J. Noailly, and D. Lacroix, The effect of sustained compression on oxygen metabolic transport in the intervertebral disc decreases with degenerative changes. PLoS Comput Biol, 2011. 7(8): p. e1002112.

137. Huang, C.Y. and W.Y. Gu, Effect of tension-compression nonlinearity on solute transport in charged hydrated fibrosus tissues under dynamic unconfined compression. J Biomech Eng, 2007. 129: p. 423-429.

138. Yao, H. and W.Y. Gu, Physical signals and solute transport in human intervertebral disc during compressive stress relaxation: 3D finite element analysis. Biorheology, 2006. 43: p. 323-335.

139. Jackson, A.R., et al., Nutrient transport in human annulus fibrosus is affected by compressive strain and anisotropy. Ann Biomed Eng, 2012. 40(12): p. 2551-8.

140. Yuan, T.Y., et al., Strain-dependent oxygen diffusivity in bovine annulus fibrosus. J Biomech Eng, 2009. 131(7): p. 074503.

141. Jackson, A.R., C.Y. Huang, and W.Y. Gu, Effect of endplate calcification and mechanical deformation on the distribution of glucose in intervertebral disc: a 3D finite element study. Comput Methods Biomech Biomed Engin, 2011. 14(2): p. 195-204.

142. Sun, D.N., et al., A mixed finite element formulation of triphasic mechano-electrochemical theory for charged, hydrated biological soft tissues. Int J Numer Meth Eng, 1999. 45(10): p. 1375-1402.

143. Gu, W.Y., et al., Streaming potential of human lumbar anulus fibrosus is anisotropic and affected by disc degeneration. J Biomech, 1999. 32(11): p. 1177-1182.

144. Iatridis, J.C., et al., The viscoelastic behavior of the non-degenerate human lumbar nucleus pulposus in shear. J Biomech, 1997. 30(10): p. 1005-13.

145. Maroudas, A., Biophysical chemistry of cartilaginous tissues with special reference to solute and fluid transport. Biorheology, 1975. 12(3-4): p. 233-48.

146. Setton, L.A., et al., Compressive properties of the cartilaginous end-plate of the baboon lumbar spine. J Orthop Res, 1993. 11(2): p. 228-39.

147. Selard, E., A. Shirazi-Adl, and J.P. Urban, Finite element study of nutrient diffusion in the human intervertebral disc. Spine, 2003. 28(17): p. 1945-53.

148. Magnier, C., et al., Nutrient distribution and metabolism in the intervertebral disc in the unloaded state: a parametric study. J Biomech, 2009. 42(2): p. 100-8.

149. Antoniou, J., et al., The human lumbar intervertebral disc: evidence for changes in the biosynthesis and denaturation of the extracellular matrix with growth, maturation, ageing, and degeneration. J Clin Invest, 1996. 98(4): p. 996-1003.

150. Gu, W.Y., et al., New insight into deformation-dependent hydraulic permeability of gels and cartilage, and dynamic behavior of agarose gels in confined compression. J Biomech, 2003. 36(4): p. 593-598.

151. Johannessen, W. and D.M. Elliott, Effects of degeneration on the biphasic material properties of human nucleus pulposus in confined compression. Spine, 2005. 30(24): p. E724-E729.

152. Iatridis, J.C., et al., Shear mechanical properties of human lumbar annulus fibrosus. J Orthop Res, 1999. 17(5): p. 732-7.

153. Iatridis, J.C., et al., Localized intervertebral disc injury leads to organ level changes in structure, cellularity, and biosynthesis. Cell Mol Bioeng, 2009. 2(3): p. 437-447.

154. Roughley, P.J., Biology of intervertebral disc aging and degeneration - Involvement of the extracellular matrix. Spine, 2004. 29(23): p. 2691-2699.

155. Iatridis, J.C., et al., Measurements of proteoglycan and water content distribution in human lumbar intervertebral discs. Spine, 2007. 32(14): p. 1493-7.

156. Setton, L.A. and J. Chen, Cell mechanics and mechanobiology in the intervertebral disc. Spine, 2004. 29(23): p. 2710-2723.

157. Iatridis, J.C., et al., Is the nucleus pulposus a solid or a fluid? Mechanical behaviors of the nucleus pulposus of the human intervertebral disc. Spine, 1996. 21(10): p. 1174-1184.

158. Nachemson, A., Towards a better understanding of low-back pain: a review of the mechanics of the lumbar disc. Rheumatol Rehabil, 1975. 14(3): p. 129-43.

159. Niosi, C.A. and T.R. Oxland, Degenerative mechanics of the lumbar spine. Spine J, 2004. 4(6 Suppl): p. 202S-208S.

160. Nixon, J., Intervertebral disc mechanics: a review. J R Soc Med, 1986. 79(2): p. 100-4.

161. Zhu, Q., A.R. Jackson, and W.Y. Gu, Cell viability in intervertebral disc under various nutritional and dynamic loading conditions: 3d finite element analysis. J Biomech, 2012. 45(16): p. 2769-77.

162. Perie, D., et al., Assessment of compressive modulus, hydraulic permeability and matrix content of trypsin-treated nucleus pulposus using quantitative MRI. J Biomech, 2006. 39(8): p. 1392-400.

163. Iatridis, J.C., et al., Degeneration affects the anisotropic and nonlinear behaviors of human anulus fibrosus in compression. J Biomech, 1998. 31(6): p. 535-44.

164. Perie, D., D. Korda, and J.C. Iatridis, Confined compression experiments on bovine nucleus pulposus and annulus fibrosus: sensitivity of the experiment in the determination of compressive modulus and hydraulic permeability. J Biomech, 2005. 38(11): p. 2164-71.

165. Goldstein, S.A., The mechanical properties of trabecular bone: dependence on anatomic location and function. J Biomech, 1987. 20(11-12): p. 1055-61.

166. Crock, H.V. and M. Goldwasser, Anatomic studies of the circulation in the region of the vertebral end-plate in adult Greyhound dogs. Spine (Phila Pa 1976), 1984. 9(7): p. 702-6.

167. Stefanovic-Racic, M., et al., Nitric oxide and energy production in articular chondrocytes. J Cell Physiol, 1994. 159(2): p. 274-80.

168. Gu, W.Y., et al., Simulation of the progression of intervertebral disc degeneration due to decreased nutritional supply. Spine, 2014. 39(24): p. E1411-E1417.

169. Perie, D.S., et al., Correlating material properties with tissue composition in enzymatically digested bovine annulus fibrosus and nucleus pulposus tissue. Ann Biomed Eng, 2006. 34(5): p. 769-77.

170. Best, B.A., et al., Compressive mechanical-properties of the human anulus fibrosus and their relationship to biochemical-composition. Spine, 1994. 19(2): p. 212-221.

171. Razaq, S., R.J. Wilkins, and J.P. Urban, The effect of extracellular pH on matrix turnover by cells of the bovine nucleus pulposus. Eur Spine J, 2003. 12(4): p. 341-9.

172. Adams, M.A., et al., Mechanical initiation of intervertebral disc degeneration. Spine, 2000. 25(13): p. 1625-1636.

173. Sato, K., S. Kikuchi, and T. Yonezawa, In vivo intradiscal pressure measurement in healthy individuals and in patients with ongoing back problems. Spine, 1999. 24(23): p. 2468-2474.

174. Goel, V.K., et al., Interlaminar shear stresses and laminae separation in a disc. Finite element analysis of the L3-L4 motion segment subjected to axial compressive loads. Spine (Phila Pa 1976), 1995. 20(6): p. 689-98.

175. Gregory, D.E., et al., Novel lap test determines the mechanics of delamination between annular lamellae of the intervertebral disc. J Biomech, 2011. 44(1): p. 97-102.

176. Marshall, L.W. and S.M. McGill, The role of axial torque in disc herniation. Clin Biomech (Bristol, Avon), 2010. 25(1): p. 6-9.

177. Kaner, T., et al., Comparison of disc and body volumes in degenerated and nondegenerated lumbar discs: a stereological study. Turk J Med Sci, 2014. 44(2): p. 237-42.

178. Peloquin, J.M., et al., Human L3L4 intervertebral disc mean 3D shape, modes of variation, and their relationship to degeneration. J Biomech, 2014. 47(10): p. 2452-2459.

179. Pfirrmann, C.W., et al., Effect of aging and degeneration on disc volume and shape: A quantitative study in asymptomatic volunteers. J Orthop Res, 2006. 24(5): p. 1086-94.

180. Masuda, K., Biological repair of the degenerated intervertebral disc by the injection of growth factors. Eur Spine J, 2008. 17 Suppl 4: p. 441-51.

181. Bayliss, M.T., B. Johnstone, and J.P. O'Brien, 1988 Volvo award in basic science. Proteoglycan synthesis in the human intervertebral disc. Variation with age, region and pathology. Spine (Phila Pa 1976), 1988. 13(9): p. 972-81.

182. Gao, X. and W. Gu, A new constitutive model for hydration-dependent mechanical properties in biological soft tissues and hydrogels. J Biomech, 2014. 47(12): p. 3196-200.

183. Hutton, W.C., et al., The effect of blocking a nutritional pathway to the intervertebral disc in the dog model. J Spinal Disord Tech, 2004. 17(1): p. 53-63.

184. Pfirrmann, C.W., et al., Magnetic resonance classification of lumbar intervertebral disc degeneration. Spine (Phila Pa 1976), 2001. 26(17): p. 1873-8.

185. Griffith, J.F., et al., Modified Pfirrmann grading system for lumbar intervertebral disc degeneration. Spine (Phila Pa 1976), 2007. 32(24): p. E708-12.

186. Benneker, L.M., et al., Correlation of radiographic and MRI parameters to morphological and biochemical assessment of intervertebral disc degeneration. Eur Spine J, 2005. 14(1): p. 27-35.

187. Hoppe, S., et al., Axial T2 mapping in intervertebral discs: a new technique for assessment of intervertebral disc degeneration. Eur Radiol, 2012. 22(9): p. 2013-9.

188. Sugiura, K., et al., Discoscopic findings of high signal intensity zones on magnetic resonance imaging of lumbar intervertebral discs. Case Rep Orthop, 2014. 2014: p. 245952.

189. Peng, B., et al., The pathogenesis and clinical significance of a high-intensity zone (HIZ) of lumbar intervertebral disc on MR imaging in the patient with discogenic low back pain. Eur Spine J, 2006. 15(5): p. 583-7.

190. Aprill, C. and N. Bogduk, High-intensity zone: a diagnostic sign of painful lumbar disc on magnetic resonance imaging. Br J Radiol, 1992. 65(773): p. 361-9.

191. Carragee, E.J., S.J. Paragioudakis, and S. Khurana, 2000 Volvo Award Winner in Clinical Studies - Lumbar high-intensity zone and discography in subjects without low back problems. Spine, 2000. 25(23): p. 2987-2992.

192. Lam, K.S., D. Carlin, and R.C. Mulholland, Lumbar disc high-intensity zone: the value and significance of provocative discography in the determination of the discogenic pain source. Eur Spine J, 2000. 9(1): p. 36-41.

193. Bogduk, N., The lumbar disc and low back pain. Neurosurg Clin N Am, 1991. 2(4): p. 791-806.

194. Iatridis, J.C., et al., Role of biomechanics in intervertebral disc degeneration and regenerative therapies: what needs repairing in the disc and what are promising biomaterials for its repair? Spine J, 2013. 13(3): p. 243-62.

195. Meisel, H.J., et al., Clinical experience in cell-based therapeutics: disc chondrocyte transplantation A treatment for degenerated or damaged intervertebral disc. Biomol Eng, 2007. 24(1): p. 5-21.

196. Ganey, T., et al., Disc chondrocyte transplantation in a canine model: a treatment for degenerated or damaged intervertebral disc. Spine, 2003. 28(23): p. 2609-20.

197. Converti, A., et al., The effects of temperature and viscosity on glucose diffusivity through Saccharomyces cerevisiae biofilms. Can J Chem Eng, 1999. 77(4): p. 618-626.

198. Burstein, D., et al., Diffusion of small solutes in cartilage as measured by nuclear magnetic resonance (NMR) spectroscopy and imaging. J Orthop Res, 1993. 11(4): p. 465-78.

199. Urban, J.P.G., Fluid and solute transport in the intervertebral disc 1977, London University.

200. Esko, J.D., K. Kimata, and U. Lindahl, Proteoglycans and sulfated glycosaminoglycans, in Essentials of Glycobiology, A. Varki, et al., Editors. 2009: Cold Spring Harbor (NY).

201. Gao, X., Q. Zhu, and W. Gu, Analyzing the effects of mechanical and osmotic loading on glycosaminoglycan synthesis rate in cartilaginous tissues. J Biomech, 2015. 48(4): p. 573-7.

202. Ishihara, H., et al., Proteoglycan synthesis in the intervertebral disk nucleus: the role of extracellular osmolality. Am J Physiol, 1997. 272(5 Pt 1): p. C1499-506.

203. van Dijk, B., E. Potier, and K. Ito, Culturing bovine nucleus pulposus explants by balancing medium osmolarity. Tissue Eng Part C Methods, 2011. 17(11): p. 1089-96.

204. van Dijk, B.G., E. Potier, and K. Ito, Long-term culture of bovine nucleus pulposus explants in a native environment. Spine J, 2013. 13(4): p. 454-63.

205. Eismont, F.J., et al., Antibiotic penetration into rabbit nucleus pulposus. Spine, 1987. 12(3): p. 254-256.

206. Fraser, R.D., O.L. Osti, and B. Vernon-Roberts, Iatrogenic discitis: the role of intravenous antibiotics in prevention and treatment. An experimental study. Spine (Phila Pa 1976), 1989. 14(9): p. 1025-32.

207. Scuderi, G.J., et al., Penetration of glycopeptide antibiotics in nucleus pulposus. Spine (Phila Pa 1976), 1993. 18(14): p. 2039-42.

208. Currier, B.L., K. Banovac, and F.J. Eismont, Gentamicin penetration into normal rabbit nucleus pulposus. Spine, 1994. 19(23): p. 2614-2618.

209. Riley, L.H., 3rd, et al., Tissue distribution of antibiotics in the intervertebral disc. Spine (Phila Pa 1976), 1994. 19(23): p. 2619-25.

210. Thomas, R.W., et al., A new in-vitro model to investigate antibiotic penetration of the intervertebral disc. J Bone Joint Surg Br, 1995. 77(6): p. 967-70.

211. Walters, R., et al., Prophylactic cephazolin to prevent discitis in an ovine model. Spine (Phila Pa 1976), 2006. 31(4): p. 391-6.

212. Gibson, M.J., et al., The penetration of antibiotics into the normal intervertebral disc. J Bone Joint Surg Br., 1987. 69(5): p. 6.

213. Lang, R., et al., Penetration of ceftriaxone into the intervertebral disc. J Bone Joint Surg, 1994. 76a(5): p. 689-691.

214. Walters, R., R. Moore, and R. Fraser, Penetration of cephazolin in human lumbar intervertebral disc. Spine (Phila Pa 1976), 2006. 31(5): p. 567-70.

215. Tai, C.C., et al., Antibiotic prophylaxis in surgery of the intervertebral disc. A comparison between gentamicin and cefuroxime. J Bone Joint Surg Br, 2002. 84(7): p. 1036-9.

216. Urban, J.P., et al., Nutrition of the intervertebral disk. An in vivo study of solute transport. Clin Orthop Relat Res, 1977(129): p. 101-14.

217. Coventry, M.B., R.K. Ghormley, and J.W. Kernohan, The intervertebral disc - its microscopic anatomy and pathology .2. Changes in the intervertebral disc concomitant with age. J Bone Joint Surg, 1945. 27(2): p. 233-247.

218. Motaghinasab, S., et al., Computational pharmacokinetics of solute penetration into human intervertebral discs - effects of endplate permeability, solute molecular weight and disc size. J Biomech, 2012. 45(13): p. 2195-202.

219. Conaughty, J.M., et al., Antifungal penetration into normal rabbit nucleus pulposus. Spine, 2004. 29(14): p. E289-E293.

220. Merrikin, D.J., J. Briant, and G.N. Rolinson, Effect of protein binding on antibiotic activity in vivo. J Antimicrob Chemother, 1983. 11(3): p. 233-8.

221. Conaughty, J.M., et al., Efficacy of linezolid versus vancomycin in the treatment of methicillin-resistant Staphylococcus aureus discitis: a controlled animal model. Spine (Phila Pa 1976), 2006. 31(22): p. E830-2.

222. Ateshian, G.A., S. Maas, and J.A. Weiss, Multiphasic finite element framework for modeling hydrated mixtures with multiple neutral and charged solutes. J Biomech Eng, 2013. 135(11): p. 111001.

223. Cloyd, J.M., et al., Material properties in unconfined compression of human nucleus pulposus, injectable hyaluronic acid-based hydrogels and tissue engineering scaffolds. Eur Spine J, 2007. 16(11): p. 1892-8.

224. Shi, S., et al., Pharmacokinetics and tolerability of intravenous cefotetan disodium for injection in healthy Chinese volunteers: A randomized, open-label, single- and multiple-dose study. Clin Ther, 2010. 32(10): p. 1832-41.

225. Pinto, N., et al., Pharmacokinetics of amikacin in plasma and selected body fluids of healthy horses after a single intravenous dose. Equine Vet J, 2011. 43(1): p. 112-6.

226. Hudson, K.D., et al., Recent advances in biological therapies for disc degeneration: tissue engineering of the annulus fibrosus, nucleus pulposus and whole intervertebral discs. Curr Opin Biotechnol, 2013. 24(5): p. 872-9.

227. Pfirrmann, C.W.A., et al., Magnetic resonance classification of lumbar intervertebral disc degeneration. Spine, 2001. 26(17): p. 1873-1878.

228. Ricketson, R., J.W. Simmons, and B.O. Hauser, The prolapsed intervertebral disc. The high-intensity zone with discography correlation. Spine (Phila Pa 1976), 1996. 21(23): p. 2758-62.

229. Ren, D.F., et al., The expression of tumor necrosis factor-alpha and CD68 in high-intensity zone of lumbar intervertebral disc on magnetic resonance image in the patients with low back pain. Spine, 2011. 36(6): p. E429-E433.

230. Zhu, Q., et al., Simulation of biological therapies for degenerated intervertebral discs. J Orthop Res, 2015. doi: 10.1002/jor.23061.

231. Rajasekaran, S., et al., ISSLS prize winner: A study of diffusion in human lumbar discs: A serial magnetic resonance imaging study documenting the influence of the endplate on diffusion in normal and degenerate discs. Spine, 2004. 29(23): p. 2654-2667.

232. DeLucca, J.F., et al., Human cartilage endplate permeability varies with degeneration and intervertebral disc site. J Biomech, 2016.

233. Zhu, Q., et al., Influences of nutrition supply and pathways on the degenerative patterns in human intervertebral disc. Spine (Phila Pa 1976), 2015. In press.

234. Xia, Y., Magic-angle effect in magnetic resonance imaging of articular cartilage: a review. Invest Radiol, 2000. 35(10): p. 602-21.

235. Mwale, F., J.C. Iatridis, and J. Antoniou, Quantitative MRI as a diagnostic tool of intervertebral disc matrix composition and integrity. Eur Spine J, 2008. 17 Suppl 4: p. 432-40.

236. Brayda-Bruno, M., et al., Advances in the diagnosis of degenerated lumbar discs and their possible clinical application. Eur Spine J, 2014. 23 Suppl 3: p. S315-23.

237. Iatridis, J.C., et al., Measurements of proteoglycan and water content distribution in human lumbar intervertebral discs. Spine, 2007. 32(14): p. 1493-1497.

238. Gao, X., Q.Q. Zhu, and W.Y. Gu, An anisotropic multiphysics model for intervertebral disk. J Appl Mech, 2016. 83(2): p. 021011.